Fibronectin binding protein A-mediated cellular infections by *Staphylococcus aureus*

(Rosenbach, 1884)

Dissertation

Zur Erlangung der Würde des Doktors der Naturwissenschaften

des Fachbereich Biologie, der Fakultät für Mathematik, Informatik und Naturwissenschaften,

der Universität Hamburg

vorgelegt von

Bernd Zobiak

aus Hamburg

Hamburg 2011

Genehmigt vom Fachbereich Biologie
der Fakultät für Mathematik, Informatik und Naturwissenschaften
an der Universität Hamburg
auf Antrag von Prof. Dr. M. AEPFELBACHER
Weiterer Gutachter der Dissertation:
Prof. Dr. W. STREIT
Tag der Disputation: 15. April 2011

Hamburg, den 31.März 2011

Universität Hamburg
64
Fakultät
Mathematik, Informatik und Naturwissenschaften

Professor Dr. Axel Temming
Leiter des Fachbereichs Biologie

Die vorliegende Arbeit wurde von Mai 2006 bis Februar 2011 unter Anleitung von Prof. Dr. Martin Aepfelbacher am Institut für Medizinische Mikrobiologie, Virologie und Hygiene am Universitätsklinikum Hamburg-Eppendorf durchgeführt.

Dissertation zur Erlangung des Doktorgrades
im Fachbereich Biologie
der Universität Hamburg
vorgelegt von
Diplom-Biochemiker Bernd Zobiak
aus Hamburg

Dissertationsgutachter:	Prof. Dr. Martin Aepfelbacher
	Prof. Dr. Wolfgang Streit
Disputationsgutachter:	Prof. Dr. Stefan Linder
	PD Dr. Dirk Warnecke

A. Abstract

Staphyloccous aureus is one of the leading pathogens in nosocomial infections and can cause life threatening diseases such as bacteremia and acute endocarditis. The surface adhesin fibronectin binding protein A (FnBPA) mediates attachment to the host cell extracellular matrix component fibronectin (Fn) and subsequent actin-dependent invasion. Bacteria-associated Fn is mainly bound to host cell integrins. While the region of Fn responsible for binding FnBPA is well defined, the domains that bind the host cell which lead to FnBPA-mediated adherence and uptake are unclear. In addition, a role for the maturation state of Fn in FnBPA-mediated infection has not been explored.

To answer these questions, we generated Fns harboring inactivating mutations in the central cell-binding RGD motif and adjacent synergy site, or purified proteolytic Fn fragments, comprising different parts of the N-terminal region. In their soluble form, bound to FnBPA-particles, these mutants or fragments were reacted with Fn-deficient cells or, in their cellularly organized form, were reacted with uncoated FnBPA-particles. For soluble Fn, the RGD motif was important for adhesion to and invasion of cells by FnBPA-particles. The synergy site was, however, important for adhesion but not invasion. Additionally, Fn 70 kDa but not Fn 30 kDa promoted invasion, suggesting a key role for the gelatin-binding domain in Fn RGD-independent invasion. In sharp contrast, the organization of Fn into fibrils reduced overall invasion and, under these conditions, neither the RGD motif nor the synergy site were important for adhesion to and invasion of cells by FnBPA-particles. Thus, we demonstrate important roles for the central cell-binding domain and the maturation state of Fn in the infection mechanism of *S. aureus*.

To further analyze the connection of mutant Fns to the integrin-linked cytoskeleton, the cell surface motility and adhesive structures formed by bacteria coated with different Fns were compared. Bacteria coated with either RGD-mutated Fn, synergy site-mutated Fn or Fn 70 kDa showed a reduced displacement and less direct transport on the cell surface. In addition, when the RGD motif was mutated, proteins important for integrin-dependent signaling and the linkage of integrins to the cytoskeleton were not recruited. These experiments show that defects in the central cell-binding domain of Fn impair the connection of integrins to the actin cytoskeleton.

The results presented here further our understanding of the mechanisms by which *S. aureus* infect the host.

B. Introduction

Infectious diseases are responsible for 15 million (26 %) of 57 million annual deaths per year (Morens et al. 2008). Through inadequate antibiotic therapy, bad healthcare management and insufficient hygiene in industrialized countries, a growing number of multi-resistant bacteria is reported worldwide, causing life threatening infections, which become more and more difficult to treat.

In community-acquired, hospital-acquired and healthcare-associated bacteremia, *Staphylococcus aureus* is one of the leading pathogens (Kern 2010). Staphylococci generally have a benign or symbiotic relationship with their hosts if they reside in the skin or mucosa, but if they gain access to deeper host tissues, they can become a life-threatening pathogen, causing severe diseases of the skin, the blood stream, and the whole organism. Invasion into deeper skin tissues or the blood stream often occurs during surgery or by the use of catheters (Bearman et al. 2005). For the invasion and infection process *S. aureus* harbors a plethora of virulence factors, e.g. adhesins, toxins and enzymes. More than 20 surface adhesins mediate binding to host cell ligands, often extracellular matrix (ECM) molecules. A well-known and important interaction is the binding of the bacteria to the ECM glycoprotein fibronectin (Fn). To date, six adhesins in *S. aureus* are known to bind to Fn, namely FnBPA, FnBPB, Eap, Emb, Ebh and Aaa/Sle1 (Henderson et al. 2010). The interaction of fibronectin binding protein A (FnBPA) with Fn has been shown to be sufficient to promote invasion into the host cells (Sinha et al. 1999; Dziewanowska et al. 1999; Sinha et al. 2000; Heying et al. 2007; Edwards et al. 2010; Heying et al. 2009; Piroth et al. 2008; A. Schröder et al. 2006; Que et al. 2005), demonstrating its significance in the process of staphylococcal infections.

Targeting Fn by bacterial Fn binding proteins is a key step in pathogenesis of a number of different gram-positive and gram-negative pathogens (Henderson et al. 2010), but the detailed molecular mechanisms, such the exact Fn modules involved, are not known.

1. *Staphylococcus aureus*

1.1. Classification

Staphylococcus aureus belongs to the family *Staphylococcaceae* of the broad *Bacillus-Lactobacillus-Streptococcus* cluster. Staphylococci are gram-positive and typically uncapsulated bacteria, 0.5-1.5 µm in diameter and occur singly or in pairs, tetrads, short chains or irregular "grape-like" clusters, the last being the origin for the name "*staphylococcus*" from the greek *staphylé*, a "bunch of grapes". The genus *Staphylococcus*

contains 32 species, 16 of which are found in humans. Most species are facultative anaerobes, nonmotile and unable to form spores. As their natural habitat, members of the *S. epidermidis* group ubiquitously colonize the skin and mucosa, but only a few of them are pathogenic under predisposing circumstances such as immunosuppression or by the introduction of foreign body implants.

The most virulent species, *S. aureus*, which is coagulase-positive and capsulated, is preferentially resident in the anterior nares and has a prevalence of 10 to 40 % in the human population. Nasal persistence is a problem especially with multi-resistant *S. aureus* (MRSA), which often resist most available antibiotics and have the propensity to spread in the community, but even more importantly in the hospital. Persistence has also been associated with an altered phenotype of so-called small colony variants (SCVs) (Proctor et al. 2006). SCVs persist intracellularly and show a different expression pattern of virulence factors and a reduced inflammatory response of the host (Tuchscherr et al. 2010).

In humans, *S. aureus* can cause local skin infections, like boils, cellulitis and impetigo, and severe diseases, such as bacteremia, pneumonia, meningitis, scalded skin syndrome, toxic shock syndrome and acute endocarditis. The overall case fatality of *S. aureus* bacteremia has been in the range of 20-30 % in the last years (Kern 2010).

1.2. Genome

To date, the whole genome sequences of 58 *S. aureus* strains in the public domain have a total size ranging from 2.7-3 Mbp (McCarthy et al. 2010), coding for 2,600-2,700 proteins. The genome consists of three different components: the core set of genes (found in 95 % or more of all strains), the auxiliary genes (found in the range of 1-95 % of all strains) and the foreign or lost genes (found in less than 1 % of all strains) (Lan et al. 2000). The core genome encodes proteins involved in processes vital to cell survival, such as metabolism, DNA and RNA synthesis and replication. The auxiliary genes cause the diversity within the species and mostly contain mobile genetic elements (MGE), including plasmids, transposons, insertion sequences, bacteriophages, pathogenicity islands and staphylococcal cassette chromosomes (Malachowa et al. 2010). Although MGEs comprise only ~25 % of the staphylococcal genome (Lindsay et al. 2004), they encode for many antibiotic determinants and virulence factors, such as toxins, enzymes and adhesins. MGEs are transferred through horizontal and vertical gene transfer and lead to selective advantage by providing a high adaptivity to the environment. This would also explain the relatively high clonality of *S. aureus* isolates found in hospitals (Lindsay 2010).

1.3. Cell wall and capsule

The gram-positive cell wall is an important target structure for antimicrobial drugs, e.g. β-lactames, which bind to and inhibit the enzymes that control peptidoglycan synthesis.

Peptidoglycan is the major component of the gram-positive cell wall, comprising ~50 % of the net weight (Lowy 1998) and consisting of alternating polysaccharide subunits of *N*-acetylglucosamine and *N*-acetylmuramic acid with 1,4-β linkages. Specific for *S. aureus*, a tetra- and pentapeptide is linked to the lactyl moiety of the glycan chains, two of which are cross-bridged by a pentaglycine chain, generating a three-dimensional network that surrounds the cell (Navarre et al. 1999). Cell wall assembly is catalyzed by penicillin-binding proteins (PBPs), which are common targets of antibiotics. In their penicillin-resistant forms, like the PBP2a of MRSA strains, they can cause antibiotic resistance.

The second biggest constituent of the cell wall are teichoic acids. Wall teichoic acids (WTA) are composed of polyribitol-phosphate polymers cross-linked to *N*-acetylmuramic acid residues of the peptidoglycan and decorated with D-alanine and *N*-acetylglucosamine residues (Navarre et al. 1999). The plasma membrane-bound counterparts are lipoteichoic acids (LTA) that contain polyglycerol phosphate and are linked to a diacylglycerol moiety that serves as a plasma membrane anchor. WTAs and LTAs are known to protect against cell damage, control the protein machineries of the cell envelope and mediate interactions with host cell receptors and biomaterials (Xia et al. 2010). Teichoic acids and enzymes responsible for their biosynthesis are also promising targets for vaccine design and antibacterial therapeutics.

Polysaccharide capsules are modified in more than 90 % of clinical *S. aureus* isolates, with additions consisting of various sugars including mannose and fucose. They are thought to hide immunogenic components of the cell wall, serving as an antiphagocytic constituent. Expression of serotype 5 or serotype 8 capsule is associated with increased virulence in animal infection models (Foster 2009). Thus, they are also promising targets for vaccination. However, to date no vaccine has been consistently successful (Bronze et al. 2010).

1.4. Surface adhesins

Surface proteins of gram-positive pathogens are widely assumed to interact with eukaryotic proteins as a means to establish residence in unique locations or to evade the immune system (Navarre et al. 1999). The primary sequence of these surface proteins is conserved, sharing an N-terminal signal peptide required for Sec-dependent secretion and a C-terminal sorting signal, containing the highly conserved LPXTG motif that is important for sortase-dependent cell wall anchoring. Sortase catalyzes a transpeptidation reaction and a model of *S. aureus*

SrtA sortase binding and catalysis of protein A LPETG motif has recently been published (Suree et al. 2009). More than 20 LPXTG-containing proteins are known in *S. aureus* and implicated in adhesion to host extracellular ligands (McCarthy et al. 2010; Roche et al. 2003), an important step in the pathogenesis. These adhesins belong to the group of "microbial surface components recognizing adhesive matrix molecules" (MSCRAMMs) and are mostly common in bacteria that do not have pili to attach to host cell extracellular matrix molecules, like Fn, fibrinogen, collagen, vitronectin or laminin (Patti et al. 1994). Many MSCRAMMs are able to bind to more than one substrate, which leads to host cell matrix molecules having more than one bacterial ligand. The same holds true for host cells, which can have, for example, more than one integrin receptor for the matrix ligand Fn (see in detail chapter 1.8).

1.5. Fn binding protein

Bacterial Fn binding proteins (FnBPs) are widely spread among pathogenic bacteria and to date more than 100 FnBPs have been identified (Henderson et al. 2010). Not only gram-positive bacteria, but also gram-negative bacteria can express FnBPs, e.g. BBK32 from *Borrelia burgdorferi*, OpaA from *Neisseria gonorrhoeae* or YadA from *Yersinia pseudotuberculosis*. In gram-positive bacteria, most knowledge about FnBPs has derived from studies of *Streptococcus pyogenes* and *S. aureus* and the family of MSCRAMMs which is only a subgroup of FnBPs. The group termed "secretable expanded repertoire adhesive molecules" (SERAMs) contains non-membrane-bound FnBPs, e.g. *S. aureus* extracellular adherence protein (Eap) or ECM protein-binding protein (Emp).

The first report of *S. aureus* binding to Fn was published in 1978 (Kuusela 1978) and only a few years later the responsible FnBP could be isolated (Espersen et al. 1982). In 1987, Flock *et al.* cloned the gene and functionally expressed it in *E. coli*, designating it as *fnb* (Flock et al. 1987). It is chromosomally encoded, but downstream of the isolated gene another gene with strong identity could be isolated, so the genes were named *fnbA* and *fnbB*, respectively (Jönsson et al. 1991).

FnBPA (Figure 1) is a protein of 106 kDa and contains the N-terminal export signal and C-terminal LPXTG motif typical for MSCRAMMs. The N-terminal A region is the most variable region, sharing only 45 % identity with FnBPB (Jönsson et al. 1991), and spans almost the first half of the protein. Two immunoglobulin-like domains in the C-terminal region of the A domain are known to bind elastin and fibrinogen, but not Fn (Loughman et al. 2008; Wann et al. 2000). The A domain is followed by the Fn binding region, consisting of 11 repetitive elements, each of which is ~40 residues in length and able to bind to Fn with

different affinities through a tandem β-zipper (Bingham et al. 2008; Ingham et al. 2004; Meenan et al. 2007; Schwarz-Linek et al. 2003). After a proline-rich region (PRR), the cell wall-anchoring (W) and membrane-spanning domain (M), including the LPETG motif, make the rest of the protein. This second half of the protein is highly conserved and 94 % identical to FnBPB, which has only 10 Fn binding repeats (FnBR).

Besides a role in binding to Fn, it could be recently shown that *S. aureus* FnBPA and FnBPB promote biofilm formation in clinical MRSA isolates (O'Neill et al. 2008).

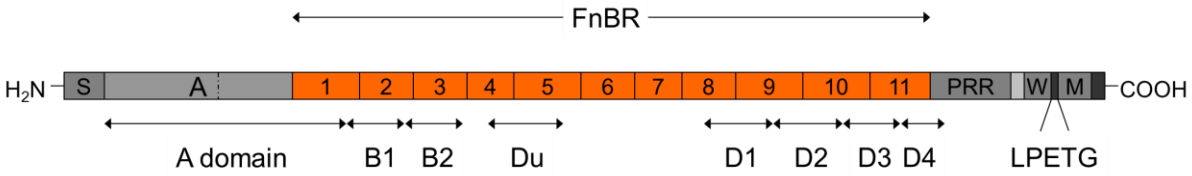

Figure 1: Domain structure of Fn binding protein A (FnBPA) from *Staphylococcus aureus*
In the current model, FnBPA is comprised of a signal peptide (S), the A domain (A), 11 Fn binding repeats with varying affinities for Fn (FnBR 1-11), a proline-rich region (PRR), the cell wall-anchoring domain (W), the LPETG domain and a membrane-spanning domain (M). The old nomenclature is given below (A domain, B1-B2, Du and D1-D4). (Meenan et al. 2007 with modifications)

1.6. Extracellular matrix

In metazoa, every cell will have close contact with the extracellular matrix (ECM), for instance, as stem or progenitor cells or during cell migration and development (Hynes 2009). In tissues, two major forms of ECM are visible, the interstitial matrix and the basement membrane. The interstitial matrix or stroma is a fibrous porous network surrounding the cells and composed of threadlike fibrils, whereas the basement membrane or basal lamina has a sheet-like structure that serves as a platform for cells and boundary between tissue compartments (Singh et al. 2010). Besides its role in providing structural support for cells and tissues, the extracellular matrix has even more functions, such as vital roles in determination, differentiation, proliferation, survival, polarity and migration of cells, in regulation, by its mechanical properties of stiffness and deformability and as a reservoir for growth factors and fluids (Hynes 2009). In vertebrates, there are hundreds of ECM proteins encoded in the genome, from ancient genes, such as some collagens, to genes evolved more recently, like Fn. The major components of the ECM are collagens, proteoglycans and glycoproteins. Most of the ECM proteins are organized in fibrils and have complex domain structures with multiple individually folded domains. Although many proteins are ubiquitously expressed, the functions of only some of them are well understood.

1.7. Fibronectin

A major component of the extracellular matrix is fibronectin (Fn; Figure 2). This highly glycosylated ~250 kDa protein is expressed and secreted as a dimer, linked by two antiparallel disulfide bonds in the N-terminal region. Fn is a modular protein composed of type I, -II and -III repeating units. It exists in two forms: a soluble form, mainly found in the blood plasma (at ~300 µg/ml) and secreted by hepatocytes and an insoluble form, expressed, secreted and organized by a range of cells into fibrils of the extracellular matrix (Hynes 1990; Pankov et al. 2002; Mao et al. 2005). The additional repeats EIIIA and EIIIB are almost exclusively found in cellular Fn (Figure 2).

Generated by alternative splicing of the single ~8 kbp mRNA transcript, Fn exists in multiple isoforms: 12 isoforms in rodents and 20 isoforms in humans. Alternative splicing occurs by exon skipping at EIIIA and EIIIB and by exon subdivision at the IIICS unit, meaning that it is mainly the cellular Fns that have a more heterogeneous group of isoforms (Ffrench-Constant 1995; Schwarzbauer 1991).

Two intramolecular disulfide bonds within each of the 12 type I and 2 type II modules stabilize the folded structure of the protein. The 15-17 type III modules are seven-stranded β-barrel structures that lack disulfide bonds (Jennifer R Potts et al. 1994). All three types of repeats are also found in other molecules, encoded by single exons and highly similar among different species rather than similar between a given type in a single molecule. This suggests that exon shuffling has been important in the evolution of Fn (Patel et al. 1987).

The domains of Fn have different bindings sites for fibrin, collagen, gelatin, heparin, integrins, syndecans, bacterial proteins and Fn itself. Proteolytic processing of Fn has helped locate some of the responsible binding sites that are still accessible after proteolysis. The diverse binding capabilities relate to Fn's important role in cell adhesion, migration, growth, differentiation and infection, as demonstrated by the early embryonic lethality of Fn knockout mice (George et al. 1993; Hynes 1990; Pankov et al. 2002).

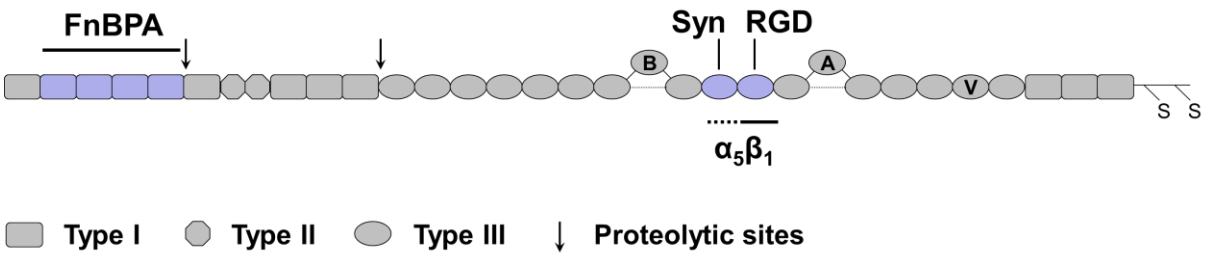

Figure 2: Domain structure of a single Fn strand
Fn is composed of 12 type I, 2 type II and 15 (plasma Fn) and 17 (cellular Fn) type III modules, respectively. Cellular Fn harbors the extra type III domains EDA and EDB and the variable region (V). An N-terminal disulfide-bridge links the ~250 kDa monomer to a ~500 kDa dimer. Fn type I(2-5) repeats contain a binding site for *S. aureus* adhesin FnBPA. The synergy site (Syn) is located in type III(9), and the RGD motif (RGD) in type

III(10) and together these mediate high affinity binding of cellular Fn integrin receptor α5β1. Proteases such as cathepsin D and trypsin cleave the molecule at specific sites. (R. Pankov 2002 with modifications)

1.8. Central cell-binding domain of Fn

The main site in Fn with which cells interact is located in the tenth type III repeat Fn III(10). It contains a sequence Arg-Gly-Asp, commonly termed as the RGD motif. This motif is not unique to Fn, but present in many other ECM molecules, such as vitronectin, laminins and collagens (Pierschbacher et al. 1984). Eight out of 24 integrin receptors are able to recognize the RGD motif, but only the α5β1 integrin receptor binds with high affinity to the central cell-binding domain, displaying a K_d in the nanomolar range (Takagi et al. 2003). The importance of this motif for development was demonstrated in mice carrying a homozygous RGD>RGE mutation. These mice die at embryonic day 10 with a shortened posterior trunk and severe vascular defects, a phenotype similar to α5 integrin-deficient mice (Yang et al. 1993; Takahashi et al. 2007). However, the RGD motif is not crucial for Fn assembly, because RGD-independent formation of Fn fibrils has been reported in many studies (Sechler et al. 1996; Sechler et al. 2000; Sottile et al. 2000; Takahashi et al. 2007; Wennerberg et al. 1996).

A second motif located in the ninth type III repeat Fn III(9) is PHSRN (in humans) or PPSRN (in mice), the so-called synergy site (Aota et al. 1994). Only α5β1 is able to recognize this site and because of this it is believed to define the specificity for the receptor. Whether integrins directly interact with this domain or not is still a matter of debate (Takagi et al. 2003; Friedland et al. 2009).

Mutational analyses of the synergy site demonstrated the important role of the proline and four arginine residues, three of which are upstream of the PHSRN region (Takagi et al. 2003; Sechler et al. 1997; S. D. Redick et al. 2000). An R1379A mutation in the PHSRN sequence resulted in an 11-fold decrease in the affinity of α5β1 to Fn III(7-10) fragment, and the triple mutant R1374A/P1376A/R1379A decreased the affinity by 45-fold (Takagi et al. 2003). Accordingly, the assembly of synergy-site mutated rat Fn [Fn(syn-)] was drastically decreased by α5-transfected CHO cells, whereas high affinity-locked α5β1 and αVβ3 were still able to assemble Fn(syn-) (Sechler et al. 1997).

1.9. Fn-FnBPA interaction

FnBPA binds to the Fn type I repeats 2-5 (Figure 3). As recently revealed by crystal structures (Bingham et al. 2008), there it forms antiparallel β-strands along the triple-stranded β-sheets of Fn I(2-5), a so-called tandem β-zipper mechanism similar to that of the Fn-gelatin

interaction. This binding-mechanism is not unique to *S. aureus*, as FnBPs of several *Streptococcus* species also bind through a tandem β-zipper to Fn (Schwarz-Linek et al. 2003; Henderson et al. 2010). Stretching the Fn molecule, and thus partially unfolding and increasing the intermodular distance of Fn type I repeats, is able to disrupt the Fn-FnBPA interaction (Diao et al. 2010; Chabria et al. 2010). The relatively small binding repeats (FnBR) of *S. aureus* FnBP (~ 40 residues) can bind a single Fn molecule with varying affinities (Ingham et al. 2004; Meenan et al. 2007). Because a single FnBPA molecule harbors 11 FnBRs, it is hypothesized that a single FnBPA molecule is able to bind multiple Fn molecules, leading to integrin clustering and uptake into host cells (Bingham et al. 2008). However, it has recently been shown that even a single high-affinity FnBR is able to mediate uptake into endothelial cells, depending on the surface density of the expressed FnBR though (Heying et al. 2009; Edwards et al. 2010).

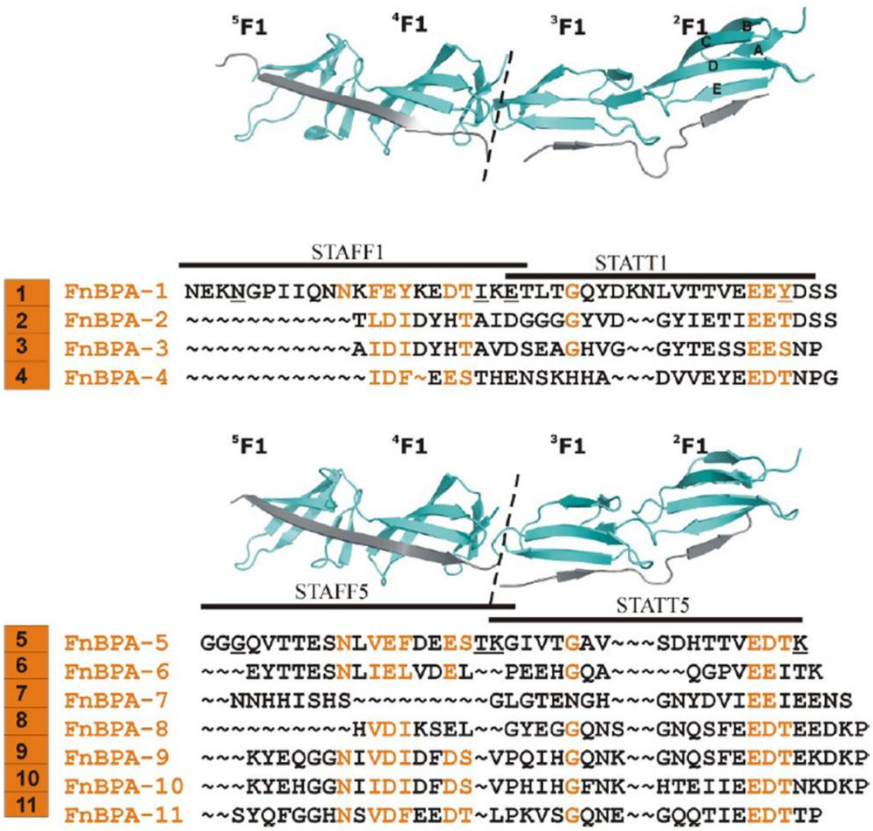

Figure 3: Crystal structures of FnBPA subdomains with Fn N-terminal domain.
X-ray diffraction data from protein crystals were achieved for synthetic peptides of Fn binding repeats (FnBR) 1 and 5 (STAFF1/STATT1, STAFF5/STATT5) from *S. aureus* FnBPA in complex with Fn I(2-3) and Fn I(4-5), respectively. FnBPA forms an antiparallel β-strand (gray) along strand E of the three antiparallel CDE-strands from Fn I (cyan), a so-called tandem β-zipper. The sequence alignment shows the 11 FnBR highlights residues that are conserved between FnBRs and participate in the interaction with Fn I. (Bingham et al. 2008 with modifications)

1.10. Assembly of Fn

The assembly of Fn into fibrils is a cell-mediated process and essential for life (George et al. 1993; McDonald 1988). Fn extracellular matrix is seen as linear and branched networks that connect cells to the substratum and to neighboring cells, the insoluble fibrils ranging in the size from 5 nm to more than 25 nm in diameter (L. B. Chen et al. 1978). These thin fibrils can cluster together to thicker bundles, up to 1 µm in diameter and are easily visible by immunological stainings and even by normal light microscopy.

In solution, Fn is present as a compact dimer that does not form fibrils *per se*, even at extremely high concentrations. This is important, as uncontrolled fibril formation in the blood would have life-threatening consequences, e.g. clot formation (Singh et al. 2010). Intramolecular self-interaction sites in the molecule are responsible for this conformation. For example, Fn III(2-3) can bind Fn III(12-14), thereby stabilizing the compact conformation (K. J. Johnson et al. 1999). Other intramolecular interactions might, however, also contribute to the compact conformation (Mao et al. 2005). The only cellular receptor able to bind native soluble Fn is the integrin heterodimer α5β1, known as the classical 'fibronectin receptor' (McDonald et al. 1987). This receptor specifically recognizes the Arg-Gly-Asp (RGD) motif in Fn III(10), with the neighbouring synergy site (PHSRN) in Fn III(9) enhancing the binding affinity. Upon binding to the receptor, intracellular proteins are recruited to integrin cytoplasmic domains and connect them to the actin cytoskeleton. Downstream signaling leads to increased actomyosin contractility, which induces integrin clustering and changes in the conformation of Fn. Firstly, end-to-end association of Fn dimers is mediated by the N-terminal 70 kDa assembly domain Fn I(1-9). Secondly, cryptic self-association sites in the Fn molecule are exposed, e.g. in Fn III(1), and free for interacting with other Fn binding sites in Fn III(1-2), Fn III(4-5) and Fn III(12-14). Straightening of the zig-zag-like ordered type III repeats (Erickson 2002) and partial unfolding of type III repeats are hypothesized to also contribute to the homophilic interactions (Mao et al. 2005; Singh et al. 2010; Ingham et al. 1997). For this process, the RGD motif is dispensable, because a recombinant Fn lacking the RGD motif is co-assembled in existing fibrils (Sechler et al. 1996). By these intramolecular interactions, Fn fibrils are formed and, during growth, are converted into a deoxycholate/detergent insoluble matrix (McKeown-Longo et al. 1983). To provide tissues with stability, rigidity and shape, insolubility is a critical property.

Irrespective of α5β1 binding to soluble Fn, at least 11 different integrin pairs are known to bind Fn, and 4 of them, namely α5β1, αVβ3, α4β1 and αIIbβ3, are able to trigger Fn fibril formation *in vitro* (Plow et al. 2000; Leiss et al. 2008). Additionally, non-integrin cell surface

receptors, i.e. syndecans-1/-2/-4, are implicated in Fn fibrillogenesis (Klass et al. 2000; Saoncella et al. 2007; Stepp et al. 2010). However, an *in vivo* relevance for α5β1-independent fibrillogenesis is still unclear.

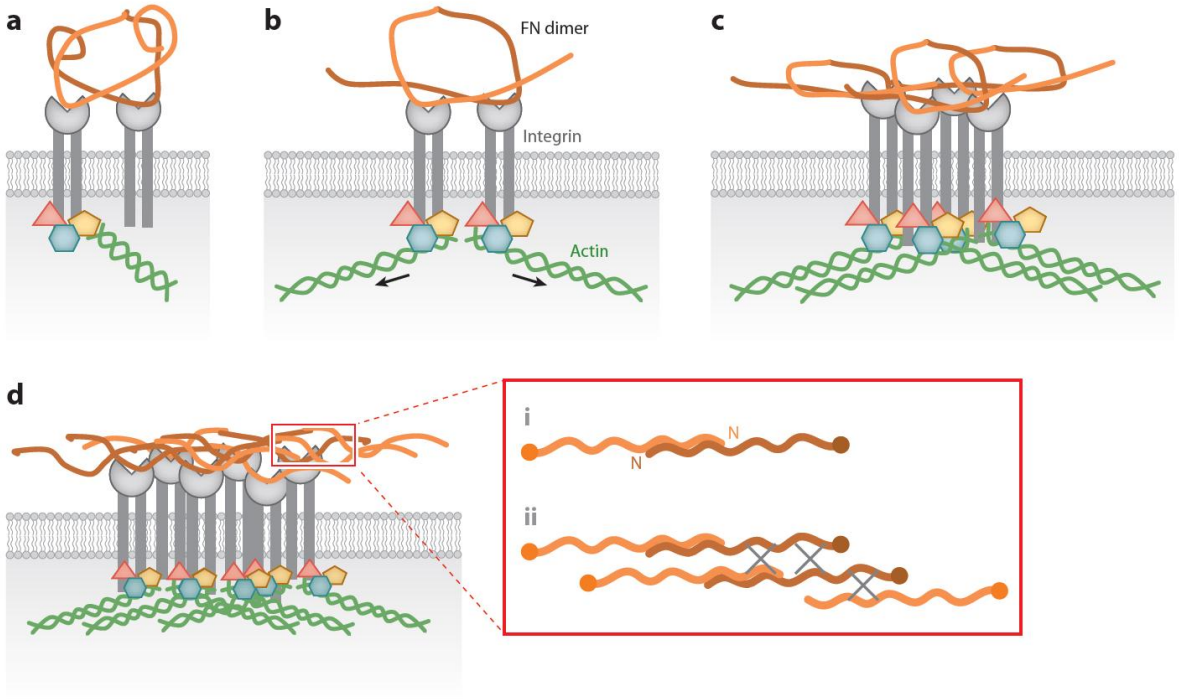

Figure 4: Assembly of Fn into fibrils
Several steps are involved in Fn fibrillogenesis. **(a)** A compact soluble Fn dimer (light and dark orange) binds to α5β1 integrins on the cell surface. **(b)** Intracellular signaling and adaptor proteins such as talin, FAK, src and paxillin, connect integrins to the actin cytoskeleton (green), leading to actomyosin contractility and exposure of cryptic self-association sites in Fn. **(c)** Integrin clustering activates signaling molecules including RhoGTPases, Ras/MAPK, and allows direct Fn-Fn interactions as well as further conformational changes in Fn. **(d)** Detergent insoluble Fn fibrils are formed through Fn self-interaction (gray crosses, highlighted in the red insert), by **(i)** end-to-end association of the N-terminal assembly domain, followed by **(ii)** lateral interactions, involving binding sites in Fn III(1-2), Fn III(4-5) and Fn III(12-14). (Singh et al. 2010)

2. Cell-matrix interactions

The interaction of cells with the extracellular matrix induces discrete plasma membrane-associated structures termed cell-matrix adhesions. They can be subdivided by size and molecular composition into so-called nascent adhesions (<0.25 µm), focal complexes (0.5 µm), focal adhesions (1-5 µm), fibrillar adhesions (>5 µm) and 3D-matrix adhesions (>5 µm) (Gardel et al. 2010; Berrier et al. 2007; Zamir et al. 2001). Supermature focal adhesions (10-30 µm) can be found in myofibroblasts under high stress conditions and show a molecular composition between classical focal and fibrillar adhesions (Hinz et al. 2003). Another type of adhesion structures are podosomes (0.5µm), mainly found in monocyte-derived cells such as

macrophages, dendritic cells and osteoclasts, but also other cells like smooth muscle cells and transformed fibroblasts (Linder 2003).

Adhesion receptors, mainly integrins that lack intrinsic enzymatic activity, bind signaling proteins via their cytoplasmic tails (Hynes 2002). They recruit different subsets of molecules: (1) integrin binding proteins, such as talin, kindlin or tensin, which regulate integrin activation and signaling, (2) adaptor/scaffolding proteins, e.g. vinculin, paxillin or α-actinin, which link integrin-associated proteins with the cytoskeleton or other proteins, and (3) enzymes, i.e. tyrosine kinases (src, FAK, Csk), serine/threonine kinases (ILK, PKC), lipid kinases (PI3 kinase), tyrosine phosphatases (SHP-2, RPTPα), modulators of small GTPases (ASAP1, Graf, PSGAP) and other proteins, like proteases (calpain II).

The large group of proteins involved in the complex interplay between the mechanical role of cell adhesions and the activation of a variety of signaling networks is termed the 'integrin adhesome', with 180 components known to date and at least 742 direct interactions (Zaidel-Bar et al. 2010; Zaidel-Bar, Itzkovitz, et al. 2007).

2.1. Focal adhesions

Focal adhesions are flat, elongated structures in the periphery of cells that mediate strong adhesion to substrates (Sastry et al. 2000; Abercrombie et al. 1975; Zamir et al. 2001). Intracellularly, they anchor bundles of actin microfilaments through a set of proteins, with typical marker proteins being αVβ3 integrin, paxillin, vinculin, α-actinin, talin, FAK and tyrosine phosphorylated proteins. It is believed that small integrin microclusters that diffuse in the plasma membrane initiate focal adhesions (Wiseman et al. 2004). Activated integrins bind to ECM molecules, where they are readily immobilized and either disassemble or interact with F-actin via adaptor proteins paxillin and talin. α-actinin bundling of F-actin in these nascent adhesions, together with myosin II-mediated retrograde actin flow, forms a link between integrins and the actin cytoskeleton. This process is controlled by Rac and CDC42 and forms focal complexes. The resulting tension leads to zyxin and vinculin recruitment, growth of actomyosin filaments and adhesions along the stress fibers. The small GTPase RhoA stimulates actomyosin driven contractility, by which focal complexes mature into focal adhesions (Gardel et al. 2010; Benjamin Geiger et al. 2001). Recently, this complex architecture could be resolved at nanometer resolution using super-resolution iPALM microscopy (Kanchanawong et al. 2010). Although focal adhesions are mainly found in cells grown on two-dimensional rigid substrates, they also exist *in vivo* (Romer et al. 2006).

2.2. Fibrillar adhesions

Fibrillar adhesions are thought to be the site of Fn matrix assembly. These dot-line or elongated structures are located more centrally in the cell and co-stain with Fn. They are positive for α5β1 integrin, tensin, paxillin and thin actin cables, but negative for phosphotyrosine and do not associate with stress fibers (Zaidel-Bar, Milo, et al. 2007; Katz et al. 2000; Zamir et al. 1999). Like focal adhesions, fibrillar adhesions also develop out of focal complexes. After binding of α5β1 to Fn in focal complexes, the integrin is connected to the cytoskeleton. In contrast to ECM proteins in focal adhesions, like vitronectin, Fn is a more flexible rather than rigid substrate, so that upon actomyosin-dependent tension, the α5β1-Fn complex translocates centripetally from focal complexes to fibrillar adhesions (Pankov et al. 2000; Benjamin Geiger et al. 2001). This translocation stretches the Fn molecule and exposes cryptic sites important for fibril formation (see chapter 1.10) (Singh et al. 2010). It could be shown that the tyrosine-dephosphorylation of paxillin is a prerequisite for the formation of fibrillar adhesions, because it promotes the recruitment of tensin (Zamir et al. 1999; Zaidel-Bar, Milo, et al. 2007). The important role of tensin in this process could be shown by expressing a dominant-negative fragment of chicken tensin containing the actin-homology 2 region fused to GFP (GFP-AH2) in human foreskin fibroblasts. In doing so, tensin remained in focal adhesions and inhibited Fn fibril formation. Blocking actomyosin contractility with pharmacological inhibitors H-7, cytochalasin-D or jasplakinolide also prevents fibrillar adhesion formation and Fn fibrillogenesis (Pankov et al. 2000; Zamir et al. 1999).
Fibrillar adhesion-like structures are also detectable at bacterial attachment sites during FnBPA-mediated infections of endothelial cells. Blocking actomyosin contractility and tensin activity with GFP-AH2 could also block the centripetal translocation of *FnBPA-S. carnosus* from peripheral attachment sites (A. Schröder et al. 2006).

2.3. Cell migration and mechanotransduction

From simple, uni-cellular organisms to complex multi-cellular organisms, cell migration is a fundamental process vital for mating, searching for food (for example, for amoeba) and tissue organization, organogenesis and homeostasis (for higher eukaryotes) (Vicente-Manzanares et al. 2005). The key-steps in cell-migration are: polarization of cells (e.g. by chemotactic stimuli, mechanical forces, substrate composition/topography), membrane extension by protrusion and adhesion and cell-body translocation, adhesion disassembly and rear retraction (Vicente-Manzanares et al. 2009; Parsons et al. 2010). Much is known from fibroblast-like

migration, where polarized cells form a leading edge (migration-front) and a trailing edge (migration-back). The leading edge is composed of actin filament-containing filopodia, the lamellipodium, consisting of highly-branched actin filaments and nascent adhesions, a transition zone, where nascent adhesions either disassemble or develop into focal complexes, and the lamellum, displaying mature focal adhesions and α-actinin/actomyosin-containing stress-fibers (Parsons et al. 2010). In the lamellipodium, actin filaments polymerize and branch by the catalytic activity of the Arp 2/3 complex at the leading edge and depolymerize in the rear, an equilibrated process defined as 'treadmilling' (Y.-L. Wang 1985). A set of proteins (ADF, profilin and capping proteins) is known to accelerate the treadmilling rate. The rapid retrograde flow of actin filaments is caused by the resistance of the plasma membrane, which is sufficient to withstand the weak protrusion force of filaments during assembly. In the lamellum, the retrograde flow of actin stress fibers is slower and mediated by the contraction of myosin II, which moves antiparallel actin strands past each other and bundles actin filaments. The interaction of adhesion-containing integrins with the centripetally flowing actin cytoskeleton is what drives cell migration (Le Clainche et al. 2008; Parsons et al. 2010). A proposed model of how this interaction mediates cell movement is the 'molecular clutch' concept (Giannone et al. 2009; Mitchison et al. 1988). Upon engagement of the clutch, cytosolic adaptor proteins such as vinculin, talin, zyxin and α-actinin connect integrin tails to the rearward flowing actin fibers. This physical link results in cell protrusions based on the forward polymerization of F-actin and traction of the cell body based on actomyosin contractility. Clutch engagement is dependent on the activation state of integrins (inside-out signaling, see chapter 3.1) as well as substrate-dependent downstream integrin-signaling (outside-in signaling, see chapter 3.2). For example, talin and vinculin act as mechanosensors by sensing the forces transmitted through integrins. Conformational switches in these molecules expose new binding-sites for other adaptor and signaling proteins, leading to integrin clustering and reinforcement of the integrin-actin linkage. This 'mechanotransduction' process is, among others, responsible for adhesion maturation and clutch engagement (J. D. Humphries et al. 2007; Giannone et al. 2009; Giannone et al. 2003; Roca-Cusachs et al. 2009; Vicente-Manzanares et al. 2009). Accordingly, partially engaged 'slipping clutches' exist during the initiation of adhesion sites at the protruding lammelipodial tip (Giannone et al. 2009).

Ligand-coated particles, for example Fn-beads or Fn-coated bacteria, have been shown to also move centripetally when attaching to the periphery of various cells, such as fibroblasts or HUVECs. This movement is coupled to the aforementioned mechanisms responsible for cell

migration, because interfering with integrin clustering, activation and signaling, adaptor binding, F-actin assembly or myosin II-contractility impaired particle transport and reinforcement of the particle-cell linkage (Cai et al. 2006; Choquet et al. 1997; Giannone et al. 2003; Nishizaka et al. 2000; Roca-Cusachs et al. 2009; A. Schröder et al. 2006; X. Zhang et al. 2008; Coussen et al. 2002).

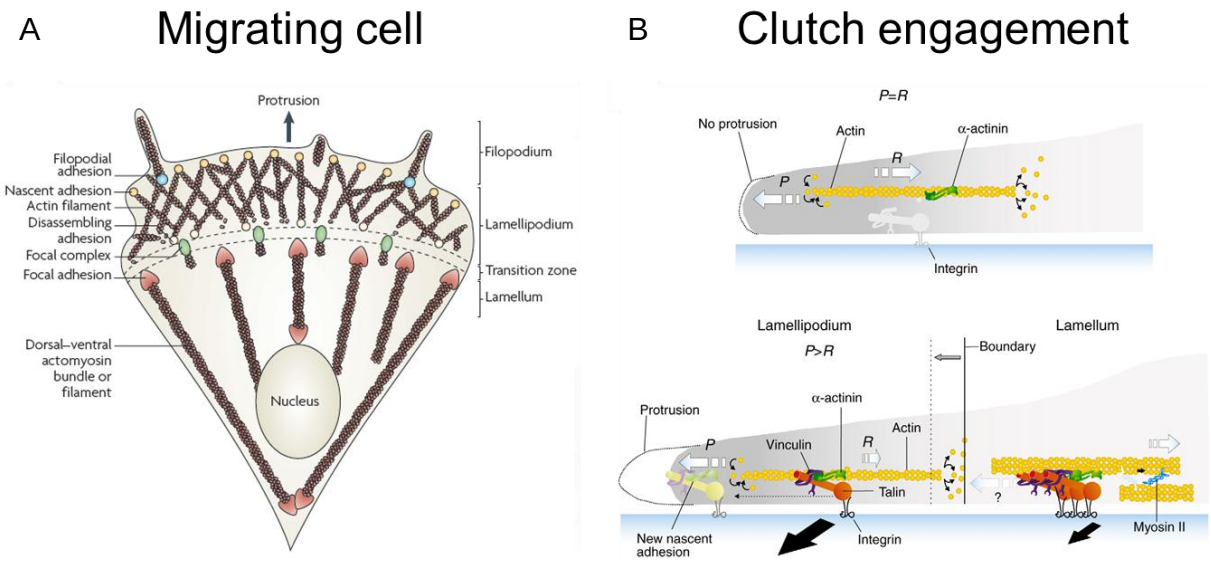

Figure 5: Structural elements and clutch engagement in a migrating cell.
(A) The leading edge of a migrating cell (filopodia and lamellipodia) contains nascent adhesions and actin filaments, which are highly branched. In the transition zone, nascent adhesions either disassemble or mature into focal complexes. Upon bundling and cross-bridging of actin filaments to stress-fibers in the lamellum, actomyosin contractility leads to elongated and stable focal adhesions. (B) Rearward actin flow in the lamellipodium is accomplished by actin polymerization and actomyosin contractility in the lamellum. Coupling of ligand-bound integrins to flowing actin filaments provides a physical link mediated by adaptor and scaffolding proteins, such as vinculin, α-actinin and talin. This engagement of the clutch results in cell protrusion and traction. (J Thomas Parsons et al. 2010; Vicente-Manzanares et al. 2009 with modifications)

3. Integrins

Integrins are transmembrane cell surface receptors expressed in all metazoans. They are heterodimers consisting of two non-covalently linked α and β subunits. In humans, there are 18 α and 8 β subunits known to form a total of 24 known receptors, which among other classifications can be grouped into subgroups based on ligand-binding properties (Hynes 2002). The subunits have large extracellular domains (~800 aa) for ligand binding, single α-helix transmembrane domains (~20 aa) and short cytoplasmic tails (13-70 aa, except for β4 [~1,000 aa]) for binding adaptor proteins or enzymes (Moser et al. 2009). Integrin receptors allow cells to adhere to the ECM or other cells and serve as a mechanical link to the actin cytoskeleton, by which they are able to permit signal transduction from the outside of the cell

to the inside and *vice versa*. Hence, they control many aspects of cell behaviour including proliferation, survival/apoptosis, differentiation, gene expression, shape, polarity and motility (Hynes 2002).

3.1. Integrin activation (inside-out signaling)

Integrin receptors exist in three conformational states: 'inactive/bent' (low affinity), 'active/extended' (high affinity), and 'ligand occupied/extended with open conformation', according to the 'switchblade' model, according to which only high affinity integrins can bind to their ligand (Askari et al. 2009; Luo et al. 2007). In the so-called 'deadbolt' model, integrin extension only occurs after binding of the ligand (Xiong et al. 2003).

Integrins interact with each other in the transmembrane region through the GXXXG motif of the α subunit, and in the cytosolic region through hydrophobic and electrostatic interactions and a salt bridge between the arginine residue within the GFKKR motif of the α subunit and the aspartate residue within the HDR(R/K)E motif of the β subunit (Gottschalk 2005; Vinogradova et al. 2002). The salt-bridge seems to maintain integrins in the low-affinity state, except for β1 integrins, where mutating Asp759 to Ala showed no defects in the activation of the integrin (Czuchra et al. 2006). To activate/stretch integrins, the subunits are thought to separate at their transmembrane and cytoplasmic regions, leading to unbending of the headpiece and resulting in an extended/activated conformation (Hughes et al. 1996; Moser et al. 2009; Takagi et al. 2001).

The mechanism by which integrins are activated involves two NPXY motifs in the cytosolic tail of the β subunit. Phosphotyrosine binding domains (PTB) recognize this motif and are found in a number of regulatory proteins, such as talins, kindlins, tensins, Shc, Dok-1 or Numb (Uhlik et al. 2005; Y.-Q. Ma et al. 2008). Among them, only talin and kindlin are known to activate integrins and act synergystically. Talin binds to the membrane proximal NPXY motif, whereas kindlin binds to the membrane distal NPXY motif. Whether they act by sequential binding, or cooperate in *cis* or *trans* is not yet clear (Moser et al. 2009). The talin head contains a FERM domain (protein 4.1, ezrin, radixin, moesin) including the PTB domain, and an extra loop of amino acids in the F3 subdomain that binds to membrane proximal sequences in the β integrin tail. The dual β integrin-binding property of the talin head domain is solely responsible for enabling the displacement of the α integrin tail and the separation of the transmembrane domains (Wegener et al. 2007).

Kindlins also contain a FERM domain but function as co-activators of integrins. Kindlin-2 alone is not sufficient to activate integrins and silencing kindlin-2 prevents talin head activating integrins (Y.-Q. Ma et al. 2008).

Integrin activation is regulated through multiple switches. Talin exists in an autoinhibitory state that propably needs to be activated through the incorporation of the lipid second messenger phosphotidylinositol-4,5-bisphosphate [PtdIns(4,5)P2] (Franco et al. 2004). Phosphorylation of the two NPXY motifs in β3 tails by src kinases inhibits binding of both talin and kindlin to their binding sites and favors binding of phosphorylation-insensitive adaptors like tensin or Dok-1 (Oxley et al. 2008; McCleverty et al. 2007; Bledzka et al. 2010). Additionally, serine/threonine phosphorylation of the sequence between the two NPXY motifs by protein kinase C (PKC) regulates binding of the actin cross-linking protein filamin and the adaptor protein 14-3-3 (Legate and Fässler 2009). Mutations in this sequence in β3 subunits are found in Glanzmann thrombasthenia disease. There, kindlin-3 cannot bind its NPXY motif and fails to activate the fibrinogen receptor αIIbβ3, which causes severe bleeding due to impaired clot formation by platelets (Moser et al. 2008). Mutating the tyrosines to unphosphorylatable phenylalanine in both NPXY motifs could be shown to decrease internalization of *S. aureus* in mouse fibroblasts (Fowler et al. 2003).

The involvement of migfilin, (Ithychanda et al. 2009), ILK (Honda et al. 2009) and FAK (Michael et al. 2009) have recently been shown to also affect integrin activation via inside-out signaling.

Integrins additionally contain binding sites for divalent cations, so-called metal ion-dependent adhesion sites (MIDAS) and adjacent to MIDAS (ADMIDAS). Binding of ions can either activate (Mn^{2+}, Mg^{2+}) or inactivate (Ca^{2+}) integrins by either changing binding affinities for the ligand or inducing conformational changes of the βA head domain (Mould et al. 2003; Xiong et al. 2002).

Finally, integrins can be activated by tensile forces (so-called catch-bonds), which are known from *E.coli* adhesin FimH-P/L-selectin- and other interactions (Sokurenko et al. 2008; Askari et al. 2009). Such catch-bonds could recently be identified for the α5β1-Fn interaction involving the synergy site (Kong et al. 2009; Friedland et al. 2009).

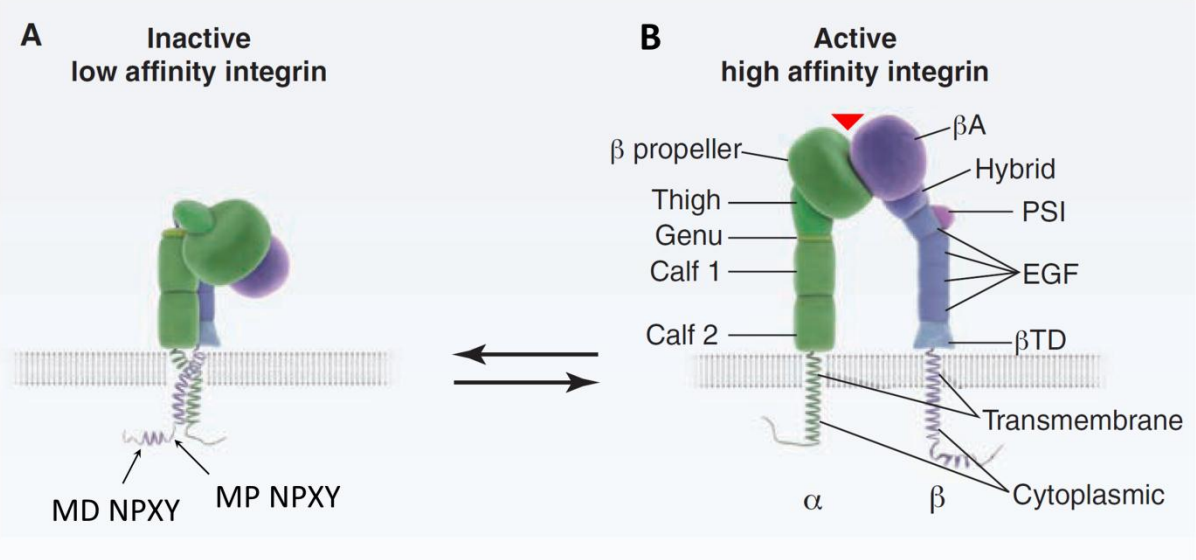

Figure 6: Structure and schematic activation of integrins
Integrins can switch between different states of activation. The inactive state (A) possesses a low-affinity for the ligand and exists in a bent conformation due to interactions in the transmembrane and cytosolic domains of the α subunit (green) and β subunit (blue). (B) During integrin activation, cytosolic adaptor proteins bind to membrane-proximal (MP, e.g. talins) and membrane-distal (MD, e.g. kindlins) NPXY motifs, leading to separation of the legs and a switch to an extended conformation. The binding of ligands (red triangle) takes place at an interface between the β propeller domain of α subunits and the βA domain of β subunits. (Moser et al. 2009 with modifications)

3.2. Outside-in signaling

Outside-in signaling through integrins is important for cell-proliferation, cell-spreading, cell-migration and mechanotransduction and can be misregulated in diseases such as cancer, or induced by pathogens during infection.

Effects that take place within minutes of integrin activation and clustering are the up-regulation of lipid kinase activity, which produces second messengers PtdIns(4,5)P2 and PtdIns(3,4,5)P3 and increases in tyrosine phosphorylation of certain substrates, like src-family kinases (SFK) and adaptor or signaling proteins such as FAK and paxillin. This is followed by changes in the actin cytoskeleton through the recruitment of additional regulatory proteins, like Rho GTPases and the Arp2/3 complex. Long-term effects (after more than 60 minutes) are mediated by MAP-kinase and other pathways and lead to changres in gene expression, which influence survival, growth and differentiation to control cell morphology.

During bacterial infection through *S. aureus*, clustering of integrins finally leads to complex remodeling of the actin cytoskeleton and bacterial uptake (Sinha et al. 1999; Agerer et al. 2003; A. Schröder et al. 2006). The precise way in which downstream signaling is transduced is not yet clear. In a first step after integrin clustering, FAK is phosphorylated and serves as a docking site for SH3 domain-containing src-family protein tyrosine kinases (PTKs). The

active src-FAK complex seems to be important during infection, because silencing either FAK or PTKs greatly reduces invasion of cells by *S. aureus* (Agerer et al. 2005; Agerer et al. 2003; Fowler et al. 2003). Active src-FAK phosphorylates substrates like cortactin, paxillin and integrins. Cortactin can directly activate the Arp2/3 complex, which mediates actin polymerization and has been shown to localize in motile attachment sites induced by *FnBPA*-*S. carnosus* (A. Schröder et al. 2006; Weaver et al. 2002). The phosphorylation of paxillin serves as a switch for focal adhesion turnover and fibrillary adhesion formation (Zaidel-Bar, Milo, et al. 2007). The phosphorylation of β integrin cytoplasmic tails at proximal and distal NPXY motifs regulates binding of adaptor proteins talin, kindlin and tensin (Oxley et al. 2008; McCleverty et al. 2007). These SH2 domain containing proteins possibly interact with Tyr-phosporylated signaling proteins such as RhoGAPs DLC-1 and DLC-3. GAPs together with GEFs regulate the activity of RhoGTPases, which also mediate actin dynamics. Accordingly, the RhoGTPases Rac and CDC42 have been shown to play a role in *S. aureus* infections of endothelial cells (A. Schröder et al. 2006).

Integrin clustering also recruits other scaffolding proteins, such as vinculin, zyxin and ILK. Recently, a vital role of the ILK-PINCH-Parvin complex could be determined in reinforcing the α5β1-actin linkage and targeting tensin to maturing adhesions (Stanchi et al. 2009). At least in epithelial cells, ILK is also known to regulate the actin cytoskeleton-remodeling activity of CDC42 and Rac and impaired ILK kinase activity results in significant reduction of *S. aureus* invasion (B. Wang et al. 2006; Filipenko et al. 2005).

Downstream from the src-FAK complex, Ras-Raf-MEK-Erk is the major pathway in integrin-related growth factor receptor signaling. *S. aureus* extracellular adherence protein Eap can block this pathway by inhibiting Erk1/2 phosphorylation, demonstrating its capability as an anti-angiogenic and anti-inflammatory agent (Sobke et al. 2006).

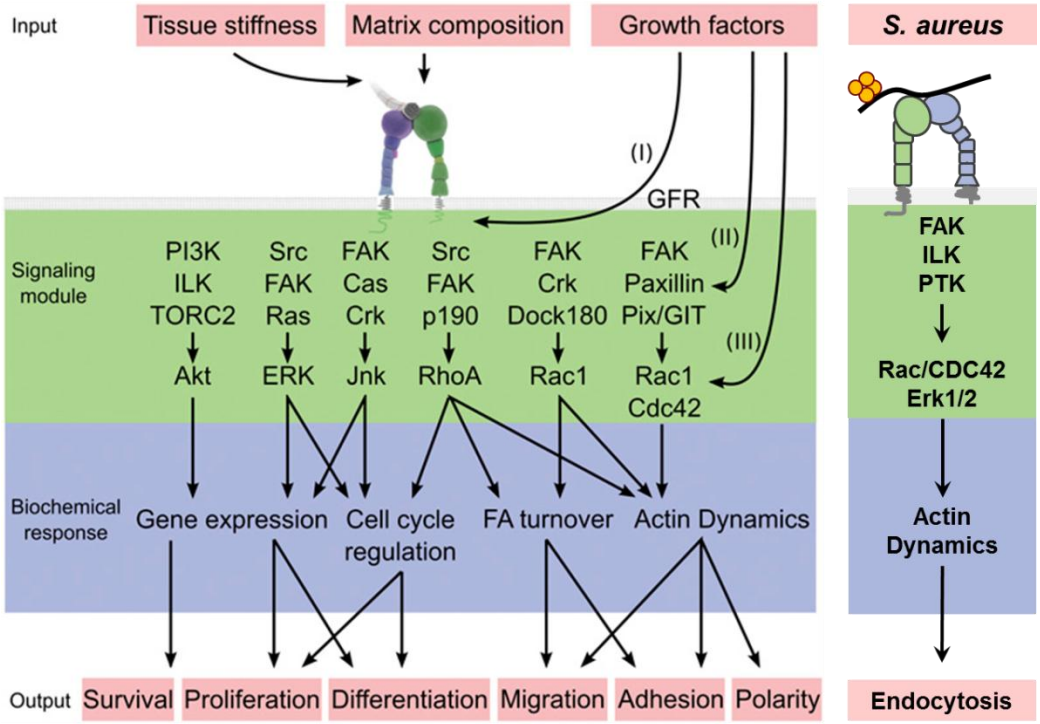

Figure 7: Integrin outside-in signaling
The composition of the extracellular matrix, its mechanical properties and growth factors are able to trigger signals from the outside to the inside of the cell. Multiple signaling pathways are activated and can influence each other as a response to extracellular factors. Downstream effectors, like RhoGTPases, control actin dynamics, focal adhesion (FA) turnover and gene expression, which have vital roles in survival, proliferation, differentiation and cell shape. (Legate, Wickström, et al. 2009 with modifications)

4. Endocytosis

The uptake of macromolecules into the cell by membrane-bound vesicles derived from the invagination and pinching-off of pieces of the membrane is a process called endocytosis. Endocytosis is an important and evolutionary historic mechanism to control processes such as hormone-mediated signal transduction, immune surveillance, antigen-presentation and cellular and organismal homeostasis. Certain molecules such as amino acids, sugars and ions can traverse the plasma membrane through the action of integral membrane protein pumps or channels. Endocytosis can be sub-divided into two broad categories: pinocytosis (the uptake of fluids and solutes) and phagocytosis (the uptake of large particles) (Conner et al. 2003). Another endocytic process called ‘entosis‘ has been described as the uptake of viable cells by another cell, forming ‘cell-in-cell’ structures (Overholtzer et al. 2007).

4.1. Pinocytosis

Depending on the size of the endocytic vesicle, the nature of the cargo and the mechanism of vesicle formation, pinocytosis occurs by different mechanisms in different kinds of cells:

macropinocytosis, clathrin-mediated endocytosis, caveolin-type endocytosis, circular dorsal ruffles, flotillin-dependent endocytosis and clathrin- and caveolin-independent (CLIC/GEEC, IL2βR, Arf6) endocytosis (Doherty et al. 2009; Conner et al. 2003).

Non-phagocytic endocytosis is used by a wide range of pathogens to enter host cells. Macropinocytosis, a growth factor-induced, actin-dependent endocytic process that leads to internalization of fluid and membrane in large vacuoles, can also be induced by larger particles, such as apoptotic bodies, necrotic cells and pathogens. Viruses known to use macropinocytosis are for example vaccinia virus, adenovirus 3, herpes simplex virus 1, human immunodeficiency virus 1, rubella virus and ebola virus (Mercer et al. 2009). Bacteria taken up through macropinocytosis are *Legionella* and *Salmonella* (Francis et al. 1993; Watarai et al. 2001).

Clathrin-mediated endocytosis (CME) is the best-characterized endocytotic pathway, implicated in the cargo of receptor tyrosine kinases, G-protein coupled receptors and toxins, among others. Clathrin forms a polymeric coat around budding membranes, which invaginate and are pinched off, aided by the large GTPase dynamin. Many viruses can be found in clathrin-coated vesicles, for example Dengue virus, hepatitis C virus, adenovirus 2/5 and influenza A virus (Mercer et al. 2010). Pathogens associated with CME are the bacteria *Listeria* (Veiga et al. 2005) and enteropathogenic *E. coli* and *S. aureus* (Veiga et al. 2007), as well as the yeast *Candida albicans* (Moreno-Ruiz et al. 2009).

Caveolae are cholesterol- and sphingolipid-rich membrane-invaginations of ~50-60 nm and can make up to 10-20 % of the endothelial surface (Conner et al. 2003). They function in transporting a wide range of molecules, such as receptors (e.g. α5β1, EGF-R, PDGF-R), signal transducers (e.g. PI3 kinase, MAP kinase, calmodulin), membrane transporters (e.g. Ca^{2+} ATPase, aquaporin-1), as well as serum and ECM proteins (e.g. Fn, albumin) (Sottile et al. 2005; F. Shi et al. 2008; W. Schubert et al. 2001; Anderson 1998). Entry of pathogens through caveolae has been mainly reported for the viruses SV40 and human papilloma virus (Mercer et al. 2010). However, very recently it could be shown that caveolin-1-deficient fibroblasts display an increased uptake of FnBPA-expressing *S. aureus* and the Fn binding protein opa50-expressing *Neisseria gonorrhaeae* compared to wild-type fibroblasts. Because caveolin-1 limits microdomain mobility, the authors speculate that caveolin-1 might contribute to integrin-meadiated uptake of particles in general (Hoffmann et al. 2010). In the same paper, the authors could demonstrate a recruitment of flotillin-1/2 to *S. aureus* attachment sites, but without any function, as shown by RNA interference and expression of dominant-negative proteins (Hoffmann et al. 2010).

4.2. Phagocytosis

Larger particles over 0.5 µm are bound, internalized and degraded by an actin-dependent and clathrin-independent zipper-like process called phagocytosis. Phagocytosis is triggered through a range of receptors, such as Fc receptors that bind the Fc region on immunoglobulins, scavenger receptors that recognize bacterial lipopolysaccharides and lipoteichoic acids, mannose receptors and complement receptors that recognize opsonins from the complement cascade, and integrins (Underhill et al. 2002; Aderem et al. 1999). In vertebrates, professional phagocytes, e.g. macrophages, dendritic cells and neutrophils, make use of phagocytosis in adaptive and innate immunity, by removal of pathogens, and for the integrin-mediated clearance of apoptotic cells. Non-professional phagocytes, such as fibroblasts, epithelial and endothelial cells, are, however, also able to perform phagocytosis, either naturally through integrin-dependent uptake of ECM compounds, such as collagen, or *in vitro* upon transfection with phagocytic receptors (Underhill et al. 2002).

Many different types of phagocytosis are known and two well investigated and phenotypically different ones are type I and II phagocytosis (Caron et al. 1998; L.-A. Allen et al. 1996). Type I is mediated through Fcγ receptors and involves activation of the small RhoGTPases Rac1 and CDC42 to induce local pseudopods and membrane ruffles to engulf particles. PI3-kinase is important for its regulation, although it is not needed for binding or actin polymerization (Underhill et al. 2002). Type II is mediated through αMβ2 and needs Rap activity to become fully activated and RhoA activity to induce actin polymerization, but without major membrane protrusions. RhoA activates two effector proteins, serine/threonine kinase Rock and formin-related elongating factor mDia, to recruit and activate the Arp2/3 complex for actin remodeling (Dupuy et al. 2008).

Besides the physiological role of integrins in phagocytosis, pathogens can hijack the machinery to gain intracellular access. Mainly β1 integrins are targeted, probably due to their central role in signaling pathways that are classically used for adhesion and spreading of cells (see chapter 2 and 3). Bacteria either activate and cluster integrins directly, for example *Yersinia* spp. through the adhesin invasin (Isberg et al. 2001), or indirectly through binding to ECM molecules, in the case of *S. aureus* FnBPA or *Yersinia pseudotuberculosis* YadA binding to Fn (see chapter 1.5). Some viruses are also believed to be phagocytosed, e.g. herpes simplex virus type I, Kaposi's sarcoma-associated simplex virus or Mimivirus (Mercer et al. 2010; Dupuy et al. 2008).

5. Aim of this study

The initial step in the infection of host cells by *Staphyloccus aureus* is mediated by the attachment to host cell extracellular matrix. Recognition of fibronectin (Fn) by the cell wall-anchored fibronectin binding protein A (FnBPA) has been shown to be sufficient to allow invasion of host cells and to induce infective endocarditis.

The N-terminal 30 kDa region in Fn is the known binding domain of FnBPA, but it is not yet clear which domains in Fn are important for the uptake of bacteria by cells. To this point, it was only known that blocking the interaction of host cell integrins with Fn reduces the internalization of bacteria. It has also never been investigated, if the physical state of Fn could contribute to FnBPA-mediated infection parameters.

We employed a system that allows the detailed and unambiguous investigation of the individual domains and the polymerization state of Fn, using cells that secreted and organized either wild-type, mutated or no Fn on the cell surface and cells that expressed either wild-type, mutated or no β1 integrin, in combination with either uncoated or soluble Fn-coated FnBPA-particles. By these and other assays, we were able to address and answer the following questions:

- Which domains in Fn contribute to the FnBPA-mediated infection by *S. aureus*?
- What are the mechanisms of the interaction with different Fns?
- Can soluble and organized Fn equally well mediate adherence to and invasion of cells by FnBPA-particles?
- Does the polymerization state of Fn alter the mechanism of cell invasion?
- How do the findings fit with the virulence strategy of *S. aureus*?

Answering these questions will provide better insight into the infection mechanisms, by which FnBPA-expressing *S. aureus* can attach to and invade human cells.

C. Results

1. Investigating the role of Fn domains in *S. aureus* FnBPA-mediated cellular infection

Assays were performed to determine the role of functional domains of fibronectin (Fn) (see chapter B.1.7 in *introduction*) during fibronectin binding protein A (FnBPA)-mediated infection of cells. In such assays, endogenous Fn produced by cells could either be secreted into the growth supernatant (generating conditioned medium) or organized on the cellular surface and could therefore interfere with the interpretation of the results. Fn-deficient (FN -/-) fibroblast-like cells were therefore used for assays in which the roles of Fn and its FnBPA-binding domains in cellular infection parameters were investigated. As proof, no endogenous Fn could be detected by Western blot (Figure 9B) or indirect immunofluorescence in FN -/- cells (Figure 8, *top row*).

Two additional fibroblast-like cell lines, FN fl/fl and FN RGE/RGE, were used in these investigations, the latter bearing an inactivating Asp>Glu mutation in the central cell-binding RGD motif. These cell lines were cultured in fibronectin-free medium and expressed and secreted wild type Fn (Fn RGD) and mutated Fn (Fn RGE), respectively. When FN -/- cells were incubated for 48 h with conditioned medium from FN fl/fl cells, the Fn-deficient cells were able to bind the exogenous Fn RGD and organize into a fibrillar matrix (Figure 8, *bottom row*). This verified that cellular receptors and signaling machineries important for the interaction with Fn were still functional in FN -/- cells (see chapters B.1.10 and B.3.2 in *introduction* for details).

For certain experiments, FN -/- cells were transiently transfected with Fn-encoding plasmids (mFNwt or mFNwt_RR1495/1500AA, which contains the mutations R1495A and R1500A in the synergy site), causing them to secrete Fn RGD or Fn Syn$^-$ in the supernatant (used for coating of bacteria or beads) or to organize it on the cell surface. In Fn Syn$^-$, the synergy site in the type III(9) module is mutated and inactivated (S. D. Redick et al. 2000). The FN -/- cells were also used for organizing exogenously added proteolytic Fn fragments (Fn 30 kDa and Fn 70 kDa) and recombinant His-Fn III(7-10).

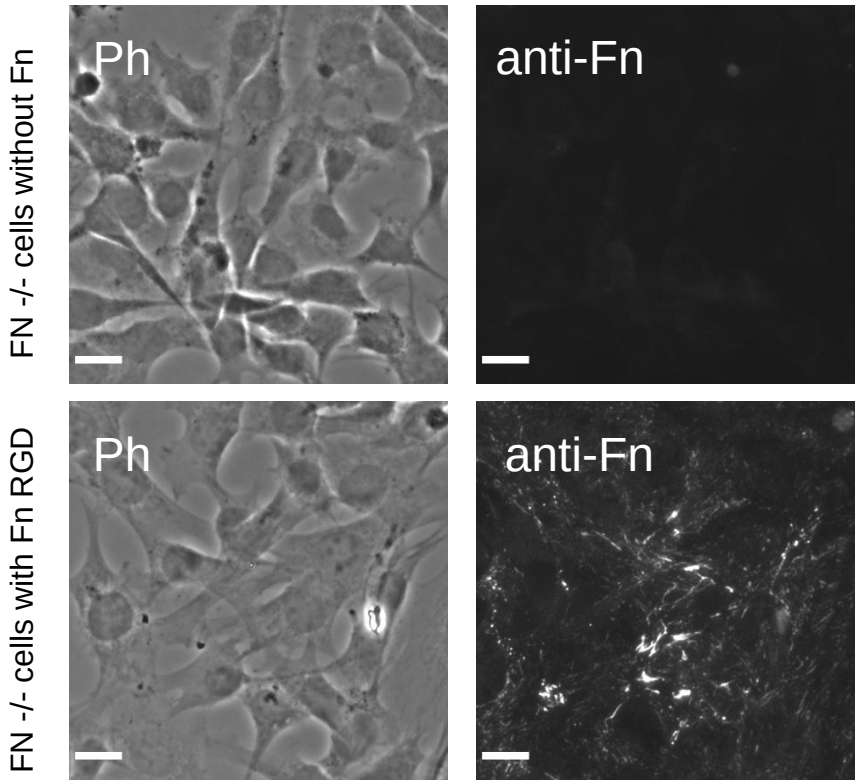

Figure 8: FN -/- cells do not express Fn but can assemble exogenous Fn into matrix
FN -/- fibroblasts were grown on ColIV-coated coverslips for 48 h without exogenous Fn or with the addition of conditioned growth medium from FN fl/fl cells, containing secreted Fn RGD. Fn matrix was detected by indirect immunofluorescence with rabbit-anti-Fn (anti-Fn) and anti-rabbit-Alexa568 antibody. Ph = phase contrast image. Bars represent 20 µm.

Staphylococcus aureus produces several adhesins, which allow binding to Fn (FnBPA, Eap, Ebh, Teichoic acids) but also to other matrix molecules such as vitronectin, laminin and collagen (Patti et al. 1994). In this study, *FnBPA-Staphylococcus carnosus* was used, which heterologously expresses FnBPA as the only adhesin on its surface (Sinha et al. 2000). As an alternative, non-bacterial model for infection, sulfate-modified polystyrene beads were coated with a GST-tagged FnBPA(DuD4)-fragment (see chapter B.1.5 in *introduction* for FnBPA domain organization). These beads have a 1 µm diameter, which corresponds to the size of staphylococci.

A summary of the experimental procedures of cellular infection, i.e. how the different cell lines, Fns, bacteria and beads were used and modified for the assays, is given below (Table 1)

Table 1: Summary of the cell lines, plasmids, Fns and infectious particles used in this study.

Cell lines	**Relevant characteristic**
FN -/-	No expression of Fn
FN fl/fl	Endogenous expression of Fn RGD
FN RGE/RGE	Endogenous expression of Fn RGE
Plasmids	
pcDNA	Empty expression vector
mFNwt	Heterologous expression of Fn RGD in FN -/- cells
mFNwt_RR1495/1500AA	Heterologous expression of Fn Syn$^-$ in FN -/- cells
Fibronectins	
Fn RGD	Wild-type Fn expressed by FN fl/fl or FN -/- cells transfected with mFNwt
Fn RGE	RGD>RGE-mutated Fn expressed by FN RGE/RGE cells
Fn Syn$^-$	Synergy site-mutated Fn expressed by mFNwt_RRAA transfected FN -/- cells
Fn III7-10	Recombinant His-tagged Fn type III(7-10)
Fn 30 kDa	Purified proteolytic 30 kDa fragment of human plasma Fn
Fn 70 kDa	Purified proteolytic 70 kDa fragment of human plasma Fn
Infectious particles	
S. carnosus TM300	No expression of adhesins
FnBPA-S. carnosus	Heterologous expression of FnBPA from *S. aureus*
BSA-beads	Latex-beads coated with BSA
FnBPA-beads	Latex-beads coated with recombinant FnBPA-fragment GST-FnBPA(DuD4)

1.1. Soluble Fn

For assays where invasion was mediated by soluble Fn, *FnBPA-S. carnosus* and FnBPA-beads were incubated with conditioned media to allow binding of soluble Fns secreted by these cells (Fn RGD, Fn RGE or Fn Syn$^-$). Thereby the bacteria or beads become surface-coated with Fns and thus are adapted to bind to integrin receptors on the surface of infected cells (Figure 9A). To verify that this method produces comparable amounts of Fn on the surface of the particles, equal numbers of coated bacteria or beads were washed, boiled in SDS sample buffer und subjected to SDS-PAGE. After transferring to a PVDF membrane, similar amounts of bound Fn could be detected by Western blot using anti-Fn antibody (Figure 9B). As an alternative approach to quantify the amount of bound Fn, indirect immunofluorescence and fluorescence quantification was employed. Serially diluted

conditioned media were incubated with beads or bacteria, washed and stained with anti-Fn primary antibody and Alexa568-labeled secondary antibody. Images were acquired using the same microscope settings for all the samples and the fluorescence signal was quantified using ImageJ software. For the different sets of conditioned media, only very small differences in the fluorescence signal could be detected between wild-type and mutated Fns (Figure 9C). The signal obtained from conditioned medium from FN -/- cells was at background level.

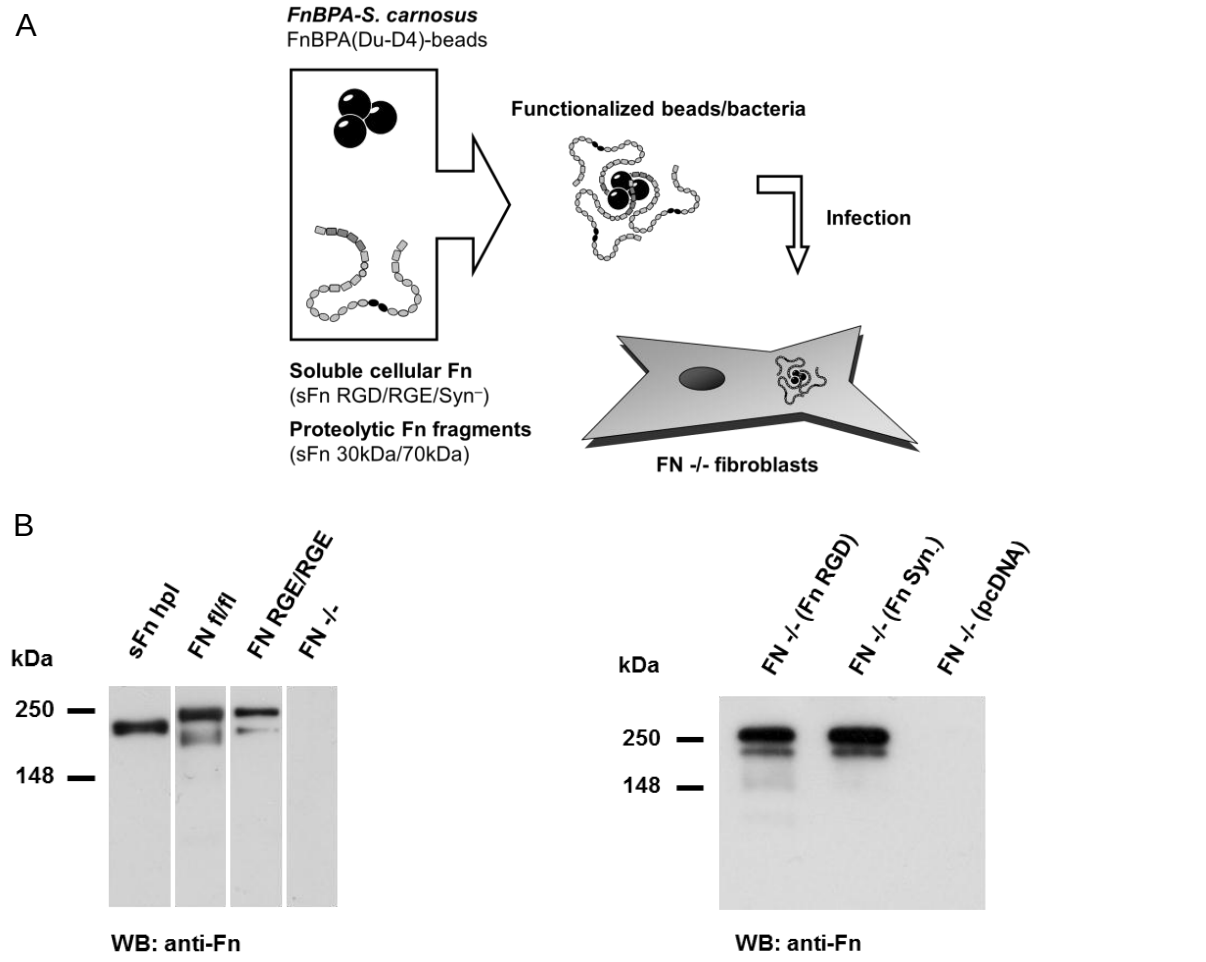

Figure 9: Quantification of the amount of secreted cellular Fn bound to *FnBPA-S. carnosus*.
Conditioned media were obtained from the following cells: FN fl/fl, FN RGE/RGE, FN -/- and the transfected FN -/- (Fn RGD), FN -/- (Fn Syn$^-$) and FN -/- (pcDNA). **(A)** *FnBPA-S. carnosus* or FnBPA(DuD4)-beads were coated with different Fn mutants and fragments. Such coated beads/bacteria were used to infect FN -/- cells. **(B)** *FnBPA-S. carnosus* were incubated with the conditioned media, washed and subjected to SDS-PAGE, followed by detection with rabbit-anti-Fn and anti-rabbit-HRP antibodies. Soluble human plasma Fn (sFn hpl) served as a positive control for the detection of Fn. **(C)** *FnBPA-S. carnosus* were incubated with serial dilutions (1:1 = undiluted) of the conditioned media, washed, sonicated and fixed on slides. Bound Fn was detected with rabbit-anti-Fn and anti-rabbit-Alexa568 antibodies. All pictures were taken with the same settings and analyzed using ImageJ software.

1.2. Organized Fn

Cultured cells express and secrete Fn into the cell culture medium and assemble it into fibrils (Hynes 1990). These Fn fibrils allow binding of FnBPA-particles, thus permitting analysis of the role of Fn domains in organized Fn-mediated infection of cells (Figure 10).

When Fn is mutated, matrix fibrils show a different morphology (Figure 11) (Sechler et al. 1997; Sottile et al. 2000; Takahashi et al. 2007). Cells expressing wild-type fibronectin (Fn RGD) established a network of thin as well as very thick fibrils on the basolateral and apical surface that colocalized with α5 integrins. When mutated Fn RGE was organized into matrix, fibrils were generally much thinner and did not colocalize with α5 integrins (Figure 12). It also seemed, as if there were fewer if any Fn RGE fibrils on the apical surface of the cells. Mutating the synergy site showed no effect on the morphology of Fn fibrils (Figure 11). In this case, matrix was localized on both the basolateral and apical surface, but also did not colocalize with α5 integrins (Figure 12). Thus, Fn RGE and Fn Syn$^-$ are assembled into fibrils by α5 integrin-independent mechanisms, as shown by others (Sottile et al. 2000; Takahashi et al. 2007; Sechler et al. 1997).

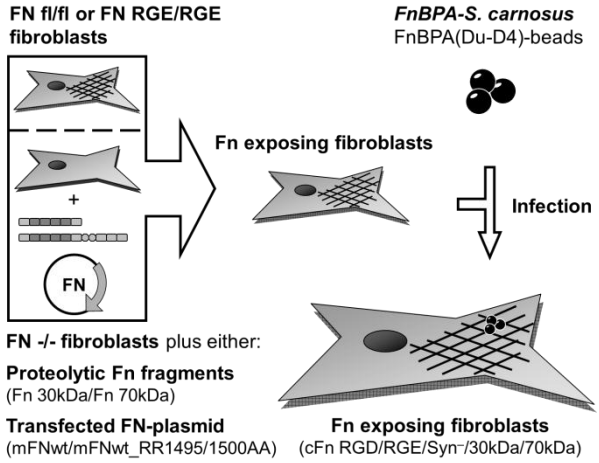

Figure 10: Outline of the experimental procedure used for infection mediated by organized Fn.
Different Fn-expressing cells, either with the Fn gene chromosomally integrated (FN fl/fl, FN RGE/RGE) or transiently transfected with Fn-encoding plasmids or after addition of proteolytic Fn fragments (FN -/-) were infected with *FnBPA-S. carnosus* or FnBPA(DuD4)-beads.

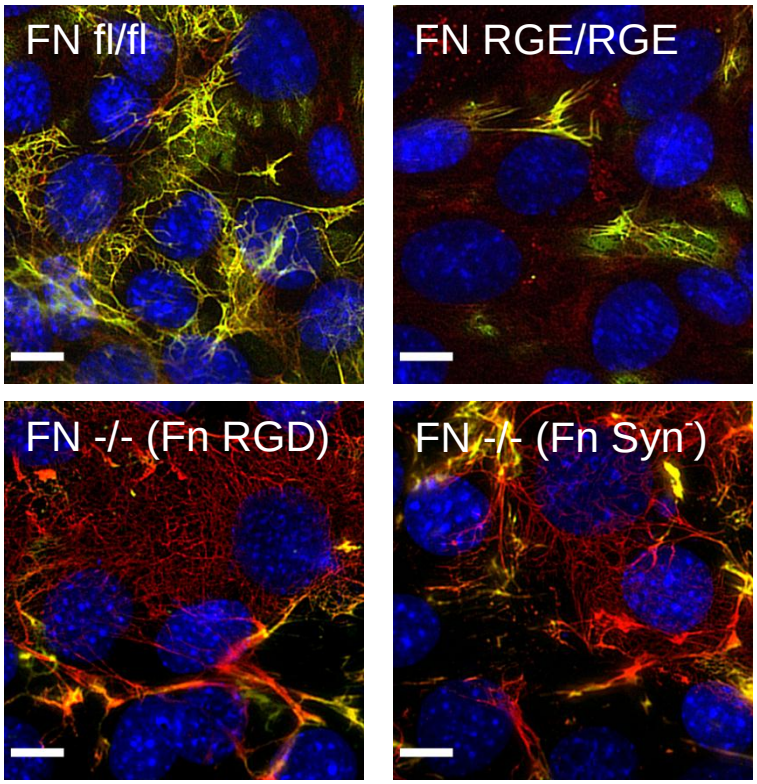

Figure 11: Endogenous and transfected Fn is assembled into matrix.
FN fl/fl, FN RGE/RGE and transfected FN -/- fibroblasts (with plasmids encoding Fn RGD or Fn Syn$^-$) were seeded for 48 h on ColIV-coated coverslips in Fn-free medium to produce Fn matrix. After fixation with non-permeabilizing PFA, cells were stained with rabbit-anti-Fn antibody and secondary anti-rabbit-Alexa488 antibody (green) to stain only surface-exposed Fn. After permeabilization with Triton-X 100, cells were stained for Fn again but with anti-rabbit-Alexa568 (red) secondary antibody to detect all Fn. Image overlays reveal surface-exposed apical Fn (yellow) and cell-masked basolateral Fn (red). Cell nuclei were stained with DAPI (blue). Bars represent 10 µm.

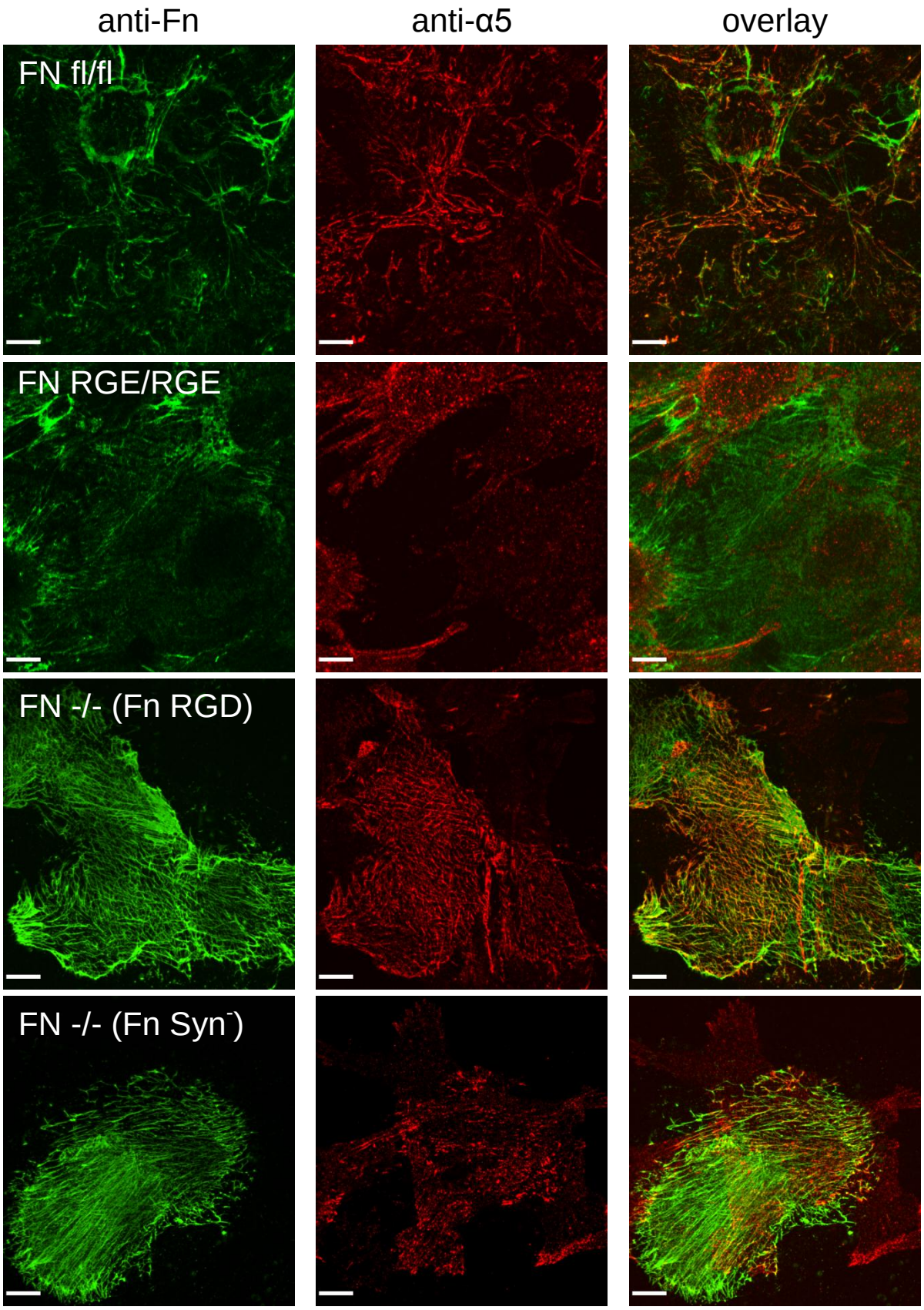

Figure 12: Fn with mutations in the central cell-binding domain does not colocalize with α5β1 integrins. FN fl/fl, FN RGE/RGE and transfected FN -/- fibroblasts (with plasmids encoding Fn RGD or Fn Syn$^-$) were seeded for 48h on ColIV-coated coverslips in Fn-free medium to produce Fn matrix. After fixation and permeabilization, cells were immunolabeled with rabbit-anti-Fn and rat-anti-α5chain primary antibodies and anti-rabbit-Alexa488 and anti-rat-Alexa568 secondary antibodies. Bars represent 10 µm.

2. FnBPA-mediated cellular infection using soluble and organized Fn

In general, bacteria can bind to soluble plasma Fn, mostly produced by hepatocytes, or cell-secreted Fn as well as cellularly organized Fn fibrils (Greene et al. 1995; Kanzaki et al. 1992; Kuusela et al. 1985; Peacock et al. 1999; Nyberg et al. 2004). To determine whether the ability of bacteria to attach to and invade cells using FnBPA depends on the type of Fn (soluble or organized) to which the FnBPA binds, two different approaches were followed. Firstly, FnBPA-bacteria or -beads were coated with soluble Fns and incubated with FN -/- cells (see Figure 9A) at a particle-to-cell ratio of 50:1 (multiplicity of infection [MOI] of 50). Secondly, Fns were organized by the respective cells and were then incubated with uncoated FnBPA-bacteria or -beads (Figure 10) at a MOI of 50. These two basic experimental designs allowed the detailed and unambiguous investigation of the role of soluble and organized Fn, as well as different Fn modules, in the infection process.

2.1. Soluble Fn

The time course of attachment to and invasion of FN -/- cells was recorded for *FnBPA-S. carnosus* and FnBPA-beads. The number of adherent bacteria (Figure 13A) was relatively constant until 60 min post infection. Between 60 min and 120 min post infection, the number of adherent Fn RGD-coated bacteria appeared to increase further by about 30 %. Invasion proceeded constantly with all the differently coated bacteria during the time window of 120 min (Figure 13B). For the assays described below, an infection time of 60 min was selected.

The mutation of RGD to RGE in Fn had an influence on both, particle adherence and invasion. At 60 min post infection, when Fn RGE-coated particles were compared with Fn RGD-coated particles, adherence was reduced by ~37 %, and invasion was even more reduced by ~81 % (Figure 13C, see Table 2 for specific values). Relative to the total number of cell-associated bacteria, only 17 % of the FnBPA-bacteria coated with Fn RGE were localized intracellularly, compared to 54 % of the Fn RGD-coated bacteria (Figure 13D). This effect was more pronounced when using FnBPA-beads instead of bacteria (86 % for RGD compared to 17 % for RGE, Figure 13F). As a control, FnBPA-negative *S. carnosus* TM300 were incubated with Fn RGD and Fn RGE containing conditioned media and exposed to FN -/- cells. No adherence or invasion could be observed (Figure 13E). The same holds true for BSA-beads coated with Fn RGD or Fn RGE. Adherence was at background level, which could also be observed for FnBPA-beads without Fn (Figure 13F).

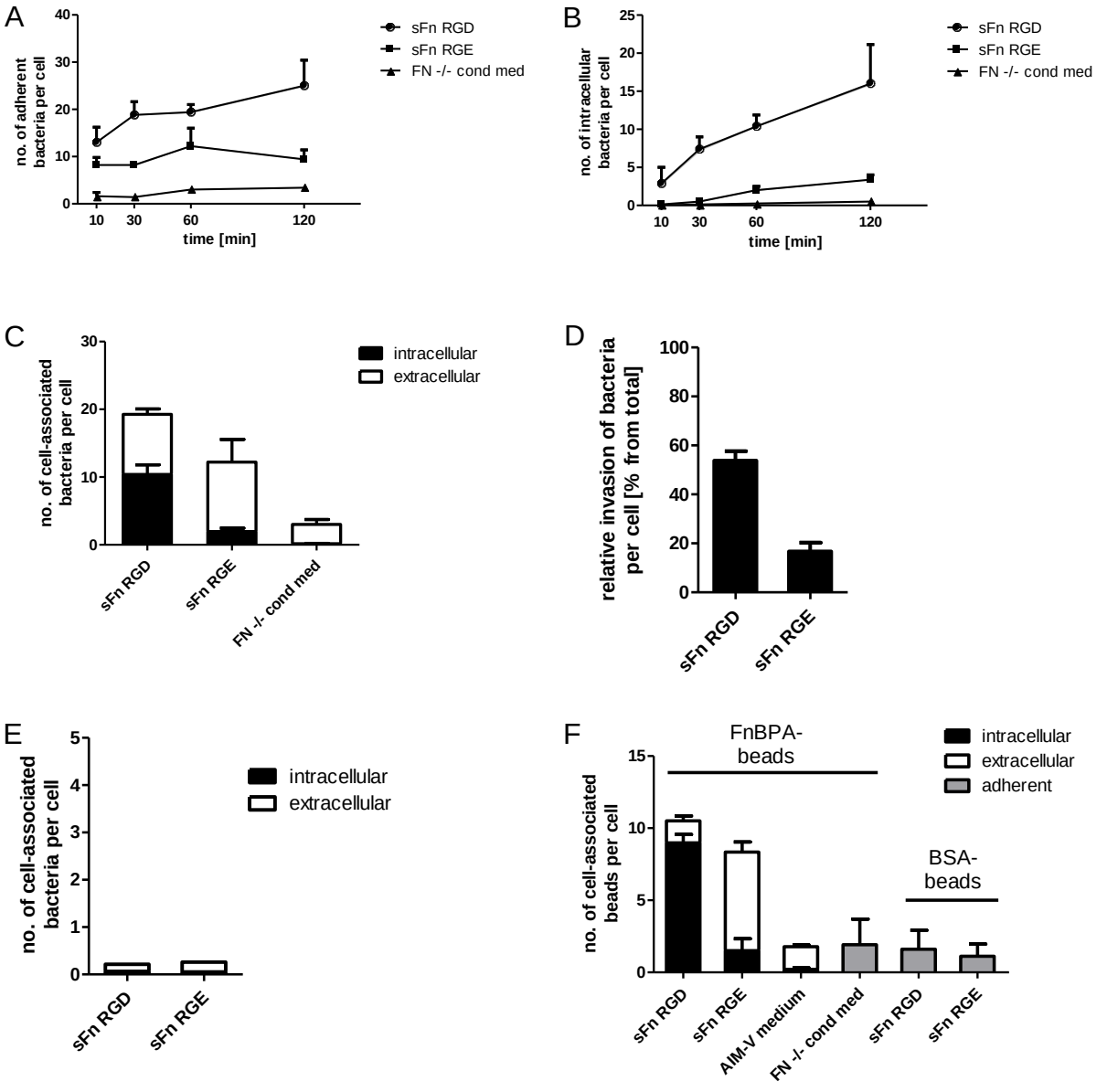

Figure 13: Mutating the RGD motif in soluble Fn causes reduced adhesion and invasion of FnBPA-particles.

(A+B) The time courses of attachment **(A)** and invasion **(B)** into FN -/- cells were recorded for *FnBPA-S. carnosus* incubated with Fn containing conditioned medium from FN fl/fl (sFn RGD) and FN RGE/RGE cells (sFn RGE). As a control, Fn-free conditioned medium from FN -/- cells (FN -/- cond med) was applied. The number of cell-associated bacteria was determined microscopically and intra- vs extracellular localization was determined by inside/outside staining of the bacteria. Values represent mean ± s.d. from three separate experiments with at least 150 cells counted per experimental condition at a MOI of 50. **(C)** The total number of intracellular bacteria at 60 min post infection is shown based on values from **A** and **B**. **(D)** The percentage of intracellular bacteria at 60 min post infection is shown based on values from **A** and **B**. **(E)** FnBPA-negative *S. carnosus* were incubated with Fn-containing conditioned medium from FN fl/fl (sFn RGD) or FN RGE/RGE cells (sFn RGE) and the number of cell-associated bacteria determined as in **C**. Each bar represents a single experiment with at least 150 cells counted per condition at a MOI of 50. **(E)** GST-FnBPA(DuD4)-coated latex-beads (FnBPA-beads) were utilized for infecting FN -/- cells after coating with Fn-containing conditioned medium from FN fl/fl (sFn RGD) and FN RGE/RGE cells (sFn RGE). As a control, plain AIM-V was used for coating and the number of cell-associated beads determined as in **C**. To determine unspecific attachment of particles, BSA-beads were coated with conditioned media as described in **C** and the number of adherent beads was counted microscopically. Each bar represents mean ± s.d. from 2-3 separate experiments with at least 150 cells counted per experimental condition at a MOI of 50.

Fn-expressing transfected cells secreted less Fn into the growth medium than FN fl/fl and FN RGE/RGE cells, probably due to a relatively low transfection efficiency. To ensure a sufficiently high concentration of Fn in the conditioned medium, needed for coating of bacteria and thus to ensure comparability in coating efficiency, the medium was 10-fold concentrated with a concentrator column.

The time course of infection of Fn Syn$^-$-coated bacteria was similar to Fn RGE-coated bacteria. The number of adhering bacteria was constant during the time window of 120 min (Figure 14A) and invasion also progressed constantly (Figure 14B). The total number of adherent Fn Syn$^-$- compared to Fn RGD-coated bacteria at 60 min post infection was reduced by ~40 % and absolute invasion was reduced by ~33 % (Figure 14C). Interestingly, however, the relative invasion of bacteria coated with these Fns did not differ (Figure 14D). Relative to the total number of cell-associated bacteria, ~39 % of Fn Syn$^-$ and ~36 % of Fn RGD-coated cell-associated bacteria were located intracellularly 60 min post infection. This would mean that mutation of either the RGD motif or the synergy site in Fn lead to impaired binding of Fn-coated bacteria to cells and that Fn Syn$^-$-coated bacteria were more invasive than Fn RGE-coated bacteria. This can only be explained with the presence of an intact RGD motif in Fn Syn$^-$, which is still accessible to host cell integrins.

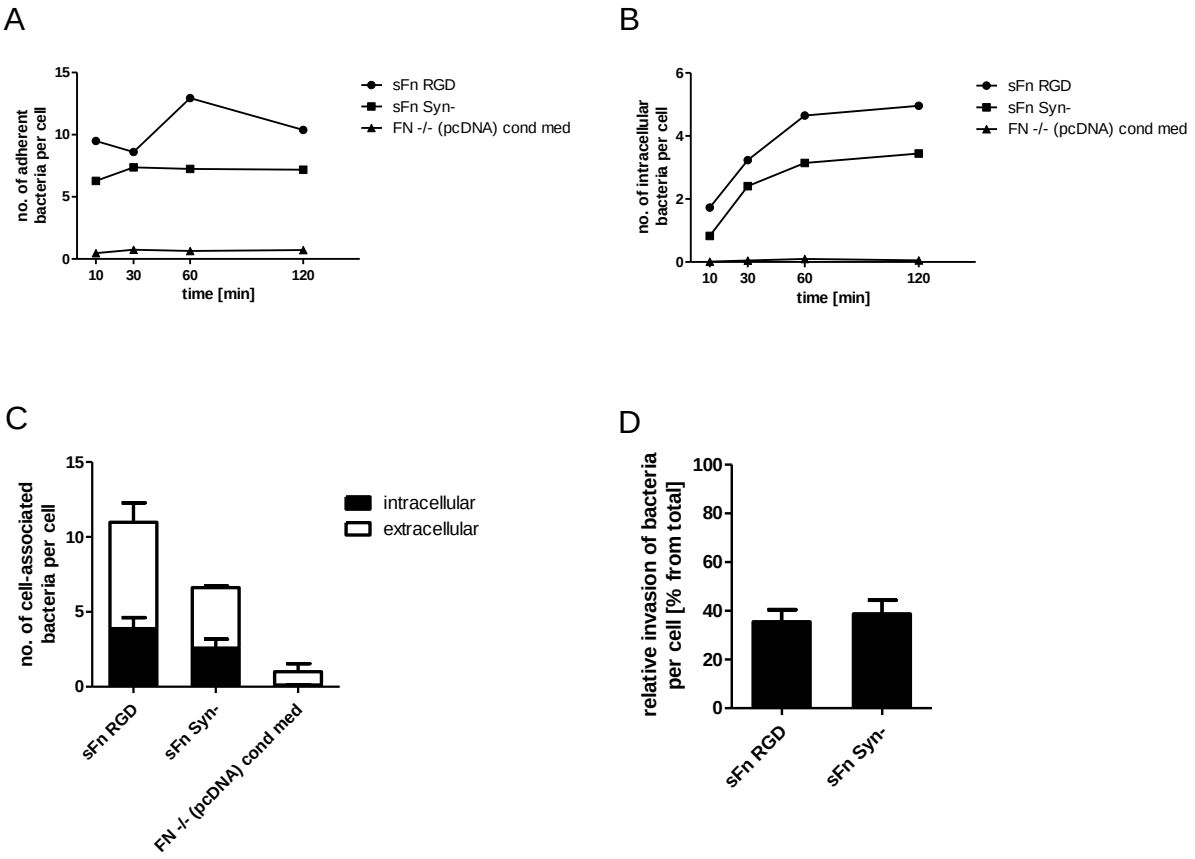

Figure 14: Mutating the synergy site in Fn reduces adhesion but not the relative invasion of FnBPA-bacteria.
(A+B) The time courses of attachment to and invasion of FN -/- cells were recorded for *FnBPA-S. carnosus* coated with Fn-containing conditioned medium from transfected FN -/- cells expressing Fn RGD (sFn RGD) or Fn Syn$^-$ (sFn Syn-). As a control, Fn-free conditioned medium from FN -/- cells transfected with the empty expression vector pcDNA [FN -/- (pcDNA) cond med] was also applied. The number of adherent bacteria **(A)** as well as the number of intracellular bacteria per cell **(B)** was determined microscopically by inside/outside staining of bacteria. Values represent mean ± s.d. from a single experiment with at least 150 cells counted per experimental condition at a MOI of 50. **(C)** The total number of cell-associated intra- and extracellular bacteria at 60 min post infection was determined for *FnBPA-S. carnosus* coated with the same conditioned media as described in **A** and **B**. Values represent mean ± s.d. from three separate experiments with at least 150 cells counted per experimental condition at a MOI of 50. **(D)** To visualize the invasion capability of bound bacteria, the percentage of intracellular bacteria at 60 min post infection is shown based on values from **C**.

Fn comprises a multitude of domains that mediate interaction with bacterial adhesins, self-association and cellular receptors such as integrins (see also Figure 2 in *introduction*). Since inactivating the RGD motif and the neighboring synergy site in Fn did not fully inhibit adherence and invasion of FN -/- cells by coated FnBPA-bacteria or -beads, shorter Fn fragments were used, either derived from Fn proteolysis (Fn 30 kDa and Fn 70 kDa) or recombinantly expressed (Fn III7-10). The Fn III(7-10) fragment, missing the N-terminal 70 kDa domain of Fn that is important for binding of FnBPA, was unable to mediate specific binding of bacteria to and invasion of FN -/- cells (Figure 15A). Conversely, the N-terminal Fn 30 kDa and Fn 70 kDa fragments alone allowed specific coating of bacteria and adhesion to cells. Compared to full-length human plasma Fn, adherence was reduced by ~80-85 %, but this was still higher than unspecific binding of bacteria incubated PBS as a control (Figure 15A). Specific binding via Fn 70 kDa to host cells could be verified by blocking the invasion of Fn RGD-coated bacteria up to 40 % with soluble Fn 70 kDa in a concentration-dependent manner. (Figure 15B). Surprisingly, the invasion of Fn RGE-coated bacteria could not be blocked, but increased ~2-fold in the presence of soluble Fn 70 kDa (Figure 15B).

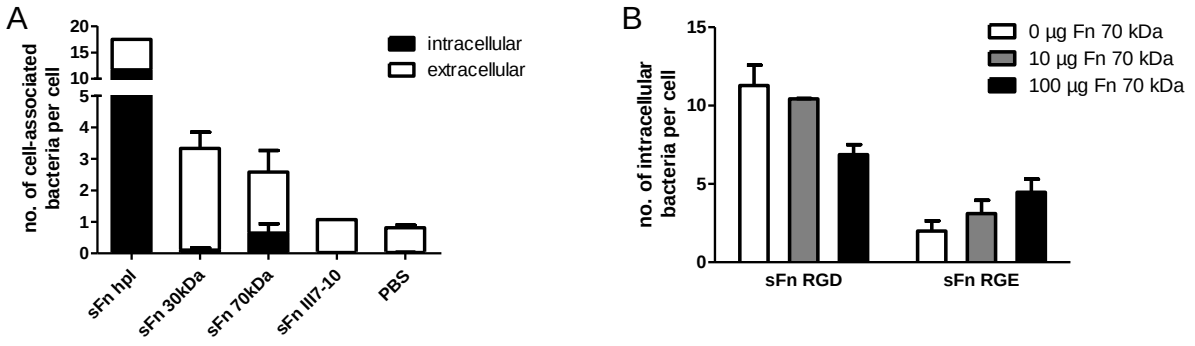

Figure 15: The N-terminal 70kDa domain of Fn is sufficient to mediate invasion of FnBPA-bacteria and inhibits sFn-dependent invasion.
(A) FN -/- cells were infected with *FnBPA-S. carnosus* coated with 10 µg/ml of full-length human plasma Fn (sFn hpl), its proteolytic fragments (sFn 30 kDa and sFn 70 kDa) or His-tagged recombinant domains Fn III(7-10) (sFn III7-10). Adherence and invasion of cell-associated bacteria were determined microscopically by inside/outside staining of bacteria. Bars are mean ± s.d. from two separate experiments with at least 150 cells counted per experimental condition at a MOI of 50. Data with sFn hpl and sFn III7-10 are derived from one experiment. **(B)** *FnBPA-S. carnosus* coated with sFn RGD or sFn RGE from conditioned medium was used to infect FN -/- cells. Different concentrations of soluble Fn 70 kDa from human plasma Fn were added to the assay. Bars represent mean ± s.d. of 2-3 separate experiments with at least 150 cells counted per experimental condition at a MOI of 50.

Table 2: Summary of the data obtained for soluble Fn-mediated adherence and invasion of FnBPA-particles into FN -/- cells.
Descriptions of the various conditions can be found in Figure 13 – Figure 15. For statistical analysis, one-way ANOVA was performed with Bonferroni's post test for selected pairs using GraphPad Prism software. P-values smaller than 0.05 were found to be significant. In columns, paired values (highlighted in gray) were selected for post test.

	number of adherent particles		**number of intracellular particles**		**percentage of intracellular particles**	
	bacteria	*beads*	*bacteria*	*beads*	*bacteria*	*beads*
sFn RGD	19.26±1.67	10.50±0.36	10.38±1.42	8.98±0.60	53.82±3.85	85.46±3.61
sFn RGE	12.21±3.72 (P<0.05)	8.34±1.39 (P<0.05)	1.97±0.49 (P<0.001)	1.50±0.82 (P<0.001)	16.69±3.61	17.36±7.50
FN -/- cond med	3.01±0.66	1.78±0.01	0.15±0.07	0.21±0.10	5.43±3.58	11.71±5.74
sFn RGD	10.98±1.76		3.89±0.74		35.50±4.97	
sFn Syn$^-$	6.62±0.59 (P<0.01)		2.59±0.59 (P<0.05)		38.75±5.64	
FN -/- (pcDNA) cond med	0.71±0.08		0.12±0.02		13.35±5.73	
sFn hpl	17.52		11.70		66.82	
sFn 30 kDa	3.33±0.45		0.11±0.07		3.36±2.42	
sFn 70 kDa	2.58±0.98		0.65±0.30		24.56±2.18	
sFn III7-10	1.07		0.02		2.30	
PBS	0.81±0.1		0.03±0.01		3.07±0.69	

2.2. Organized Fn

The time course of infection of cells exposing surface-associated organized Fn RGD (FN fl/fl cells) or Fn RGE (FN RGE/RGE cells) by uncoated FnBPA-bacteria and -beads was recorded. The time courses of attachment and invasion for *FnBPA-S. carnosus* mediated by organized Fn on the host cell surface differed slightly from those of *FnBPA-S. carnosus* bound to soluble Fn. For both Fn RGD- and Fn RGE cells, adherence and invasion increased with increasing time of infection (Figure 16A+B). The total number of bacteria adhering to cellularly organized Fn RGE was reduced by ~20 % when compared to cellularly organized Fn RGD after 60 min. Under these conditions invasion was reduced by ~39 % in Fn RGE cells (see Table 3 for specific values). However, in sharp contrast to the situation with FnBPA-bound, soluble Fn, invasion of Fn RGE cells was not significantly reduced relative to the total number of cell-associated bacteria. The difference in relative invasion between organized Fn RGD and Fn RGE was only 7 % (Figure 16C) compared to 37 % difference with the soluble Fns (Figure 13D and Table 2). The respective results obtained with FnBPA-beads were similar to those obtained with the bacteria. Here, adherence via Fn RGE was reduced by ~43 % and invasion was reduced by ~33 % compared to Fn RGD (Figure 16D). Consistent with the results obtained for bacteria, invasion relative to the total number of cell-associated beads was almost equal under the two conditions (~8 % for Fn RGD compared to ~9 % for Fn RGE).

Finally, no differences between the number of either adhering or intracellular bacteria could be detected in Fn Syn^- vs. Fn RGD expressing cells (Figure 16E).

To produce fragments of Fn organized on the cell surface, FN -/- cells were incubated for 24 h with Fn 30 kDa, Fn 70 kDa or recombinant Fn III(7-10). The results for uncoated FnBPA-bacteria adhesion to and invasion of cells exposing the different organized Fn fragments on the cell surface were similar to those seen for invasion of FnBPA-bacteria coated with soluble Fn fragments (Figure 15A). While Fn III(7-10) mediated neither adhesion nor invasion, Fn 70 kDa was able to promote invasion (23 % intracellular bacteria, Figure 16F) and Fn 30 kDa lead to only bound but not invading bacteria. Again, adhesion and invasion using proteolytic Fn fragments organized on the cell surface was greatly reduced compared to full-length Fn (for Fn 70 kDa ~80 % reduction in adherence and 70 % reduction in invasion).

Comparing the results obtained for organized Fn with those for soluble Fn, it is clear that the capability of bacteria or beads to invade using organized Fn is less efficient compared to in the case of soluble Fn. Except for the conditions when Fn RGE (soluble or organized) was

used for mediating invasion of FnBPA-bacteria, the percentage of intracellular particles was lower with organized Fns than with soluble Fns. In summary this suggests that the polymerization state of Fn has a huge impact on the Fn domains that are involved in internalization of Fn-ligated particles and we can show for the first time here that the central integrin binding RGD-site is required for cell invasion using soluble but not cellularly organized fibronectin.

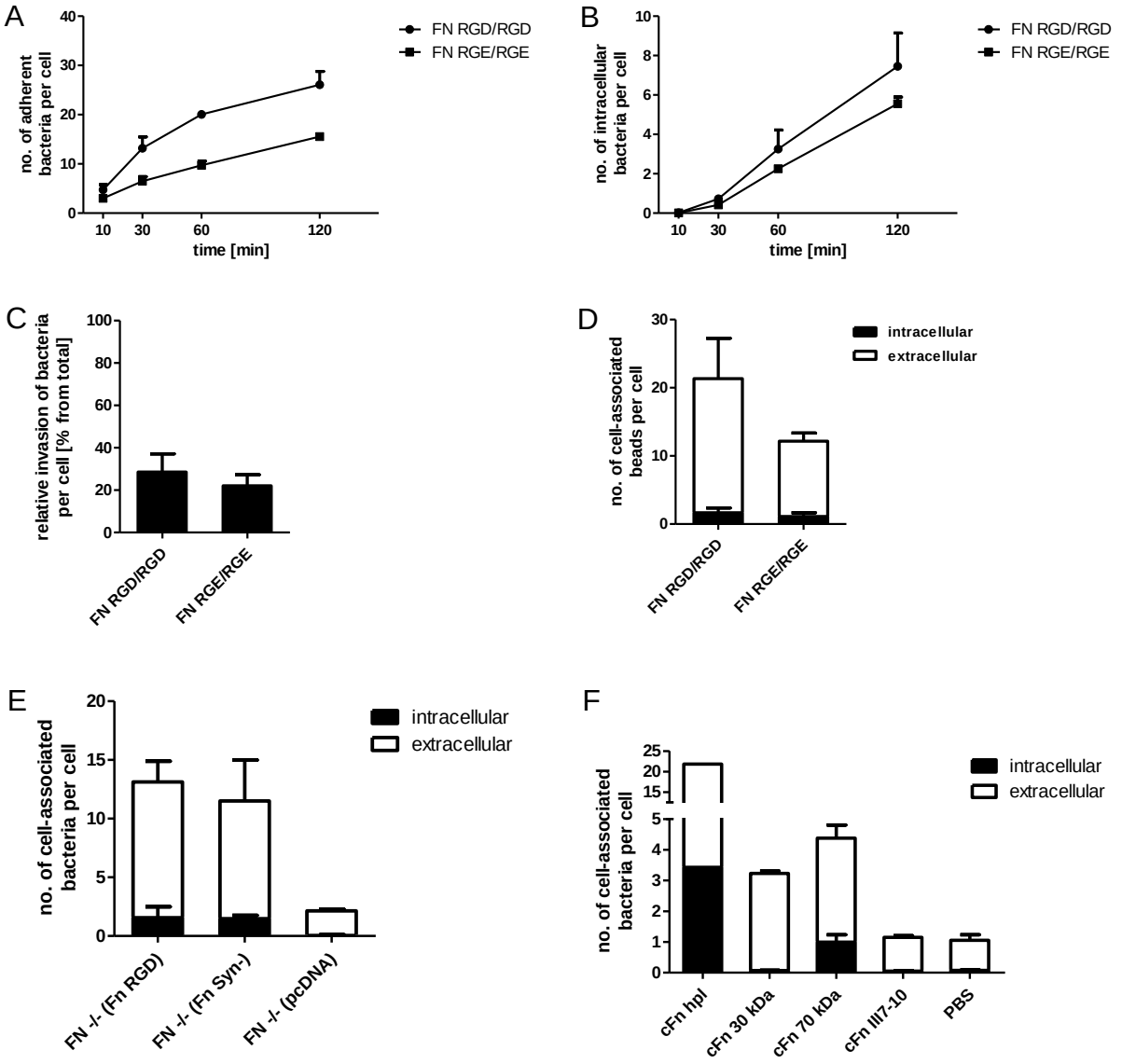

Figure 16: Organized Fns differentially modulate adherence and invasion by *FnBPA-S. carnosus*.
Uncoated *FnBPA-S. carnosus* was used to infect cells organizing various types of Fn. **(A+B)** The time course of attachment to and invasion of cells expressing Fn RGD (FN fl/fl) and Fn RGE (FN RGE/RGE) or no Fn (FN -/-) by FnBP-bacteria and was monitored. The number of adherent bacteria **(A)** as well as the number of intracellular bacteria per cell **(B)** was determined microscopically by inside/outside staining of bacteria. Values represent mean ± s.d. from two separate experiments with at least 150 cells counted per experimental condition at a MOI of 50. **(C)** The percentage of intracellular FnBPA-bacteria at 60 min post infection is shown for the same conditions as described in **A** and **B**. Values represent mean ± s.d. from three separate experiments with at least 150 cells counted per experimental condition at a MOI of 50. **(D)** Using untreated GST-FnBPA(DuD4)-coated latex-beads to infect the same Fn-expressing cells as in **A+B** confirmed the results in **C**. Values represent mean ±

s.d. from two separate experiments with at least 150 cells counted per experimental condition at a MOI of 50. **(E)** Transfected cells expressing Fn with an inactivating mutation in the synergy site [FN -/- (Fn Syn-)] or wild-type Fn [FN -/- (Fn RGD)] were infected with uncoated FnBPA-bacteria. Cells transfected with empty vector served as a control [FN -/- (pcDNA)]. The number of adherent and intracellular bacteria was determined as described in **A+B**. Values represent mean ± s.d. from two separate experiments with at least 150 cells counted per experimental condition at a MOI of 50. **(F)** Attachment to and invasion of host cells by FnBPA-bacteria using organized full-length human plasma Fn (cFn hpl), proteolytic Fn 30 kDa (cFn 30 kDa) or Fn 70 kDa fragment (cFn 70 kDa), and recombinant His-tagged Fn III(7-10) (cFn III7-10) was achieved by adding 10 µg/ml of the respective Fns to FN -/- cells for 24 h prior to infection. PBS (solvent of the the Fns) served as a control. The number of adherent and intracellular bacteria was determined as described in **A+B**. Bars are mean ± s.d. from two separate experiments with at least 150 cells counted per experimental condition at a MOI of 50. Data with cFn hpl derived from one experiment.

Table 3: Summary of the data obtained for organized Fn-mediated adherence and invasion of *FnBPA-S. carnosus* into cells.

Descriptions of the various conditions can be found in Figure 13 – Figure 15. For statistical analysis, one-way ANOVA was performed with Bonferroni's post test for selected pairs using GraphPad Prism software. P-values smaller than 0.05 were found to be significant. In columns, paired values (highlighted in gray) were selected for post test.

	number of adherent particles		**number of intracellular particles**		**percentage of intracellular particles**	
	bacteria	*beads*	*bacteria*	*beads*	*bacteria*	*beads*
FN fl/fl	10.77±2.35	21.33±6.66	3.21±1.66	1.66±0.72	28.55±8.60	7.62±0.98
FN RGE/RGE	8.60±2.71	12.17±1.76	1.97±0.92	1.12±0.56	22.07±5.23	8.96±3.27
FN -/-	0.97±0.34		0.09±0.06		11.29±9.28	
FN -/- (Fn RGD)	13.13±2.69		1.56±0.92		11.43±4.68	
FN -/- (Fn Syn$^-$)	11.51±3.76		1.48±0.28		13.13±1.90	
FN -/- (pcDNA)	2.14±0.07		0.05±0.07		2.26±3.19	
cFn hpl	21.83		3.43		15.69	
cFn 30 kDa	3.23±0.06 (P<0.05)		0.07±0.02		2.13+/0.50	
cFn 70 kDa	4.38±0.67 (P<0.01)		1.00±0.24 (P<0.05)		22.61±2.03	
cFn III7-10	1.15±0.08		0.05±0.02		4.19±1.35	
PBS	1.05±0.20		0.08±0.02		7.23±0.42	

3. Bacterial motility on the surface of fibroblasts

The infection of cells by FnBPA-expressing bacteria has been demonstrated to be a dynamic process (A. Schröder et al. 2006). Instead of simply being taken up, the bacteria attach at the cell edges and move centripetally on the cell surface, towards the nucleus. It is believed that connection of ligand-bound integrins to the rearward moving actin cytoskeleton is responsible for the centripetal movement of particles on cells (Cai et al. 2006; Choquet et al. 1997; A. Schröder et al. 2006). Changes in the affinity state of integrins and their downstream signaling are known to interfere with the integrin-actin connection and thereby affect motility of ligand-coated particles on cells (Roca-Cusachs et al. 2009; A. Schröder et al. 2006; X. Zhang et al. 2008; Coussen et al. 2002; Giannone et al. 2003; Nishizaka et al. 2000). To reveal the impact of Fn domains on integrin outside-in signaling during FnBPA-mediated infection, bacterial motility was recorded and quantified using time-lapse imaging of infected cells. After adding bacteria, three parameters were analyzed:

1) Displacement, which is the length in µm of a straight line drawn between the bacterial position in the first and the last frame of a track
2) Directionality, which is the ratio between the displacement and the absolute length of the bacterial track
3) Track velocity, which is the average speed of the bacterium (absolute track length/track recording time)

3.1. Soluble Fn

FN -/- fibroblasts were infected with *FnBPA-S. carnosus* coated with either Fn RGD or Fn RGE from conditioned media or proteolytic Fn 70 kDa (see Table 1 and 9A). It could be observed, that Fn RGD-coated bacteria were transported with a directionality value of 0.55 compared to 0.34 for Fn RGE- and 0.35 for Fn 70 kDa-coated bacteria (Figure 17B + Table 4). Also the displacement was affected because all Fn RGD-coated bacteria moved centripetally to the perinuclear region without shifting or stopping, but in contrast, Fn RGE- and Fn 70 kDa-coated bacteria both had a shortened travel distance (Figure 17A), which was reduced by 46 % (Fn RGE) and 33 % (Fn 70 kDa) vs. Fn RGD, respectively. Despite these large differences in displacement and directionality, the track velocity was essentially the same for all coatings (Figure 17C).

Next, the motility of Fn Syn$^-$-coated bacteria was investigated. Mean displacement was reduced by ~20 % and the directionality values (0.43 for Fn Syn$^-$ versus 0.60 for Fn RGD; Table 4) pointed to a less straight movement of Fn Syn$^-$-coated compared to Fn RGD-coated bacteria (Figure 17D+E). The speed of bacteria was the same for both treatments (Figure 17F).

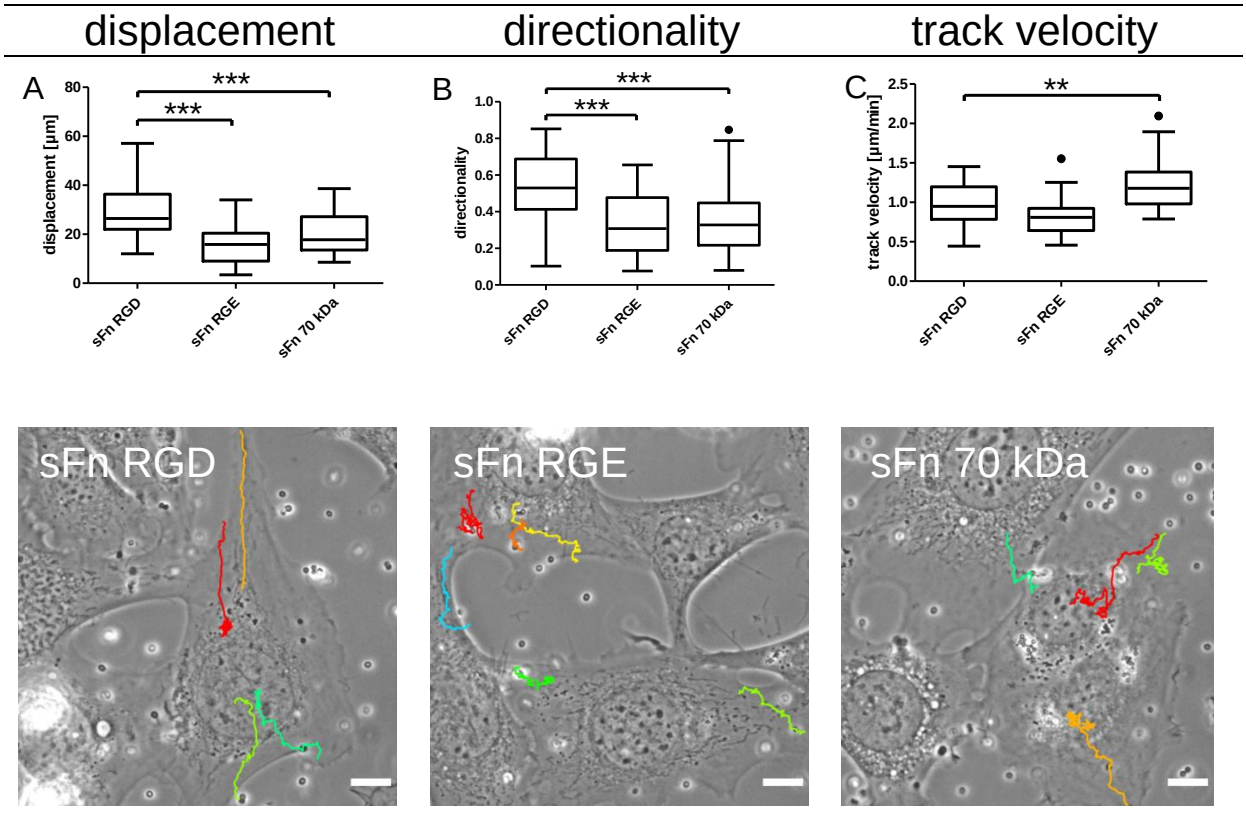

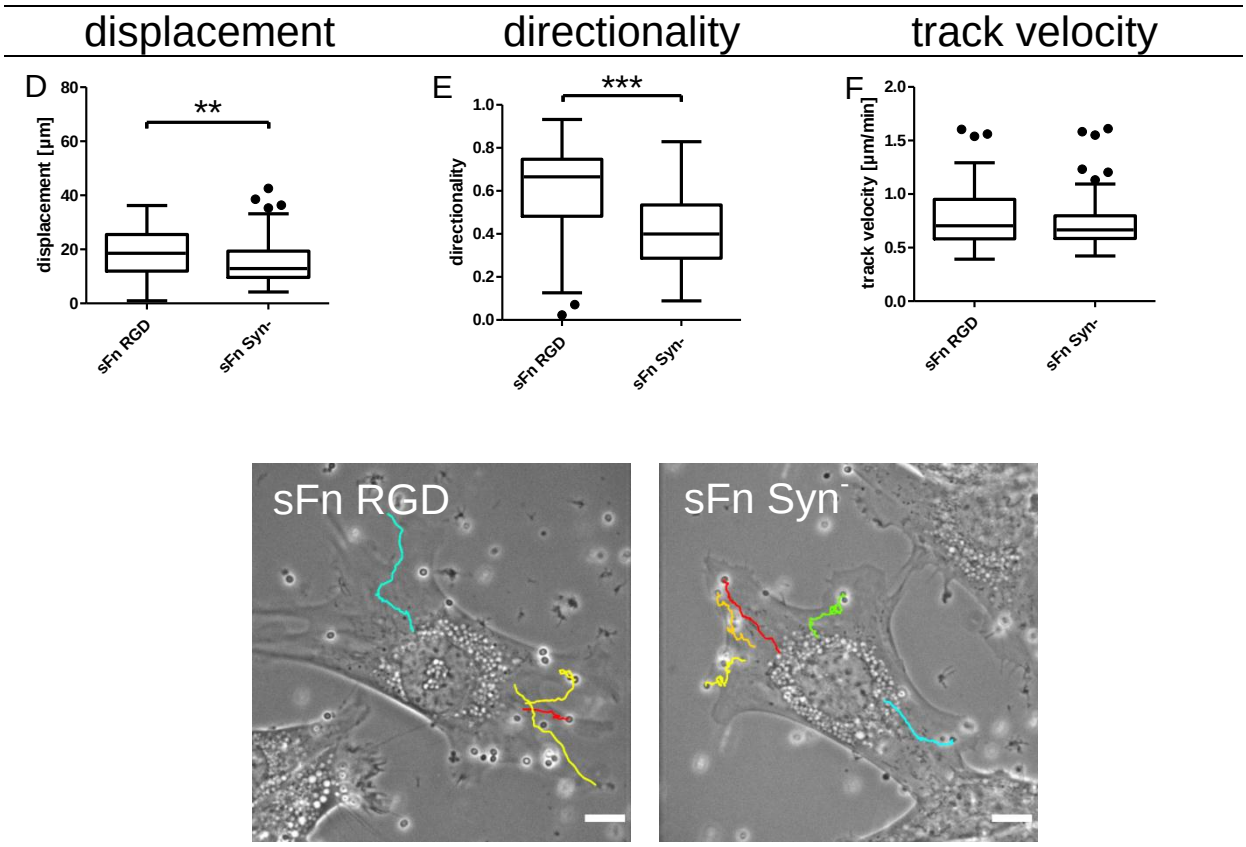

Figure 17: The central cell-binding domain in Fn is important for the motility of *FnBPA-S. carnosus* on FN -/- cells.

Motility parameters of individual Fn-coated *FnBPA-S. carnosus* bacteria were investigated during 60 min infection of FN -/- cells using time-lapse microscopy. The depicted phase contrast images were taken from the movies at an early timepoint. Tracks of selected bacteria are indicated by lines. Bars represent 10 µm. **(A-C)** Bacteria were coated with Fn containing conditioned media from FN fl/fl cells (sFn RGD) and FN RGE/RGE cells (sFn RGE) or 10 µg/ml proteolytic Fn 70 kDa fragment (sFn 70 kDa). **(D-F)** Bacteria were coated with Fn-containing conditioned media from transiently transfected FN -/- cells expressing Fn RGD (sFn RGD) and Fn Syn$^-$ (sFn Syn-). **(A-C)** Whisker-Tukey plots were generated from two independent experiments with 32 (sFn RGD) and 36 (sFn RGE) tracks analyzed. Statistical analyses were performed with GraphPad Prism software using one-way ANOVA with Bonferroni's post test. **, $p < 0.01$; ***; $p < 0.001$. **(D-F)** Whisker-Tukey plots were generated from two independent experiments with 77 tracks analyzed for each condition. Statistical analyses were performed with Graph Pad Prism software using Student's unpaired t-test. **, $p < 0.01$; ***; $p < 0.001$.

3.2. Organized Fn

Fibroblasts with surface-associated, organized Fn RGD (FN fl/fl cells) or Fn RGE (FN RGE/RGE cells) were infected with uncoated *FnBPA-S. carnosus*. No significant differences in displacement, directionality or track velocity were apparent for the bacteria adhering to these two different Fn forms (Figure 18A-C). These bacteria moved centripetally to the perinuclear region at the same speed and covered the same distance.

Bacterial motility mediated by binding to cell surface-organized Fn RGD- or Fn RGE-bacteria was ~20-30 % slower than that mediated by the corresponding soluble Fns. However, whereas directionality was unchanged between movements mediated by organized or soluble Fn RGD, displacement via organized Fn RGD was reduced by ~40 % compared to soluble Fn RGD. In contrast, displacement and directionality stayed essentially the same when bacterial movements were mediated by soluble Fn RGE vs. organized Fn RGE. This suggests that the polymerization state of Fn has a considerable impact on the Fn domains participating in the integrin activation, coupling to the cytoskeleton and thereby in the centripetal transport of Fn-ligated particles.

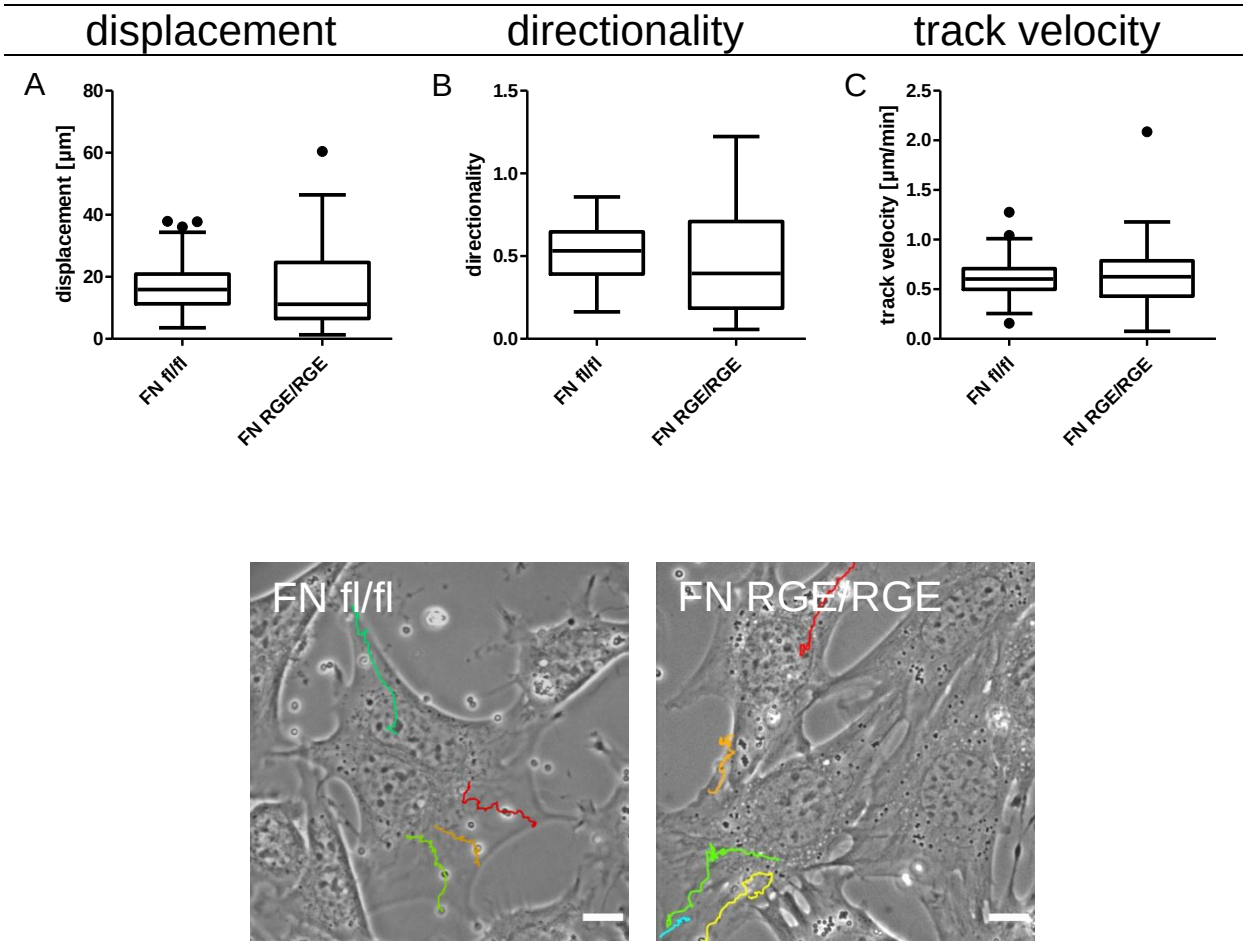

Figure 18: Mutating the RGD motif in cellularly organized Fn does not affect the motility of *FnBPA-S. carnosus* during infection.
(A-C) The motility of individual uncoated *FnBPA-S. carnosus* bacteria was investigated during 60 min infection of Fn-expressing FN fl/fl cells and FN RGE/RGE cells using time-lapse microscopy. The depicted phase contrast images were taken from the movies at an early timepoint. Tracks of selected bacteria are indicated by lines. Bars represent 10 µm. Whisker-Tukey plots were generated from three separate experiments with 82 (FN fl/fl) and 68 (FN RGE/RGE) tracks analyzed.

Table 4: Summary of the data obtained for soluble and organized Fn-mediated motility of FnBPA- bacteria during infection.
Descriptions of the various conditions can be found in Figure 17 + Figure 18.

	Displacement [µm]	**Directionality**	**Track velocity [µm/min]**
sFn RGD	29.22 ± 10.73	0.55 ± 0.19	0.98 ± 0.26
sFn RGE	15,72 ± 7.70 (p < 0.001)	0.34 ± 0.18 (p < 0.001)	0.82 ± 0.23 (p < 0.01)
sFn 70 kDa	19,50 ± 7.63 (p < 0.001)	0,35 ± 0.19 (p < 0.001)	1.21 ± 0.31 (p < 0.01)
sFn RGD	19.18 ± 8.40	0.60 ± 0.20	0.78 ± 0.26
sFn Syn$^-$	15.21 ± 8.36 (p < 0.01)	0.43 ± 0.19 (p < 0.001)	0.74 ± 0.24
FN fl/fl	16.89 ± 7.67	0.51 ± 0.18	0.62 ± 0.19
FN RGE/RGE	16.26 ± 13.27	0.45 ± 0.31	0.64 ± 0.30

4. Integrin activation and signaling

Integrins are the main receptors responsible for FnBPA-induced invasion. Upon Fn-mediated binding to the receptors, integrins become activated and clustered and outside-in signaling results in remodeling of the actin cytoskeleton (for details see chapter B.1.9 + B.3.2 in *introduction*). In this work we wanted to investigate which part of this cascade of signaling events is affected by different Fns and by fragments that have been used to decipher Fn domains functional in cell interactions. αVβ3 integrins were therefore blocked by the use of inhibitory peptides or knocked down with small interfering RNAs (siRNAs). Additionally, cell lines were used, in which β1 integrins were knocked out or where Tyr-phosphorylatable NPXY binding motifs for cytosolic adaptor proteins were modified to nonphosphorylatable NPXF motifs. Under these conditions, adherence and invasion assays for FnBPA-bacteria were performed and bacterial motility was recorded and quantified using time-lapse microscopy. To further characterize the impact of Fn's central cell-binding domain on integrin activation during attachment and invasion, the recruitment of integrin adaptor and signaling proteins to bacterial adhesion structures was investigated.

4.1. Integrin inhibition and activation

It is known that blocking the α5β1 integrin receptor by RGD-inhibiting peptides or antibodies reduces adhesion and invasion of *Staphylococcus aureus* (Sinha et al. 1999; Dziewanowska et al. 2000; Fowler et al. 2000; Agerer et al. 2003). By infecting β1 integrin knockout cells (GD25) with *FnBPA-S. carnosus* we verified that β1 integrins are essential for Fn-mediated uptake of bacteria into host cells. Recomplementation of these cells with β1A integrins (GD25-β1A) fully restored the capability of bacteria to invade the cells (Figure 19A). Despite these results it has been proposed, that αVβ3 may function as an alternative receptor that mediates Fn-triggered invasion during bacterial infections (Ozeri et al. 1998; Fowler et al. 2000). We also found that inactivating the Fn RGD motif, the major α5β1 integrin binding site, did not fully inhibit adhesion and invasion of FnBPA-particles (see chapter 2). To elucidate a potential role of αVβ3 in RGD-independent infection, αVβ3-specific cyclic peptides (cycRGD) were used to block the Fn binding site of the αVβ3 receptor. A concentration of 10 µg/ml cycRGD, which blocked spreading of endothelial cells (Figure 23, *material and methods*), did not impair adhesion to or invasion of GD25-β1A cells by *FnBPA-S. carnosus* coated with either Fn RGD or Fn RGE (Figure 19B). On the contrary, adhesion even increased by ~1.5-2 fold and invasion increased by ~3-3.5 fold, and no differences

between Fn RGD and Fn RGE could be observed. Integrin α5β1-mediated invasion via cellularly organized endogeneous or FCS-derived plasma Fn could not be excluded in these cells, which could perhaps mask the previously observed differences for adhesion and invasion through soluble Fn RGE (see chapter 2.1). However, the increase in adhesion and invasion in the presence of cycRGD seems to be related to the coating of bacteria with soluble Fn, because uncoated bacteria showed no increase when infecting these cells in the presence of cycRGD or control peptide cycRAD (Figure 19C).

In another approach, binding of Fns to the αVβ3 receptor was blocked by siRNA-induced knock down of the αV integrin. For this, human ubilical cord vein endothelial cells (HUVEC) were subjected to αV siRNA for 72-96 h and infected with *FnBPA-S. carnosus* for 60 min. Again, no reduction in the number of adherent or intracellular bacteria could be detected (Figure 19D). These results support our hypothesis that invasion is regulated differently in the presence of soluble and organized Fns, whereas the role of αVβ3 in this context needs further investigations. It is possible that αVβ3 modulates the function of β1 integrin receptors, since they seem to be mandatory for Fn-mediated infection. The fact that αVβ3 enables mechanotransduction and α5β1 determines adhesion strength in the connection of Fn to the cytoskeleton (Roca-Cusachs et al. 2009), suggests investigations may find the role of αVβ3 in bacterial adhesion and invasion to be more sensitive under flow than under the static conditions used here.

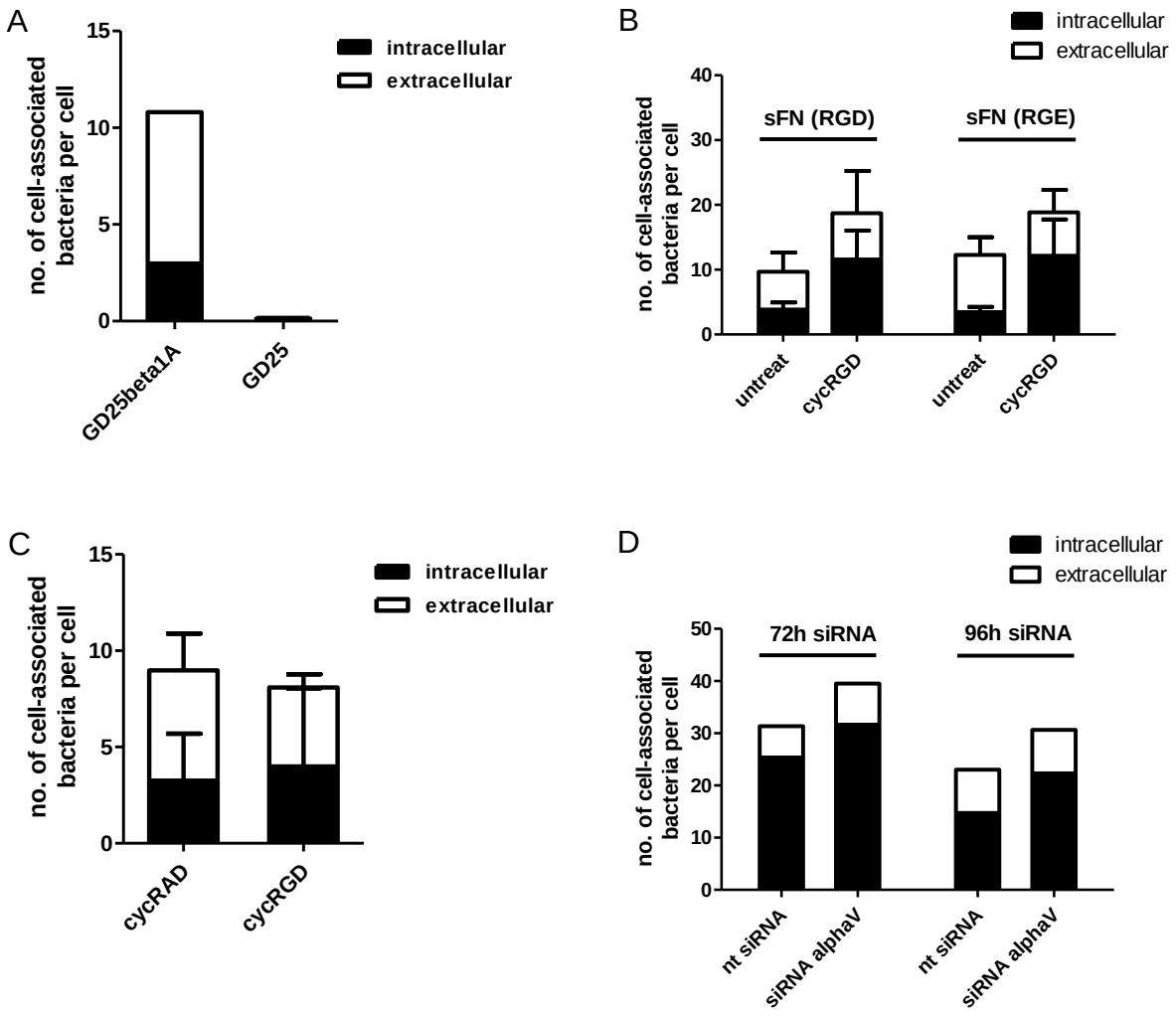

Figure 19: *FnBPA-S. carnosus* infection via Fn requires β1 integrins, but not αVβ3 integrin.
(A-D) The number of cell-associated bacteria was determined microscopically at 60 min post infection with *FnBPA-S. carnosus* and localization was determined by inside/outside staining. **(A)** β1 integrin-deficient mouse fibroblasts (GD25) and β1A-complemented GD25 (GD25beta1A) cells were infected with uncoated bacteria. Values represent mean ± s.d. from a single experiment with at least 150 cells counted per experimental condition at a MOI of 50. **(B)** Prior to infection, GD25-β1A cells were incubated for 60 min with 10 µg/ml αVβ3-specific inhibitory peptide cyclic RGDfV (cycRGD). Bacteria were coated with soluble Fn-containing conditioned medium from FN fl/fl (sFn RGD) or FN RGE/RGE cells (sFn RGE). Values represent mean ± s.d. from two separate experiments with at least 150 cells counted per experimental condition at a MOI of 50. **(C)** Prior to infection with uncoated bacteria, GD25-β1A cells were incubated for 60 min with 10 µg/ml of cyclic RGDfV (cycRGD) or the control peptide cyclic RADfV (cycRAD). Values represent mean ± s.d. from two separate experiments with at least 150 cells counted per experimental condition at a MOI of 50. **(D)** Human umbilical cord vein endothelial cells were transfected with siRNA against αV integrin (siRNA alphaV) or a non-targeting control (nt siRNA) for either 72 h or 96 h prior to infection with uncoated bacteria. Values represent mean ± s.d. from a single experiment with at least 150 cells counted per experimental condition at a MOI of 50.

Downstream signaling of integrins is mediated for the most part through the cytoplasmic region of the β-chain. A key step is the binding of the adaptor proteins talin and kindlin to the membrane-proximal and -distal NPXY motifs, respectively. Tyrosine phosphorylation of these motifs is thought to regulate binding of these adaptors and downstream signaling via src kinases (see chapter B.3.1, *introduction*). A Tyr>Phe mutation in these motifs prevents phosphorylation of the tyrosines but leaves intact the aromatic ring of the tyrosines and thus the binding sites for talin and kindlin (H. Chen et al. 2006; Czuchra et al. 2006). Several studies could show that this mutation leads to impaired signaling through src kinases and FAK resulting in altered rates of Fn fibrillogenesis, organization of focal contacts and cytoskeleton, cell spreading and migration (T. Sakai et al. 1998; Wennerberg et al. 2000; H. Chen et al. 2006). Defects in signaling through FAK and src kinases have been shown to negatively affect the internalization of *S. aureus* (Fowler et al. 2003; Agerer et al. 2003; Agerer et al. 2005).

We used mouse embryonic fibroblasts (MEF) derived from beta1-FF mouse embryos, in which both NPXY motifs were Tyr>Phe-mutated. The invasion of these cells compared to the control beta1-YY MEFs was not impaired when infection with *FnBPA-S. carnosus* (Figure 20A). Surprisingly, the number of intracellular bacteria did not change at 60 min post infection. Because the bacterial motility assay was shown to be a sensitive assay for Fn-triggered integrin activation and coupling to the cytoskeleton, bacteria were tracked during the infection of beta1-YY and beta1-FF MEFs. Again, no differences with respect to displacement, directionality or track velocity were detectable (Figure 20B). In agreement with these findings, two studies using genetically modified mice, in which both β1 integrin cytoplasmic tyrosines have been replaced by phenylalanine, could detect no obvious phenotype and concluded a Tyr phosphorylation-independent function of β1 integrins *in vivo* (H. Chen et al. 2006; Czuchra et al. 2006).

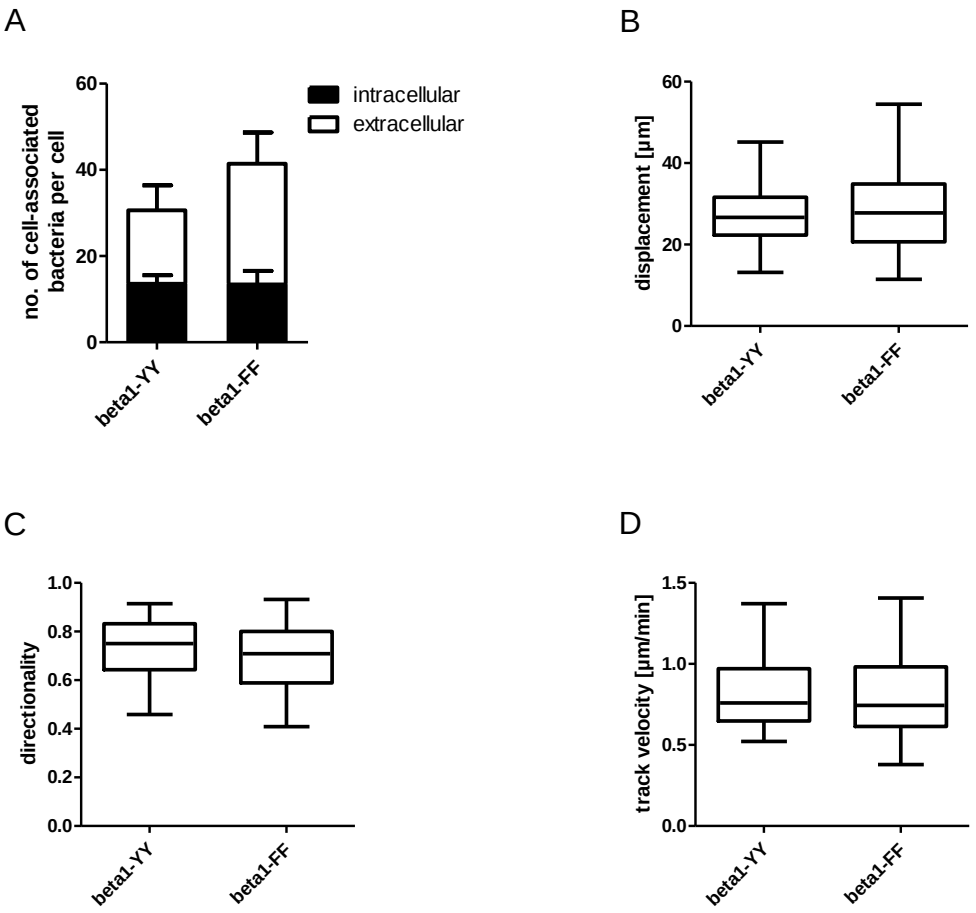

Figure 20: Phosphorylation of cytosolic NPXY motifs in β1 integrin tails is not important for the invasion or motility of *FnBPA-S. carnosus*.
(A-D) Mouse embryonic fibroblasts (MEFs) with YY>FF mutations in the membrane proximal and membrane distal NPXY motifs of the integrin β1 tails (beta1-FF), and wild-type control MEFs (beta1-YY) were infected with uncoated *FnBPA-S. carnosus* for 60 min. **(A)** Adherence and invasion of cell-associated bacteria was determined microscopically by inside/outside staining of bacteria. Bars are mean ± s.d. from four separate experiments with at least 150 cells counted per experimental condition. **(B-D)** The motility of individual uncoated bacteria was investigated during 60 min infection cells using time-lapse microscopy. Whisker-Tukey plots were generated from a single experiment with 41 (beta1-YY) and 42 (beta1-FF) tracks analyzed.

4.2. Recruitment of regulators and adaptors to FnBPA/Fn-mediated bacterial adhesion sites

To gain further data supporting the idea that FnBPA/Fn-mediated integrin activation and adaptor recruitment depends on the RGD motif, the translocation of regulating and scaffolding proteins to the site of bacterial adhesion was investigated.

Experiments allowed discrimination between marker proteins specific for so-called focal adhesions, namely focal adhesion kinase (FAK), vinculin, paxillin, talin and phosphotyrosine (pY), and for fibrillary adhesions, namely α5 and β1 integrins and tensin-3. The molecular composition of the adhesion complex produced in response to soluble Fn RGD-coated *FnBPA-S. carnosus*, was strikingly different from the Fn RGE-induced adhesion structure. (Figure 21). Whilst all of the aforementioned marker proteins could be found in Fn RGD-mediated adhesion complexes, in Fn RGE-triggered sites only talin and β1 integrins could be detected. Since α5 was absent from Fn RGE adhesion sites, and inhibiting the αVβ3 receptor did not reduce Fn RGE-mediated adhesion or invasion (Figure 19B), this may mean that a β1 integrin receptor other than α5β1 is the adhesion-mediating molecule. However, this interaction was sufficient for the infection of these cells, leading to actin reorganization (Figure 21A), coupling to the cytoskeleton (Figure 17) and internalization, albeit a greatly reduced level (Figure 13B+D). Further experiments should focus on the molecular composition of Fn 70 kDa and Fn Syn$^-$-mediated adhesion complexes and on possible differences of organized Fn-induced adhesion sites, as well as downstream signaling mediated by the various Fn.

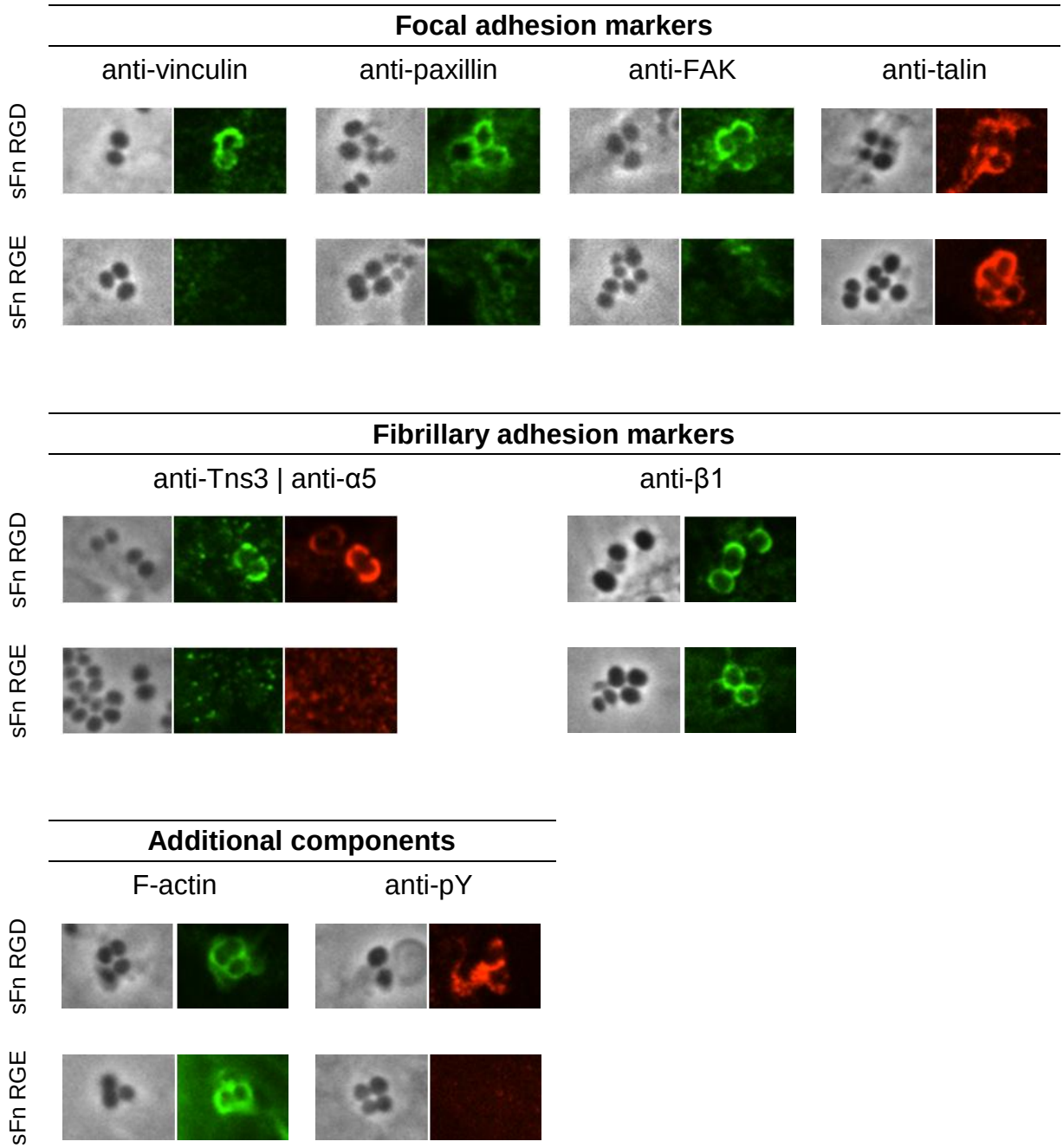

Figure 21: Mutating the RGD domain alters the recruitment of adaptor and signaling proteins to bacterial adhesion sites.
FN -/- cells were infected for 60 min with *FnBPA-S. carnosus* coated with Fn-containing conditioned media from FN fl/fl (sFn RGD) or FN RGE/RGE cells (sFn RGE). The recruitment of marker proteins specific for focal adhesions or fibrillary adhesion was assessed by immunofluorescence using the antibodies mouse-anti-vinculin, mouse-anti-paxillin, mouse-anti-FAK, mouse-anti-talin and rabbit-anti-tensin3 (anti-Tns3), rat-anti-alpha5chain (anti-α5) and hamster-anti-β1, respectively. Additionally, F-actin was detected using Phalloidin-Alexa488 and phosphotyrosine (anti-pY) using mouse-anti-pY(4G10).

D. Discussion

1. Role of Fn domains and the polymerization state of Fn on adherence to and invasion of host cells by FnBPA-particles

The initial step of *Staphylococcus aureus* infection of host cells is mediated, amongst other things, by the interaction of cell wall-anchored fibronectin binding proteins (FnBPs) with the extracellular matrix compound fibronectin (Fn). Binding of multiple Fn binding repeats (FnBR) within the FnBP molecule to the N-terminal type I domains 2-5 of several Fn molecules is sufficient to cluster Fn-bound integrins. This leads to downstream signaling through focal adhesion kinase (FAK), protein tyrosine kinases (PTKs) and Rho GTPases, reorganization of the actin cytoskeleton and finally bacterial uptake. Although it could previously be shown that blocking the interaction of cells with Fn reduces FnBP-mediated invasion of cells by bacteria, the underlying mechanisms and roles of individual Fn domains as well as the physical state of Fn in *S. aureus* infections have remained unclear.

In this work we used a model system that allowed the detailed and unambiguous investigation of the role of various Fn domains and Fn maturation state in FnBPA-mediated infection. Fn-deficient cells (FN -/-) clearly showed a reduced number of adherent and intracellular FnBPA-particles that were coated with soluble RGD>RGE-mutated Fn (Fn RGE) compared to wild-type Fn (Fn RGD). It was previously reported that inhibiting the interaction between α5β1 and Fn, using GRGDS peptides or β1-inhibitory antibodies, reduced internalization of *S. aureus* (Dziewanowska et al. 2000; Agerer et al. 2003; Fowler et al. 2000; Sinha et al. 1999). However, this is the first time that mutated Fn has been used to show a direct role of the RGD motif in FnBPA-mediated infection and the first time that inhibition of uptake could be unambiguously attributed to an effect on soluble Fn bound to FnBPA. The bacterial adhesin-Fn-α5β1 interaction is not only of functional importance in *S. aureus* FnBPA-mediated infections. Several other pathogens also attach to the N-terminal 70 kDa domain of fibronectin through a tandem β-zipper mechanism, e.g. *Streptococcus pyogenes* via protein F1/Sfb1, *Streptococcus dysgalactiae* via FnBA/B, *Streptococcus zooepidemicus* via FnZ and *Borrelia burgdorferi* via BBK32 (Schwarz-Linek et al. 2003; Atkin et al. 2010; Raibaud et al. 2005). For *S. pyogenes*, it could be shown that RGD-containing peptides and α5β1-inhibitory antibodies decreased internalization into epithelial cells (Ozeri et al. 1998; Cue et al. 1998; Cue et al. 2000). Similarly, internalization of *Yersinia pseudotuberculosis* YadA-expressing *E. coli* into HEp-2 cells could be blocked by GRGDS peptides and α5β1-inhibitory peptides

(Heise et al. 2006). Other pathogens are, however, capable of interacting directly with host cell α5β1 integrins via surface adhesins bearing a RGD- or functionally similar motifs, further demonstrating the importance of this interaction. *Bordetella pertussis* is harbors an RGD motif in the filamentous hemagglutinin protein, which promotes adhesion to and invasion of respiratory epithelial cells and thus could be specifically blocked by GRGDS peptides, α5β1-inhibitory antibodies and by an RGD>RAD mutation (Ishibashi et al. 2001). Another *Yersinia pseudotuberculosis* adhesin, 'invasin', acts similarly by binding with its C-type-lectin-like domain directly to β1 integrins. Mutating the participating Asp911 to Glu in invasin, similarly to the results presented here for RGD>RGE in Fn, prevented bacteria from entering M-cells (J. M. Leong et al. 1995), demonstrating the conserved function of the Asp residue in the interaction with cell surface integrins. In the cellular context, the importance of the RGD motif is well-known. Introducing a homozygous RGD>RGE mutation into mice leads to early embryonic lethality, similarly to in both α5- and β1-knock-out mice (Takahashi et al. 2007; Brakebusch et al. 2005; Fässler et al. 1995). Not only in the FN RGE/RGE mice themselves, but also in *in vitro* cultures of fibroblast-like cells isolated from these mice, Fn fibrillogenesis was still possible (Takahashi et al. 2007), a phenomenon we could also see in our assays (Figure 11). The authors could prove that αVβ3 integrins were the main receptors mediating α5β1-independent fibrillogenesis (Takahashi et al. 2007). In another model system, rat FN -/- cells could assemble FnΔRGD into fibrils in an αV-dependent fashion (Sottile et al. 2000). Accordingly, the interaction of αVβ3 integrins with Fn RGE-coated FnBPA-particles could be an explanation for the invasion into FN -/- cells seen in our assays (Figure 13B+D), as speculated elsewhere (Fowler et al. 2000). To further test this notion, we inhibited the αVβ3 receptor by specific peptides or αV-knockdown in various cell types. None of the applied conditions reduced adherence or invasion, but interestingly the opposite could be observed (Figure 19). A possible explanation could be an elevated surface expression of β1 integrins, because cross-talk between integrins and its effect on surface availability is a described phenomenon (Retta et al. 1999). This idea is supported by the fact that β1 integrins could be detected in Fn RGE-induced adhesion sites (Figure 21), and β1-heterodimers other than α5β1 have been shown to bind Fn (Leiss et al. 2008). We only saw a reduction in adherence and invasion, when cells were seeded on vitronectin (data not shown), since this has been described to deplete αVβ3 from the cell surface and to suppress assembly of Fns, especially Fn RGE, into fibrils (Fath et al. 1989; Bae et al. 2004; Takahashi et al. 2007). In our assays, we did not, however, observe the almost equally efficient αVβ3-mediated invasion of *S. pyogenes* into GD25 cells lacking β1 integrins that has been previously reported (Ozeri et al.

1998) (Figure 19A). In the same report, bacteria were not able to invade using soluble Fn 70 kDa, but in our assays, *FnBPA-S. carnosus* could invade (Figure 15A), pointing to a difference in the invasion mechanism, although both bind to Fn 30 kDa through a tandem β-zipper (Schwarz-Linek et al. 2003). It must be noted that we made every effort to exclude the presence of uncleaved full-length Fn in our assays (as documented in Figure 24). Very recently, an extended tandem β-zipper conformation could be demonstrated for streptococcal adhesin F1/Sfb1, binding additionally to the gelatin-binding domain in Fn I(8-9) (Atkin et al. 2010; Maurer et al. 2010) and this interaction has been shown to be important for invasion of epithelial cells (Talay et al. 2000). This extended conformation might explain the differences compared to α5β1-independent invasion by *S. aureus* FnBPA. However, invasion of *FnBPA-S. carnosus* using soluble Fn 30 kDa did not occur, suggesting a significance of the gelatin-binding domain in RGD-independent invasion.

We also investigated whether the synergy site located in the Fn III(9) repeat, adjacent to the RGD-containing Fn III(10) repeat, also contributes to adherence and invasion. The introduction of two RR1495/1500AA mutations into the PPSRN motif inactivates the synergy site, as demonstrated by mutational analyses (S. D. Redick et al. 2000). *FnBPA-S. carnosus* coated with Fn Syn$^-$ showed reduced adherence and invasion into FN -/- cells compared to Fn RGD, but interestingly the percentage of intracellular bacteria was not changed (Figure 14D). We therefore propose that the synergy site is important for adhesion, but not invasion. It is not yet clear, however, which cellular receptors mediate adhesion and invasion of bacteria via soluble Fn Syn$^-$. It has been described that adhesion of cells to recombinant, synergy site-mutated Fn III(6-10) (Danen et al. 1995) and synergy site-mutated full-length rat Fn (Sechler et al. 1997; Mao et al. 2006) is mediated either by αVβ3 integrins or artificially activated α5β1 integrins. Co-staining of α5 and Fn Syn$^-$ revealed almost no colocalization (Figure 12), so it seems likely that αVβ3 is the main receptor for Fn Syn$^-$ fibrillogenesis. However, there still seems to be a difference in cellular receptor usage and/or downstream signaling compared to with Fn RGE, because, once adherent, FN -/- cells were better able to internalize Fn Syn$^-$- than Fn RGE-coated FnBPA-bacteria, as demonstrated by the percentage of intracellular bacteria (Table 2). It is feasible that activated α5β1 integrins contribute to this phenomenon by binding to the RGD-site, which is not possible in Fn RGE. Thus, the exact mechanisms and signaling events downstream of soluble Fn RGE- and Fn Syn$^-$-mediated invasion remain to be elucidated.

During infection, bacteria encounter two forms of Fn, soluble and cellularly organized matrix Fn. We hypothesized that there may be a difference in the usage of both in FnBPA-dependent

attachment and invasion. Very surprisingly, our assays revealed firstly that invasion using organized Fn is decreased compared to for soluble Fn and, secondly, that the organization of Fn abrogated the inhibitory effects on adhesion and invasion of the RGE- and synergy site, respectively. Adherence of FnBPA-particles to organized Fn RGE was still lower compared to Fn RGD, but this might easily be explained by the reduced presence of cell surface-exposed matrix (Figure 11). However, the percentage of intracellular bacteria was comparable between the two Fns (Figure 16C). Cells transiently transfected to express Fn RGD and Fn Syn$^-$ displayed similar amounts of surface-exposed Fn, allowing equal binding of bacteria with no detectable differences in the number of intracellular bacteria. The presence of trace amounts of secreted soluble Fn could not completely be ruled out in our assays, because, although medium was changed and the cells were washed before infection, during the 60 min of infection, cells were still able to secrete Fn. To address whether this poses a problem, we incubated FnBPA-bacteria with medium incubated for 60 min with Fn-secreting cells, but were not able to detect any bacteria-bound Fn by Western blot analysis (data not shown). Bae and co-workers have speculated that integrin-bound Fn is released from the cell and presented on the cell-surface (Bae et al. 2004). This would resemble soluble Fn and therefore be accessible for FnBPA to bind. For future studies, therefore, either blocking endogenous protein synthesis by drugs such as cycloheximide or using FN -/- cells with an external source of Fn for matrix assembly would be a possibility to completely exclude the presence of soluble Fn. Such an approach was applied to demonstrate that invasion (albeit at a low level) was possible via organized Fn 70 kDa, but not via Fn 30 kDa (Figure 16F). Soluble Fn 70 kDa, which can also mediate invasion, should not have been present and has been shown to be assembled into short, linear fibrils by FN -/- cells (Tomasini-Johansson et al. 2001). Thus, we clearly show here that the polymerization state of Fn has an influence on the FnBPA-mediated infection of cells and that the RGD motif is dispensable for invasion via organized Fn.

In a pathological situation like infective endocarditis, FnBP-expressing bacteria in the blood stream should become instantly coated with plasma Fn due to the high amount of Fn in the blood plasma (~300 µg/ml). When facing sub-endothelial extracellular matrix in cardiac lesions, the question arises whether soluble or organized Fn promotes the adhesion to and invasion of cells or if bacteria-bound soluble Fn would inhibit binding to organized Fn. Most reports dealing with *S. aureus*-related infections were unable to inhibit adherence to and invasion of cells or adherence to immobilized Fn with soluble Fn, but could even demonstrate the significance of soluble Fn for adhesion and invasion (Sinha et al. 1999; Fowler et al. 2000; Edwards et al. 2010; Kuusela et al. 1985). Conversely, invasion of epithelial cells by

S. aureus strain 8325-4 could be inhibited, even using small amounts of soluble Fn (Dziewanowska et al. 1999; Dziewanowska et al. 2000). To decipher the roles of soluble plasma and cellularly organized Fn in *S. pyogenes* FnBP F1/Sfb1-mediated infection, Nyberg and co-workers used plasma Fn-deficient transgenic mice and the derived FN -/- cells, as were used in our assays (Nyberg et al. 2004). They could show that Fn-dependent uptake into cells was solely mediated by soluble Fn, both in the absence and presence of organized Fn. Interestingly, dissemination to the spleen after intraperitoneal injection of FnBP-bacteria was reduced in wild-type mice compared to plasma Fn-null mice and the lack of the Fn binding domain in F1/Sfb1 lead to an increased virulence in wild-type mice. The authors speculate that both soluble plasma Fn-mediated invasion and cellularly organized Fn-mediated adhesion retain bacteria at the infection site. In *S. aureus* FnBPA-mediated infections, the presence of FnBPs decreased virulence in a rat model of pneumonia (McElroy et al. 2002) but increased virulence in a rat model of endocarditis and mouse model of sepsis (Que et al. 2005; Piroth et al. 2008; Edwards et al. 2010). Confusingly, a recent report using a large number of clinical FnBPA/B-expressing *S. aureus* isolates in a rat model of endocarditis could again prove the importance of adhesion to Fn for pathogenesis in experimental endocarditis, but even the least adherent strain had the ability to induce infection (Ythier et al. 2010). Hence, it would be interesting to also test the infectivity of FnBPA-expressing staphylococci in soluble Fn-null mice to assess whether invasion at a much reduced level via cellularly organized Fn seen occurs, in our assays.

2. Role of Fn domains and the polymerization state of Fn on the motility of bacteria during infection

Investigating the motility parameters of bacteria during FnBPA/Fn-mediated cell surface transport extended the results obtained for adherence and invasion in the respective internalization assays. Firstly, coating of *FnBPA-S. carnosus* with soluble Fn (other than wild-type Fn RGD), i.e. Fn RGE, Fn Syn^- and Fn 70 kDa, reduced directionality and displacement of bacteria. Secondly, regarding FnBPA-mediated transport controlled by cell-attached polymerized/mature Fn, the modulatory effects of the RGD>RGE mutation in Fn was abolished.

In our assays, as opposed to in flow conditions, directional movement of bacteria was in theory only possible by two mechanisms, either by rapid actin polymerization inducing so-

called ‘comet tails’ (J. M. Stevens et al. 2006; A. Schröder et al. 2006) or by integrin-mediated connection to the rearward moving actin cytoskeleton (Cai et al. 2006; Choquet et al. 1997). Both have already been observed in the FnBPA/Fn-mediated infection of endothelial cells (A. Schröder et al. 2006). In our assays, however, track velocities of >10 µm/min, which would resemble movement by actin comet tails, were not detected. This might be due to the different cell type that was used for our investigations. Further indication that the FnBPA/Fn-particles in our assays were connected to the rearward actin flow, is provided by the fact that our recorded track velocities match the published data on rearward flowing actin and Fn/integrin-ligated particles (Alexandrova et al. 2008; Cai et al. 2006; Choquet et al. 1997; Coussen et al. 2002; Nishizaka et al. 2000). It is also known that the amount and density of Fn bound to the surface of particles has an influence on motility parameters (Roca-Cusachs et al. 2009; Coussen et al. 2002; Choquet et al. 1997). It was therefore important to verify that equal amounts of the various soluble Fns were bound to the particles in our experiments (Figure 9). This allowed us to draw the conclusion that mutating either the RGD motif or the synergy site impaired the connection of the integrin to the actin cytoskeleton. An explanation for these effects could be alterations in the affinity state of integrins and/or their downstream signaling, both of which are known to interfere with the integrin-actin connection (Roca-Cusachs et al. 2009; A. Schröder et al. 2006; X. Zhang et al. 2008; Coussen et al. 2002; Giannone et al. 2003). Our experiments showed no involvements of the β1 integrin MP/MD NPXY motifs, known to regulate integrin signaling, in the motility and invasion of cells by bacteria, even though a previous report could show an inhibitory effect on Fn-mediated uptake of *S. aureus* (Fowler et al. 2003). This could be explained by the different cells that have been used in these assays and is supported by the fact that the transgenic YY>FF-mice, from which the beta1-FF cells used in our study are derived, also showed no obvious phenotype compared to the control mice (Czuchra et al. 2006). Biochemical assays to detect Fn RGE- and Fn Syn$^-$-dependent changes in the downstream signaling during infection, for example FAK phosphorylation at Tyr397 (Agerer et al. 2005), should therefore be a subject of future investigations. An involvement of the synergy site in FAK phosphorylation and Rho/Rac acitvity has already been shown in assays analyzing spreading of fibroblasts on Fn (Hotchin et al. 1999).

The connection of integrin cytoplasmic tails to the cytoskeleton is mediated by adaptor and scaffolding proteins and so we therefore sought to determine the molecular composition of the Fn RGE-induced adhesion sites. We found the majority of the previously identified proteins to be absent from Fn RGE-induced sites, except for talin. Talin is the major protein that links

integrins to the cytoskeleton and a prerequisite for this connection (Critchley et al. 2008; X. Zhang et al. 2008; Giannone et al. 2003). It also serves as a scaffold for the other adaptor proteins such as vinculin, although some of the interaction sites are cryptic and only accessible after conformational changes in the molecule, e.g. during mechanotransduction. Hence, it could be speculated that integrin binding of Fn Syn$^-$ or Fn RGE fails to generate mechanosensory stimuli, meaning that important adaptor proteins cannot then strengthen the link to the actin cytoskeleton. This would explain why directionality values for bacterial movement were decreased compared to for Fn RGD. In some experiments, especially in the case of Fn Syn$^-$-coating, particles could be seen to detach having traveled only a short distance (data not shown). It can be speculated that this is caused by a destabilized integrin-cytoskeleton linkage (Nishizaka et al. 2000), supporting the idea that a fully activated α5β1 integrin receptor, resulting from synergistic binding of type III modules 9 and 10, as well as cooperative binding by αVβ3-talin (Roca-Cusachs et al. 2009) is needed to permit efficient coupling to the cytoskeleton. Establishing, whether the activation state of integrins is changed upon binding of the various Fns used in this study, would help further understand the individual roles of Fn domains during infection. Since it could be shown that the adhesion structures induced by *S. aureus* have a fibrillary adhesion-like composition (A. Schröder et al. 2006), it would be interesting to see whether the fibrillary-adhesion- and activation-specific α5β1 integrin antibody SNAKA-51 is able to recognize and modulate these in the infection process (Clark et al. 2005). Additionally, using atomic force microscopy (AFM) with Fn fragments it could be shown that Fn RGE and Fn Syn$^-$ contribute differently to the binding kinetics in Fn-integrin interactions, defining inner and outer energy barriers in the adhesion complex (Li et al. 2003; Kokkoli et al. 2004). Very recently, a report could show, AFM, the activation of αVβ3 by acidic extracellular pH, e.g. during the early stages of wound healing (Paradise et al. 2011). We are currently applying single-cell force spectroscopy, an AFM variant, to further characterize the binding complex of our various full-length Fn proteins in conjunction with FnBPA-functionalized microspheres and living FN -/- cells. This might help further understanding of the specific roles of the Fn domains as seen in our assays.

In our motility assays, organized Fn on the surface of cells also provided a molecular basis for the adherence of bacteria. However, whether the fibrils themselves provided bacterial displacement is uncertain. The velocity of bacteria adherent to organized Fn was lower compared to bacteria coated with soluble Fn (~ 0.6 µm/min and ~1 µm/min, respectively, see Table 4), but was still 5-fold higher than the reported velocities for Fn fibril elongation or integrin movement (Ohashi et al. 2002; Pankov et al. 2000). Whether surface Fn fibers can be

transported with the rearward cytoskeleton has, to our knowledge, not yet been reported. Hence, it is possible that the velocity is lower because either the fibrils display a more rigid and connected network, which provides more resistance or because very short fibrils (or even residual soluble Fn) bound to the integrins were sterically hindered during the transport of bacteria. To test this, fluorescently labeled Fn (recombinant with e.g. FITC or endogenously expressed with, for example, GFP-tag) could be used to determine the localization of bacteria in relation to Fn fibrils during transport, by time-lapse microscopy. Modern super-resolution imaging techniques could overcome the problems of precisely localizing the bacteria to Fn fibrils (Toomre et al. 2010; Coombes et al. 2010). However, the polymerization state of Fn also abrogated the modulatory roles seen for the synergy site and the RGD motif in soluble Fn-mediated motility of FnBPA-bacteria. This role of Fn should be considered when developing anti-adhesive/invasive strategies for the future treatment of *S. aureus* infections.

E. Material and Methods

1. Devices

1.1. General devices

Äkta Purifier System	GE Healthcare, Munich (D)
Cassette for film exposure	Hartenstein, Würzburg (D)
Cell counter	Neubauer improved, Hartenstein, Würzburg (D)
Cell transfection	Nucleofector II, Amaxa, Cologne (D) Neon Transfection System, Invitrogen, Darmstadt (D)
Centrifuge	Sorvall RC-5B, Sorvall RC 28S, Thermo Scientific, Rockford (USA) Table centrifuges: 5417R, 5810R, Eppendorf, Hamburg (D); 3-18K, Sigma, Osterode (D)
Chromatography columns	HiTrap NHS-activated HP 1 ml columns, Superdex 75 10/300 GL, Superdex 200 10/300 GL, GE Healthcare, Munich (D)
Electrophoresis	Agarose gels: Roth, Karlsruhe (D); OWL EasyCast, Thermo Scientific, Rockford (USA); SDS-PAGE: Mini-Protean II Cell, BioRad, Munich (D)
Gel dryer	Gel dryer 543, BioRad, Munich (D)
Incubator	BBD 6220, Heraeus, Hanau (D); CB series, Binder, Tuttlingen (D)
Incubator (shaking)	Certomat BS-1, Sartorius, Göttingen (D); Thermomixer comfort / compact, Eppendorf, Hamburg (D)
Magnetic stirrer	RCT-basic, IKA-Labortechnik, Staufen (D)
Microwave	900 W, Panasonic, Osaka (J)
PCR-Cycler	Primus 96, MWG-Biotech, Ebersberg (D); Mastercycler gradient, Eppendorf, Hamburg (D)
pH Meter	Seven easy, Mettler-Toledo, Giessen (D)
Photometer	Ultrospec 3100 pro, Amersham / GE Healthcare Europe, Munich (D); NanoDrop 2000,

	ThermoScientific, Rockford (USA)
Pipettes	2, 10, 20, 100, 200, 1000 µl, Gilson, DenHaag, Netherlands; 5000 µl Research, Eppendorf, Hamburg (D); Accu-jet pro, Brand, Wertheim (D)
Power supply	Power Pac 200 / universal, BioRad, Munich (D)
Processor for X-ray development	Curix 60, Agfa, Mortsel (B)
Refrigerator	profi line, Liebherr, Bulle (CH)
Balance	440-47N, Kern, Balingen-Frommern (D)
Scanner	CanoScan 4400F, Canon, Amsterdam (NL)
Sonifier	digital Sonifier 250-D, Branson, Danbury (USA)
UV-transilluminator	ETX, Vilber Lourmat, Eberhardzell (D)
UV-transilluminator + documentation	ChemiDoc XRS, BioRad, Munich (D)
Vortex	REAX top, Heidolph Instruments, Schwabach (D)
Water bath	GFL Typ 1013, GFL, Burgwedel (D)
Western blot apparatus	Micro Bio Tec Brand, Gießen (D)

1.2. Microscopes

LiveCell Spinning Disk Confocal:

Provider	Improvision, Coventry (UK)
Stand	Axiovert 200M, Zeiss, Jena (D)
Objective	Plan-Apochromat 63x / 1.4 Ph3 oil immersion
Confocal unit	Spinning disk CSU22, Yokogawa, Tokyo (J)
Camera	EM-CCD C9100-02, Hamamatsu (J)
Laser	Cobolt Calypso CW 491 nm, Cobolt Jive 561 nm, Stockholm (S)
Laser combiner	LMM5, Spectral Applied Research, Richmond Hill (CDN)
Emission filters	ET 525/50 (green), ET 620/60 (red), Chroma Technology, Rockingham (USA)
UV lamp	X-cite series 120 W with Hg-lamp, EXFO, Mississauga (CDN)
Halogen lamp	Standard housing 100 W, Zeiss, Jena (D)

Incubation chamber	Temperature / humidity / CO_2 control, Solent Scientific, Regensworth (UK)
Equipment	Motorized BioPrecision inverted XY stage and PiezoZ stage, Ludl Electronic Products, Hawthorne (USA)
Software	Volocity versions 4.2-5.4, PerkinElmer, Waltham (USA)

Epifluorescence microscope I:

Provider	Visitron Systems, Puchheim (D)
Stand	Axioplan (upright), Zeiss, Jena (D)
Objective	Plan-Neofluar 40x / 0.75 Ph2
Camera	CCD SPOT Pursuit 1.4MP monochrome, Diagnostic Instruments, Sterling Heights (USA)
Emission filters	Filter set 02 (blue) / 09 (green) / 15 (red), Zeiss, Jena (D)
UV lamp	HBO 50 W with Hg lamp, Zeiss, Jena (D)
Halogen lamp	Standard housing 100 W, Zeiss, Jena (D)
Software	SPOT version 4.6, Diagnostic Instruments, Sterling Heights (USA)

Epifluorescence microscope II:

Provider	Zeiss, Jena (D)
Stand	Axiovert 200M
Objectives	LD Plan-Neofluar 20x / 0.4 Ph2 korr
	Plan-Neofluar 40x / 0.75
Camera	CCD Axiocam MRm 1.4MP monochrome
Emission filters	Filter set 49 (blue) / 44 (green) / 43 (red) / 50 (far-red)
UV lamp	HBO 100W with Hg lamp
Halogen lamp	Standard housing 100 W
Software	Zeiss Axiovision version 4.7

Transmitted light microscope I:

Provider	Zeiss, Jena (D)
Stand	Axiovert 25 (inverted)
Objectives	A-Plan 10x / 0.25 Ph1
	LD A-Plan 20x / 0.3 Ph1
	LD Achroplan 40x / 0.6 Ph2
Emission filter	Filter set 02 (blue) / 09 (green)
UV lamp	HBO 50 W with Hg lamp
Halogen lamp	Standard housing 30 W

Transmitted light microscope II:

Provider	Nikon, Tokyo (J)
Stand	Eclipse TS100
Objectives	Plan Fluor 4x / 0.13 PhL
	LWD 10x / 0.25 Ph1
	LWD 20x / 0.4 Ph1
	LWD 40x / 0.55 Ph1
Camera	Nikon D5000 digital camera
Emission filters	Filter set HQ EGFP (green) / HQ Calcium Crimson, Chroma Technology, Rockingham (USA)
UV lamp	Nikon Intensilight 130 W with Hg lamp
Halogen lamp	Standard housing 30 W

2. Disposables

Conical centrifuge tubes	Sterile 15 ml / 50 ml, BD Biosciences, New Jersey (USA)
Cell culture dishes	35 mm µdish, Ibidi, Munich (D); 10 cm SUREGrip, Sarstedt, Nümbrecht (D)
Cell culture flasks	T-25 nunclonΔ, ThermoScientific / Nunc, Rockford (USA)
Centrifugal concentrator columns	Vivaspin 2 / 6, Sartorius Stedim Biotech,

	Göttingen (D)
Cryo tubes	1.6 ml, Sarstedt, Nümbrecht (D)
Cuvettes	1.5 ml semi-micro, Brand, Wertheim (D); 50 µl micro UVette, Eppendorf, Hamburg (D)
Filter papers for Western blot	190 g / m^2, Hartenstein, Würzburg (D)
Glass coverslips	round 12 mm diameter No. 1, Hartenstein, Würzburg (D)
Glass pasteur pipettes	230 mm, Heinz Herenz Medizinalbedarf, Hamburg (D)
Inoculating loops	10 µl, Sarstedt, Nümbrecht (D)
Microscopy slides	76 x 26 mm cleaned with frosted end, Karl Hecht, Sondheim (D)
Multiwell plates	6- / 12-well nunclonΔ, ThermoScientific / Nunc, Rockford (USA)
Petri dish	92 x 16mm, Nerbe plus, Winsen/Luhe (D)
Reaction tubes	Standard 0.5, 1.5, 2 ml, and Protein LoBind 1.5 ml, Eppendorf, Hamburg (D); 0.2 ml, Biozym Scientific, Hessisch Oldendorf (D)
Pipette tips	Sterile Biosphere filter tips and non-sterile 10, 200, 1000 µl, Sarstedt, Nümbrecht (D); 5000 µl, Eppendorf, Hamburg (D); Prot / Elec tips, BioRad, Munich (D)
Polypropylene columns	5 ml, Qiagen, Hilden (D)
PVDF membrane	Immobilon-P, 0.45 µm pore size, Millipore, Billerica (USA)
Serological pipettes	Sterile 2, 5, 10, 25 ml, BD Biosciences, New Jersey (USA)
Scalpel	Sterile, B. Braun, Melsungen (D)
Syringe filters	SFCA 0.2 µm, Thermo Scientific / Nalgene, Rockford (USA)
Syringes	Sterile 1, 2, 5, 10, 25 ml, B. Braun, Melsungen (D)

3. Kits and Enzymes

α-Chymotrypsin	Sigma-Aldrich, Munich (D)
Expand Long Template PCR System	Roche, Mannheim (D)
FastDigest restriction enzymes (EcoRI, XbaI, XhoI)	Fermentas, St. Leon-Rot (D)
GoTaq DNA Polymerase	Promega, Madison (USA)
PCR Extender System	5 Prime, Hamburg (D)
Revert Aid First Strand cDNA Synthesis Kit	Fermentas, St. Leon-Rot (D)
T4 DNA Ligase	Promega, Madison (USA)
TA Cloning Kit (with pCR2.1 and One Shot competent TOP10 E. coli)	Invitrogen, Darmstadt (D)
TrypLE Express	Invitrogen, Darmstadt (D)
Trypsin 0.05 %, 0.53 mM EDTA x 4 Na	Invitrogen, Darmstadt (D)
QuikChangeII XL Site-Directed Mutagenesis Kit	Strategene, Amsterdam (NL)
QIAEX II Gel Extraction Kit	Qiagen, Hilden (D)
NucleoSpin Extract II Kit	Macherey-Nagel, Düren (D)
EndoFree Plasmid Maxi Kit	Qiagen, Hilden (D)
HUVEC Nucleofector Kit	Lonza, Basel (CH)
Neon Transfection System 100 µl Kit	Invitrogen, Darmstadt (D)
SuperSignal West Femto detection reagents	Thermo Scientific, Rockford (USA)
ECL Western Blotting detection reagents	GE Healthcare, Munich (D)
BioRad Protein Assay	BioRad, Munich (D)
Complete Mini Protease Inhibitor Cocktail Tablets	Roche, Mannheim (D)
RNeasy Mini Kit	Qiagen, Hilden (D)

4. Chemicals and antibiotics

All chemicals and antibiotics were obtained from: Amersham / GE Healthcare (Munich [D]), Biozym (Oldendorf [D]), Dianova (Hamburg, [D]), Fermentas (St. Leon-Rot [D]), Invitrogen (Karlsruhe [D]), Merck (Darmstadt [D]), PAA (Pasching, [A]), PromoCell (Heidelberg [D]), Roche (Mannheim [D]) Roth (Karlsruhe [D]) and Sigma-Aldrich (Munich [D]).

4.1. Antibiotics

Antibiotic	Dissolved in	Final concentration
Ampicillin	ddH_2O	100 µg/ml
Chloramphenicol	Ethanol	20 µg/ml
Kanamycin	ddH_2O	50 µg/ml

4.2. Inhibitory agents

siRNA

For RNA interference, a pool (siGENOME SMARTpool) of 4 different small interfering ribonucleic acids (siRNA) against human αV integrin and a non-targeting (nt) control were obtained from ThermoScientific (Rockford [USA]). In order to validate functional knock-down of αV integrins, various assays were used. Human umbilical cord vein endothelial cells (HUVECs) were transfected for 48, 72 and 96 h with siRNAs and the amount of αV protein was determined by Western blot (Figure 22, *top left*). Between 72 and 96 h after transfection there was no further decrease in the amount of αV and the knock-down after 72 h was also visible by indirect immunofluorescence (Figure 22, *bottom*). Although knock-down was not complete, αV function was impaired as validated by spreading assays (Figure 22, *top right*). After 72 h of transfection with αV siRNA, HUVEC cells showed impaired αVβ3-mediated spreading on vitronectin (Horton 1997) compared to nt siRNA.

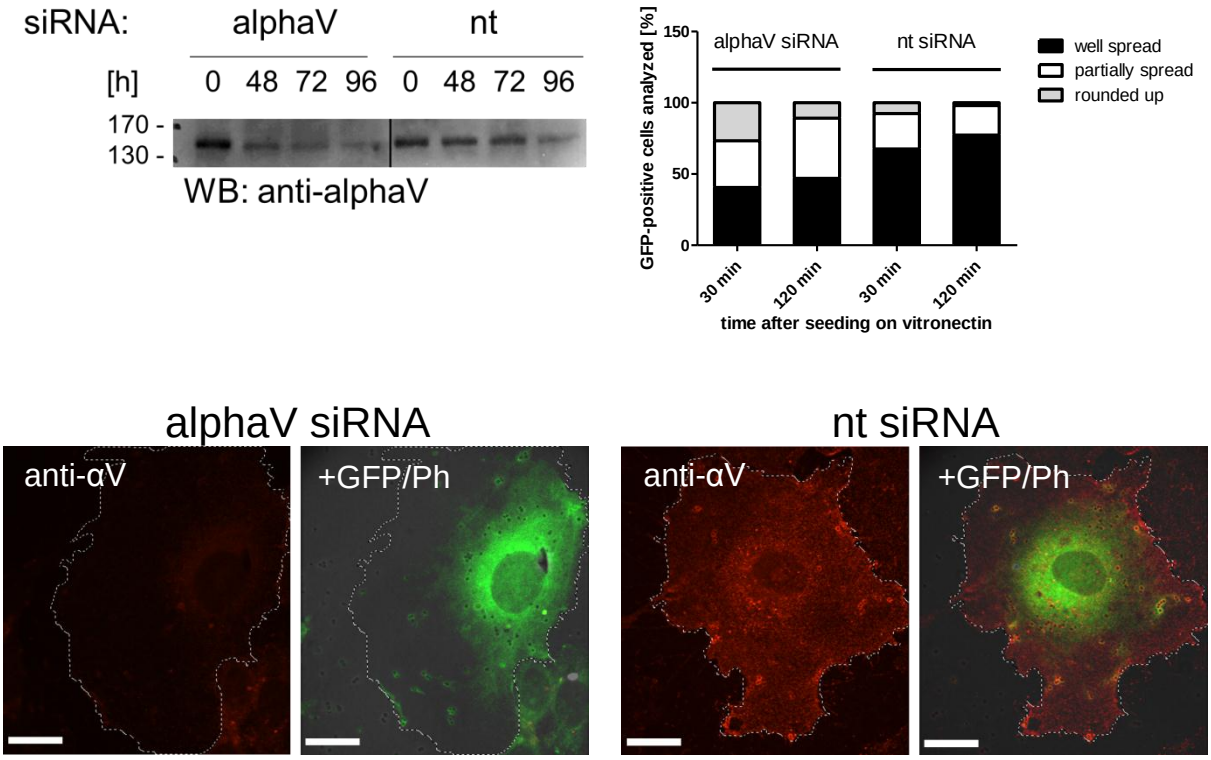

Figure 22: Functional knock-down of αV integrin in HUVEC using siRNA.
HUVEC were transfected with siRNA for αV integrin (alphaV), non-targeting control (nt) or plasmid encoding GFP (GFP). (Top panel, *left*) At indicated timepoints after transfection with siRNA, equal amounts of protein were analyzed by Western blot using anti-αV antibody. (Top panel, *right*) After 72 h of transfection with siRNA and GFP plasmid, cells were seeded on vitronectin-coated coverslips for 30 min or 120 min and the degree of spreading analyzed microscopically. Values represent mean spreading from one representative experiment with at least 50 cells analyzed per condition. (Bottom panel) After 72 h of transfection with siRNA and GFP plasmid, cells were infected with *FnBPA-S. carnosus* for 60 min and stained with rabbit-anti-αV and anti-rabbit-Alexa568 antibodies. All pictures were taken with the same settings to obtain comparable fluorescence signals.

Cyclic peptides

To specifically block αV integrins, cyclic peptides cyclo-(Arg-Gly-Asp-D-Phe-Val) [cycRGD] and the control peptide cyclo-(Arg-Ala-Asp-D-Phe-Val) [cycRAD] were purchased from Bachem (Weil am Rhein, [D]). To validate the αVβ3-specific inhibition of the peptides, trypsinized HUVECs were incubated with 10 µg/ml of the peptides and seeded for 2 h on vitronectin or gelatin. αVβ3-mediated spreading on these substrates was greatly reduced by cycRGD compared to the control peptide cycRAD (Figure 23).

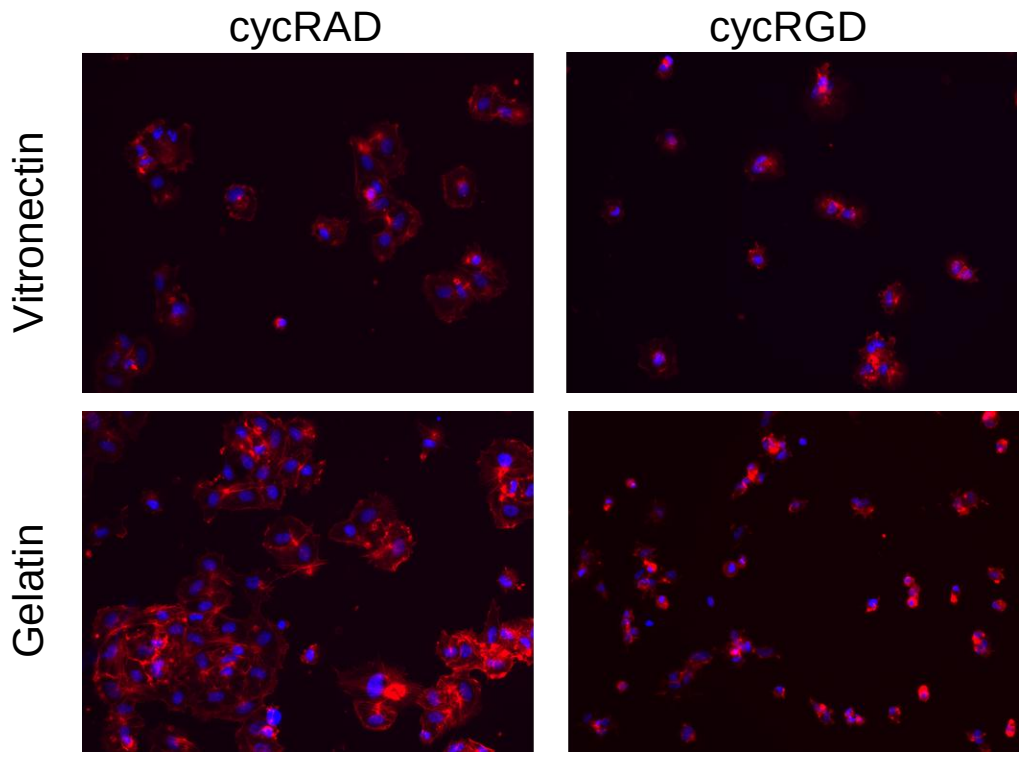

Figure 23: Functional inhibition of αVβ3 integrin receptor in HUVEC using cyclic peptides.
HUVECs were trypsinized and incubated for 1 h in basal medium with 10 µg/ml cyclic peptides specific for αVβ3 (cycRGD) or unspecific control (cycRAD). Cells were seeded for 2 h on vitronectin- or gelatin-coated coverslips and stained for nuclei (DAPI, blue) and F-actin (Phalloidin-Alexa568, red).

4.3. Buffers

Anode I		**Anode II**	
Tris/HCl	0.3 M (7.26 g)	Tris/HCl	25 mM (0.605 g)
Methanol	10 % (20 ml)	Methanol	10 % (20 ml)
ddH_2O	200 ml, pH 10.4	ddH_2O	200 ml, pH 10.4

Cathode buffer		**Coomassie staining solution**	
Tris/HCl	25 mM (0.605 g)	Coomassie Brilliant Blue R-250	0.1 %
6-amino-n-caproic acid	40 mM (1.0494 g)	Methanol	25 %
Methanol	10 % (20 ml)	Glacial acetic acid	10 %
ddH_2O	200 ml, pH 9.4	ddH_2O	

Destain solution

Methanol	25 %
Glacial acetic acid	10 %
ddH_2O	

MOPS buffer (10x)

MOPS	400 mM
Sodium acetate	100 mM
EDTA	10 mM
ddH_2O	pH 7.0

PBS (10x)

NaCl	1.37 M (80 g)
KCl	26.5 mM (2 g)
Na_2HPO_4	0.1 M (17.8 g)
KH_2PO_4	17.6 mM (2.4 g)
ddH_2O	1 l, pH 7.7

PBST (10x)

NaCl	1.37 M (80 g)
KCl	26.5 mM (2 g)
Na_2HPO_4	0.1 M (17.8 g)
KH_2PO_4	17.6 mM (2.4 g)
Tween 20	0.5 % (5 ml)
ddH_2O	1 l, pH 7.7

Resolving gel buffer

Tris/HCl	1.5 M (45.3 g)
SDS	1 g
ddH_2O	250 ml, pH 8.8

SDS loading buffer (5x)

0.5 M Tris/HCl	5 ml, pH 6.8
Glycerol	2 ml
SDS	0.8 g
0.5 % Bromophenol blue	1 ml
ddH_2O	2 ml

SDS-PAGE running buffer (10x)

Tris-Base	0.025 M (30.3 g)
Glycine	0.192 M (144 g)
SDS	0.1 % (10 g)
ddH_2O	1 l

TAE (50x)

Tris Base	242 g
Glacial acetic acid	57.1
0.5 M EDTA	100 ml
ddH_2O	1 l

5. Fibronectins

5.1. Secreted and cellularly organized Fns

The various mouse cell lines used express and secrete fibronectin (Fn) into the cell culture supernatant, generating conditioned medium. Secreted Fn could either be assembled into fibrils or be used to coat particles (see 12.10). The following full-length Fns were applied in the assays:

Fibronectins	**Relevant characteristic and origin**
Fn RGD	Wild-type Fn expressed by FN fl/fl or mFNwt-transfected FN -/- cells
Fn RGE	RGD>RGE-mutated Fn expressed by FN RGE/RGE cells
Fn Syn^-	Synergy site-mutated Fn expressed by mFNwt_RR1495/1500AA-transfected FN -/- cells

5.2. Proteolytic Fn fragments

30 kDa and 70 kDa proteolytic fragments from human plasma Fn were purchased from Sigma-Aldrich (Munich, [D]). The purity of the proteolytic fragments was ~90 % in accordance with the specifications of the manufacturer. However, SDS-PAGE revealed high molecular weight bands in the original sample (Figure 24, lanes “30” and “70”, respectively), which were positive for Fn in the immunoblot (Figure 24, Fn means full-length human plasma Fn as positive control). To avoid interference with downstream assays, size-exclusion chromatography was applied to remove the high molecular weight bands. The 30 kDa and 70 kDa fragments were eluted as sharp and clear peaks. After collecting the correct fractions, no high molecular weight bands then contaminated the sample (Figure 24, fraction 9 for Fn 30 kDa and fraction 11+12 for Fn 70 kDa). After measuring the protein concentration, equivalent amounts (10 µg) of 30 kDa and 70 kDa Fn were used for coating beads or bacteria.

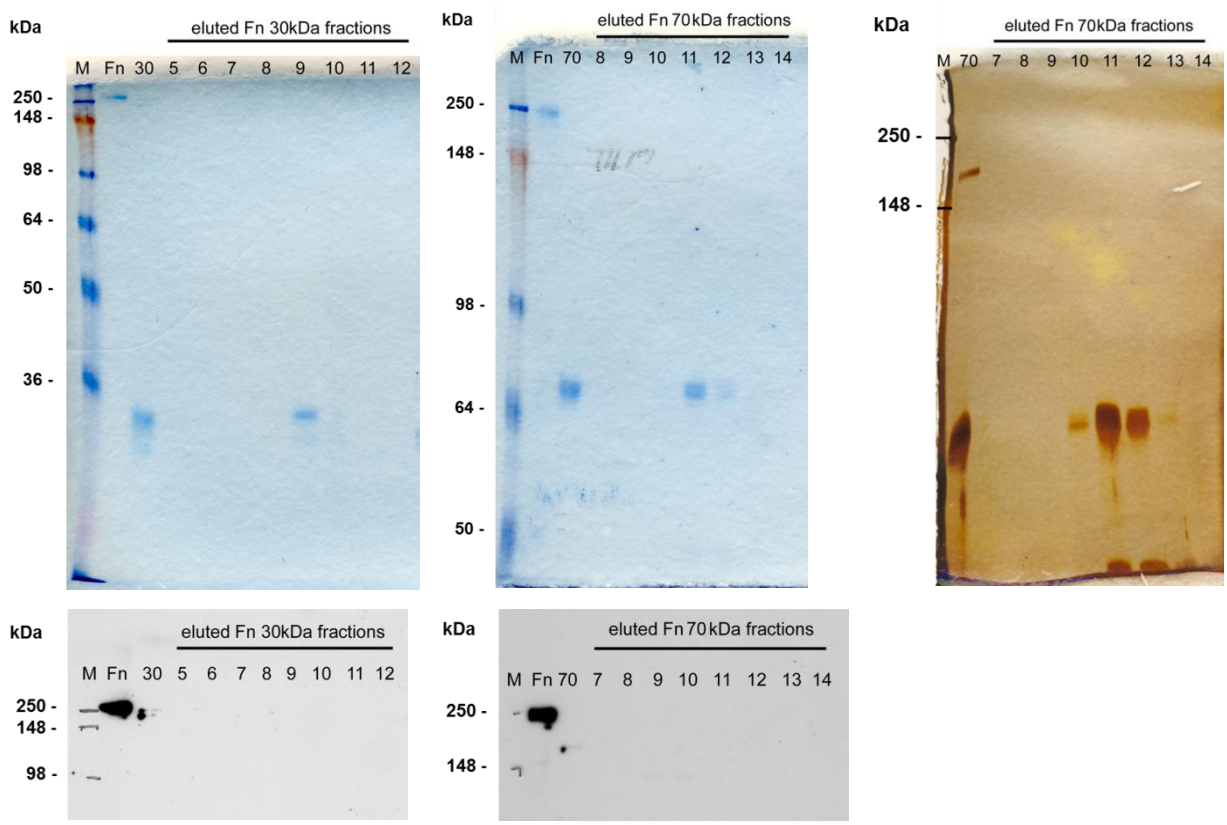

Figure 24: Purification of 30 kDa and 70 kDa proteolytic fragments from human plasma Fn by size-exclusion chromatography.
Left panel: Fn 30 kDa before purification with Fn-positive high MW contaminants (lanes "30") and the eluted fractions "5-12", with fraction "9" containing solely Fn 30 kDa. *Middle + right panel*: Fn 70 kDa before purification with Fn-positive high MW contaminants (lanes "70") and the eluted fractions "8-14", with fraction "11+12" containing solely Fn 70 kDa. *Top row*: Coomassie-stained (*left+middle*) and silver-stained (*right*) SDS-gels. *Bottom row*: Western blot against Fn of the same samples as depicted in the SDS gels.

6. Bacterial strains

All bacteria were grown in LB-medium (Roth, Karlsruhe, [D]) or plated on LB-Agar (Roth, Karlsruhe, [D]) containing the appropriate antibiotics.

6.1. *E. coli* strains

Strain	Genotype	Reference
TOP10	F$^-$ *mcr*A Δ(*mrr-hsd*RMS-*mcr*BC) φ80*lac*ZΔM15Δ*lac*X74 *nup*G *rec*A1 *ara*D139 Δ(*ara-leu*)7697 *gal*E15 *gal*K16 *rps*L(Str^R) *end*A1 λ$^-$	(Grant et al. 1990)
BL21	F$^-$ *ompT gal dcm lon hsdS$_B$*(r_B- m_B-) λ	(Studier et al. 1986)

6.2. *S. carnosus* strains

Strain	Relevant characteristic	Reference
TM300	No expression of adhesins	(Schleifer et al. 1982)
TM300(pFNBA4)	Overexpression of FnBPA from *S. aureus* strain 8325-4 in *S. carnosus* TM300	(Sinha et al. 2000)

7. Plasmids

Plasmid name	Description	Reference
pcDNA3.1(-)	Mammalian expression vector; empty vector used as a negative control	Invitrogen
mFNwt	pcDNA3.1(-)-mFNwt; expression of murine wild-type Fn RGD	This study
mFNwt_RR1495/1500AA	pcDNA3.1(-)-mFNwt_RRAA; expression of murine Fn Syn$^-$ with two inactivating RR1495/1500AA mutations in the synergy site	This study
pCR2.1	Cloning vector with two T overhangs	Invitrogen
IMAGE:3915400 (5')	pCMV-SPORT6 containing a part of human Tensin-3 cDNA sequence (RefSeq BE888943)	LGC Standards
pGEX-4T	Vector for prokaryotic protein expression	GE Healthcare
GST-FnBPA	pGEX-fnbpa-DuD4; expression of *S. aureus* FnBPA domains Du-D4 (aa 605-881) with N-terminal GST-tag	(A. Schröder et al. 2006)
GST-hTNS-3	pGEX-hTNS-3; expression of a human Tensin-3 fragment (aa 399-597) with N-terminal GST-tag	This study
pmaxGFP	Expression of green fluorescent protein	Lonza

8. Primers

Primers for cloning hTNS-3 from IMAGE:3915400 (5') into pGEX-4T-3 via EcoRI/XhoI:

hT3_EcoRI_F1 5‘ – ACTCTAC**GAATTC**TGCCAGGAC – 3‘

hT3_XhoI_R1 5’ – TATAC**CTCGAG**ACCTACAACCATCT – 3‘

Primers for sequencing pGEX-4T constructs:

pGEX 5’ 5’ – GGGCTGGCAAGCCACGTTTGGTG – 3‘

pGEX 3‘ 5’ – CCGGGAGCTGCATGTGTCAGAGG – 3‘

Primers for cloning murine Fn (RefSeq NM_010233) from cytosolic RNA including reverse transcription and sub-cloning into pcDNA3.1(-) via XbaI (recognition sequences in bold letters):

oligo(dT)18 5’ – $(T)_{18}$ – 3’

mFN_fwd2 5’ – **TCTAGA**CCTCCTGGGGAGGGCGACTC – 3‘

mFN_rev1 5’ – **TCTAGA**CCACGGGGCGATGCTTGGAG – 3‘

Primers for introducing two R>A mutations at positions aa 1495 and 1500 in the synergy site of murine Fn using the QuikChangeII XL Site-Directed Mutagenesis Kit (Stratagene) and the Fn RGD-encoding mFNwt plasmid (mutated triplets in bold letters):

mFN_RRAA_F2

5’ – CCCAGGCAGGAT**GCA**GTGCCGCCCTCG**GCG**AATTCCATCACC – 3‘

mFN_RRAA_R2

5’ – GGTGATGGAATT**CGC**CGAGGGCGGCAC**TGC**ATCCTGCCTGGG – 3‘

Primers for sequencing the cloned Fn transcripts:

mFN_walk_F1 5’ – CAGAAACAGATGCAACGATC – 3‘

mFN_walk_F2 5’ – CACAACCAATGAAGGGGTC – 3’

mFN_walk_F3 5’ – GGTGACCGGAGAGACTGC – 3‘

mFN_walk_F4 5’ – ACATGGGCAGAGGCTGC – 3‘

mFN_walk_F5 5’ – ACTGTCTCCTGGGAGAGGAG – 3‘

mFN_walk_F6 5’ – CGAACAACATGAGAGCATCC – 3‘

mFN_walk_F7 5’ – CATCAAAAACTAAAACTGCCAG – 3‘

mFN_walk_F8	5’ – GCTACAGAGACCACCATCAC – 3‘
mFN_walk_F9	5’ – ACCCCCGTCAGGCTTAG – 3‘
mFN_walk_R1	5’ – GTAGCCAGTGATATCTGGGG – 3‘
T7	5’ – TAATACGACTCACTATAGGG – 3‘
SP6	5’ – TATTTAGGTGACACTATAG – 3’

9. Antibodies

9.1. Primary antibodies

The following antibodies were used either for indirect immunofluorescence or Western blot analysis:

Antigen	**Species**	**Supplier**
α5 integrin chain	rat	BD Biosciences
αV integrin	rabbit	Millipore
β1 integrin	armenian hamster	Pharmingen
FAK	mouse	BD Biosciences
fibronectin	rabbit	Sigma-Aldrich
GST	rabbit	BD Biosciences
paxillin	mouse	Transduction Lab
phospho-tyrosine (4G10)	mouse	Millipore
Staphylococci	rabbit	(Mack et al. 1992)
talin (8d4)	mouse	Sigma-Aldrich
tensin-3	rabbit	this study
vinculin	mouse	Sigma-Aldrich

Actin was stained with AlexaFluor 488- or AlexaFluor 568-labeled phalloidin (Invitrogen) and DNA was stained with DAPI (Invitrogen).

9.2. Secondary antibodies

The following secondary antibodies were used for indirect immunofluoresence or Western blot analysis:

Description	Supplier
AlexaFluor 488 goat anti mouse	Invitrogen
AlexaFluor 488 goat anti rabbit	Invitrogen
AlexaFluor 568 goat anti mouse	Invitrogen
AlexaFluor 568 goat anti rabbit	Invitrogen
AlexaFluor 568 goat anti rat	Invitrogen
DyLight 488 goat anti hamster (syrian + armenian)	Rockland
Cy5 donkey anti rabbit	Millipore
Horseradish peroxidase-linked anti rabbit IgG	GE Healthcare

10. Molecular Biology Methods

10.1. Isolation of RNA

Cytoplasmic RNA was isolated from eukaryotic cells with the RNeasy Mini Kit (Qiagen) according to the manufacturer's protocol from May 2006. ~4.8 x 10^6 cells were lysed with RLN buffer without the addition of DTT or RNase inhibitors. For eluting, 30 µl RNase-free water was passed twice over the column, yielding a final concentration of c > 0.5 µg/µl.

10.2. Agarose gel analysis of RNA

The integrity of isolated RNA was verified by agarose gel analysis. 1-5 µg RNA was incubated at 70 °C for 10 min in RNA sample-buffer and loaded onto a 1 % agarose gel (MOPS system). Visualized by ultra-violet (UV) light, RNA displayed three bands, representing 28S, 18S and 5S ribosomal RNA and if smearing was absent, was considered suitable for further proceedings.

10.3. cDNA synthesis

To obtain complementary DNA (cDNA), cytosolic RNA was reverse-transcribed (RT) using the Revert Aid First Strand cDNA Synthesis Kit (Fermentas) according to the manufacturer's protocol. In order to transcribe solely messenger RNA (mRNA), an oligo$(dT)_{18}$ primer included with the kit was chosen for the RT reaction together with 100-200 ng RNA.

10.4. Standard PCR

Polymerase chain reactions (PCR) for preparative gels were performed in 0.2 ml reaction tubes in a volume of 50 µl using the PCR Extender System (5 Prime), which contains proof-reading polymerase for accurate amplification. The reaction mixture was kept on ice during pipetting to avoid the formation of unspecific products.

Reaction setup and conditions:

	Temp.	**Time**	**Cycles**
Initial denaturation	94 °C	2 min	1
Denaturation	94 °C	30 s	29
Annealing	58 °C	30 s	
Elongation	72 °C	1 min / 1 kbp	
Final elongation	72 °C	10 min	1

Reagent	**Amount**
10x buffer	5 µl
DNA template	10-100 ng
Primer forward (10 µM)	1.5 µl
Primer reverse (10 µM)	1.5 µl
dNTP (10 mM each)	1 µl
Enzyme mix	1 µl
ddH_2O	Fill up to 50 µl

10.5. Long-range PCR

For the very large Fn transcript, amplification by polymerase chain reaction (PCR) had to be adapted to obtain long DNA amplificates. Expand Long Template PCR System (Roche) was found to be suited for the reaction. Highest yield of products was obtained with buffer 2 included with kit. PCR was performed according to the manufacturer's protocol and amplificates were checked with agarose gel analysis and by sequencing.

Reaction setup and conditions:

Reagent	**Amount**
10x buffer	5 µl
cDNA template	2 µl from RT rxn
Primer forward (10 µM)	1.5 µl
Primer reverse (10 µM)	1.5 µl
dNTP (25 mM each)	1 µl
Enzyme mix	0.75 µl
ddH_2O	Fill up to 50 µl

	Temperature	**Time**	**Cycles**
Initial denaturation	94 °C	2 min	1
Denaturation	94 °C	10 s	10
Annealing	58 °C	30 s	
Elongation	68 °C	8 min	
Denaturation	94 °C	15 s	11-30
Annealing	58 °C	30 s	
Elongation	68 °C	8 min + additional 20 s for each successive cycle	
Final elongation	68 °C	7 min	1
Cooling	4 °C	Unlimited time	

10.6. DNA mutagenesis

Amino acid substitutions were introduced with the QuikChangeII XL Site-Directed Mutagenesis kit (Stratagene) according to the manufacturer's instructions. In brief, mutagenic primers (see chapter 8) containing two amino acid substitution codons were designed and used in a PCR to incorporate the mutation of interest into newly synthesized DNA. Methylated and hemimethylated parental DNA was specifically digested with the DpnI restriction enzyme. The mutagenic strands were transformed into competent *E. coli* XL10-Gold and transformants were checked for the desired mutation by DNA sequencing.

10.7. DNA sequencing

DNA sequencing was performed in the MWG-Biotech sequencing lab (Ebersberg, [D]) using 1.5 µg of plasmid DNA. The resulting sequences were analyzed with Vector NTI software or ApE software.

10.8. Agarose gel analysis of DNA

Agarose gels were prepared by mixing an appropriate proportion of agarose with 1x TAE buffer (40 mM Tris/Acetate, pH 8.3, 10 mM EDTA). Gel concentrations varied between 0.8 % (> 5.000 bp) and 2 %, depending on the size of the DNA molecule. The mixture was boiled in a microwave, cooled down and poured into agarose gel chambers. DNA was mixed, if necessary, with 6x DNA loading buffer (Fermentas), loaded onto the gel and separated by application of voltage (10 V per cm electrode distance). After separation, the gel was stained for 5-10 min in ethidium bromide solution and DNA was visualized under ultraviolet light. The size of DNA molecules was estimated by comparison with a ready-to-load "1kb ladder" (Fermentas).

10.9. Restriction digestion of DNA

Type-II restriction enzymes recognize specific palindromic sequences within a DNA molecule and cut them by hydrolyzing two phosphodiester bonds, generating "sticky" (5' and 3' overhangs) or "blunt" (no 5' or 3' overhangs) ends. DNA digestions were performed with "fast-digest" (FD) restriction enzymes purchased from Fermentas. Digestions were performed at temperatures recommended by the manufacturer (normally 37 °C) in a thermo block for 5-15 min with FD-buffer. Usually 1 µl of enzyme was sufficient to cut 1 µg of DNA in 5 min.
Restriction digestion reaction:

Reagent	**Amount**
10x buffer (ready-to-load)	1 µl
DNA	1-2 µg
Restriction enzyme	1 µl
ddH_2O	Fill up to 20 µl

10.10. DNA extraction from agarose gels

In order to isolate PCR fragments or digested DNA fragments for (sub-) cloning, the desired DNA was excised from the gel and extracted either with the NucleoSpin Extract II kit (Macherey-Nagel) or the QIAEX II Gel Extraction Kit (Qiagen) according to the protocol of the manufacturer.

10.11. Ligation of DNA fragments

To ligate vector DNA with the desired insert DNA, both molecules need compatible ends, i.e. complementary sticky-ends or two blunt-ends. For TA-cloning, the unspecific 3'-A overhang produced by *Taq* polymerase after PCR is sufficient to anneal with cloning vectors containing a 5'-T overhang. Ligases catalyze the formation of a phosphodiester bond between the 5'-phosphate and 3'- hydroxyl residue by ATP hydrolysis. Ligation reactions were performed overnight at 16 °C.

Ligation reaction:

Reagent	**Amount**
10X ligation buffer	1 µl
Vector DNA	25 ng
Insert DNA	X ng (molar ratio 3:1 [insert:vector])
T4 Ligase	0.5 µl
ddH_2O	Fill up to 10 µl

10.12. In-gel ligation

Standard sub-cloning of large DNA fragments from cloning vectors into expression vectors was not successful. A protocol from Michael Koelle (Yale University) was found to work with larger fragments.

- Digested cloning vector with the desired insert and linearized target vector were separated on a 0.8 % low melting-point agarose gel (TAE system) at 4 °C with 10 V per cm electrode distance
- DNA was visualized by ethidium bromide staining on a UV table and the bands of interest were excised from the gel

- 2 µl 10x ligase buffer (Invitrogen) and 2 µl water were added to a reaction tube
- The gel slices were melted in a 70 °C water bath and 10 µl of insert gel slice and 5 µl of vector gel slice were added, mixed with a pipette tip and incubated for ~30 s at room temperature to cool
- 1 µl of T4 DNA ligase (Invitrogen) was added, mixed by pipetting up and down, and immediately placed on ice to cool
- The ligation mixture was incubated overnight at 16 °C or at room temperature for ~3 h

10.13. Preparation of plasmid DNA

Successful transfection of eukaryotic cells is strongly dependent on the quality of plasmid DNA used. The DNA needs to be free of endotoxins, be in a super-coiled state and should have a low protein content. Plasmid DNA was therefore always freshly prepared with the ZR Plasmid Miniprep – Classic Kit (Zymo Research) from 6 ml of bacterial overnight culture, according to the manufacturer's recommendations for large plasmids. DNA was eluted in 50 °C warmed elution buffer for 5-10 min. Concentration of isolated DNA was measured with a spectrophotometer at a wavelength of 260 nm (Ultraspec 3001 or Nano Drop). To determine purity grade, DNA was measured at a wavelength of 260 nm and 280 nm. An $A_{260/280}$ coefficient < 1.8 and > 2 indicated (protein-) contamination of the DNA.

10.14. Preparation of chemically competent *E. coli*

- 50 ml LB-medium were inoculated with 1 ml of an overnight culture and incubated with vigorous shaking at 37 °C to an OD_{600} of 0.6
- Cells were centrifuged for 10 min at 5500 g at 4 °C
- The pellet was resuspended in 25 ml of ice cold 0.1 M $CaCl_2$ and incubated for 30 min on ice
- Cells were centrifuged for 10 min at 5500 g at 4 °C
- The pellet was resuspended in 5 ml of ice-cold 0.1 M $CaCl_2$ / 20 % glycerol
- Bacteria were aliquoted, frozen in liquid nitrogen and stored at -80 °C

10.15. Heat-shock transformation of competent *E. coli*

- 100 µl competent *E. coli* were thawed on ice
- The following amounts of DNA were added:
    - 10 µl standard ligation mixture or
    - 100 µl in-gel ligation mixture, containing 20 µl 70 °C heated ligation mix and 80 µl 0.1 M Tris pH 7.5 or
    - 10-50 ng of purified plasmid DNA
- The bacteria-DNA-mixture was incubated for 10 min on ice
- A heat-shock was performed for 1 min at 42 °C in a water-bath
- The bacteria-DNA-mixture was incubated for an additional 10 min on ice
- 900 µl of warm SOC (Invitrogen) medium was added to the cells and agitated at 350 rpm and 37 °C on a thermomixer
- 100 µl bacterial cell suspension was plated on a LB-agar plate containing appropriate antibiotics and X-gal (if suitable) for positive selection and blue/white screening of the transformants
- Remaining cells were centrifuged for 1 min at 13,000 rpm, the pellet resuspended in 100 µl LB-medium and plated on another selective LB-agar plate
- Plates were incubated overnight at 37 °C

10.16. Colony PCR

For a rapid and larger scale screening of transformants, bacterial colonies were picked with a pipette tip and dipped into a mixture for PCR amplification of small fragments (< 1,000 bp). Primers were located in the vector and in the insert, with the PCR therefore providing evidence about the correct orientation of the insert. GoTaq polymerase and a ready-to-load reaction buffer from Promega were used for screening.

Reaction setup and conditions:

	Temperature	Time	Cycles
Initial denaturation	98 °C	2 min	1
Denaturation	98 °C	30 s	29
Annealing	58 °C	30 s	
Elongation	68 °C	1 min	
Final elongation	68 °C	10 min	1

Reagent	Amount
5x buffer	3 µl
Primer forward (10 µM)	0.6 µl
Primer reverse (10 µM)	0.6 µl
dNTP (10 mM each)	0.2 µl
Taq polymerase (5 U/µl)	0.1 µl
ddH_2O	10.5 µl

11. Biochemical Methods

11.1. Protein expression and purification

The purification of an expressed protein of interest is facilitated by the introduction of a protein tag, which can bind with high affinity to its ligand. Glutathione S-transferase is an enzyme of M_r 26 kDa and binds with high affinity and specificity to the tripeptide glutathione. The protein of interest is fused to the C-terminus of GST using the bacterial pGEX-4T expression vector (GE Healthcare). Expression of the fusion protein can be induced and the protein then purified from the bacterial lysate with a glutathione-coupled Sepharose 4B matrix (GE Healthcare). A thrombin recognition sequence allows cleavage of the target protein from the GST-tag.

GST-fused constructs were transformed into *E. coli* strain BL21, which is deficient in OmpT and Lon protease and allows high-level expression of GST-fusion proteins. Overnight bacterial cultures were diluted 1:20 in fresh LB-medium containing the selective antibiotic and grown at 37 °C to an OD_{600} of 0.5-0.7. Protein expression was induced by adding 0.4 mM IPTG (isopropyl β-D-1-thiogalactopyranoside) and bacteria were incubated at 37 °C for 4 h. Cells were harvested at 6,000 rpm for 15 min at 4 °C, the pellet resuspended in 5 ml lysis buffer (PBS + 0.1 mM PMSF) per 100 ml culture and sonicated 10 times for 10 s at 25 %. Cell debris was centrifuged for 30 min at 20,000 rpm and GST-fused proteins in the

supernatant were purified by applying each 5 ml of bacterial lysate to 100 µl Glutathione Sepharose 4B matrix. After several washing steps with lysis buffer, proteins were either eluted with lysis buffer containing reduced glutathione (30 mM glutathione, 50 mM Tris pH 7.5) or cleaved on the column using 10 U thrombin per 50 µl sepharose matrix and eluted subsequently with PBS. Expression of fusion-proteins was monitored by SDS-PAGE and Western blotting against GST.

11.2. Determination of protein concentration

The concentration of solubilized protein was measured with the BioRad protein assay, based on the method of Bradford. As a protein standard, bovine serum albumine (BSA) at different concentrations was used (20 µg/ml, 15 µg/ml, 10 µg/ml, 5 µg/ml and 1 µg/ml). To determine protein concentration, 800 µl of diluted sample or 800 µl standard solution was mixed with 200 µl of the assay reagent. After vortexing and an incubation of 5 min at room temperature, the absorbance at 595 nm was measured in a spectro-photometer.

11.3. SDS-PAGE

During sodium-dodecyl-sulfate-polyacrylamide gel electrophoresis (SDS-PAGE), proteins are separated on the basis of their electrophoretic mobility as they migrate through a porous gel. SDS is an anionic detergent, which denatures secondary and tertiary structures and applies a negative charge to proteins relative to their mass with a constant weight ratio of 1.4 g/g polypeptide. Accordingly, proteins may be separated roughly by their size.

For analysis, a discontinuous Tris-Glycine-System was chosen. Protein samples were mixed with 5x Laemmli SDS loading buffer (with a 5 % final concentration of β-mercapto-ethanol), boiled for 5 min at 95 °C and subjected to electrophoresis. Mini-gels were run at 100 V during stacking and 150 V during separation. Larger Hoefer-gels were run at 25 mA during stacking and 35 mA during separation. To estimate approximate molecular weights, a protein marker (prestained protein markers PeqLab GoldIV or Invitrogen SeeBlue Plus2) was additionally loaded onto the gel.

Stacking gel	**Mini**	**Höfer**
ddH_2O	1.55 ml	9.15 ml
Stacking gel buffer	625 µl	3.9 ml
Acrylamide	325 µl	1.995 ml
10 % ammonium persulfate	12.5 µl	100 µl
TEMED	5 µl	20 µl

	========== **Mini** ==========			**Höfer**
Resolving gel	**7.5 %**	**10 %**	**12.5 %**	**7.5 %**
ddH_2O	2.43 ml	2.09 ml	1.6 ml	17 ml
Resolving gel buffer	1.25 ml	1.25 ml	1.25 ml	9.05 ml
Acrylamide	1.25 ml	1.67 ml	2.08 ml	8.8 ml
10 % ammonium persulfate	25 µl	25 µl	25 µl	200 µl
TEMED	2.5 µl	2.5 µl	2.5 µl	40 µl

11.4. Western blot

Proteins that were separated by SDS-PAGE were transferred ("blotted") onto a polyvinylidene fluoride (PVDF) membrane (Immobilion-P) by electrophoretic transfer with a semi-dry Western blot apparatus. From bottom (anode) to top (cathode), two filter papers soaked in anode buffer 1 and one filter paper soaked in anode buffer 2 were followed by a piece of methanol-activated PVDF membrane and the SDS gel placed directly on top of it, layered by three filter papers soaked in cathode buffer. The transfer stack was relieved off any trapped air bubbles and proteins blotted for 1 h at 1.2 mA/cm^2. After the transfer, the membrane was blocked with PBST / 5 % fat-free milk powder or PBST / 2 % bovine serum albumin for 1 h at room temperature or overnight at 4 °C. The membrane was incubated with primary antibody in blocking solution for 1 h at room temperature (or 4 °C, overnight for anti-pY antibody), washed three times with PBST for 5 min, followed by incubation with horseradish peroxidase-linked secondary antibody in PBST for 1 h (1:100,000). After three more washing steps with PBST, detection solution was added to the membrane according to manufacturer's instructions (SuperSignal West Femto, Thermo Scientific). Emitted light was detected by exposing the membrane to an X-ray film (Fuji) which was then developed in a processor for X-ray film development (Agfa Curix 60).

11.5. Coomassie staining

Proteins were visualized by staining with Coomassie staining solution for 5-15 min depending on the thickness of the gel, followed by destaining with destain solution for several hours and then in water overnight. All steps were applied under constant shaking at room temperature.

11.6. Silver staining

Silver staining is a highly sensitive method to stain SDS gels conatining proteins with quantities low as 0.4 ng. The SilverSNAP Kit (Pierce / Thermo Scientific) was used according to the manufacturer without overnight incubations. The gel was washed and fixed to remove salts. Silver stain was then added, releasing silver ions that interact with the proteins. Developer was introduced, which causes the protein bands to darken as the bound silver reduces. The color development was stopped by lowering the pH to the desired level using acetic acid.

11.7. Size exclusion chromatography

Another method to purify proteins according to their molecular weight is size exclusion chromatography. Molecules of different sizes are applied to a gel filtration medium densely packed in a column. The medium is a porous matrix in the form of spherical particles, so that molecules diffuse in and out of the pores of the matrix. Depending on the size of the pores, larger molecules are unable to diffuse into the pores and pass through the column, whereas smaller molecules move further into the matrix and so stay longer on the column.

Purification by such a method was necessary in order to remove high molecular weight proteins from proteolytic Fn fragments Fn 30 kDa and Fn 70 kDa, as well as the bacterial contaminating proteins (mainly 70 kDa chaperone DnaK) and degradations products of recombinantly expressed Tensin-3 ~23 kDa fragment hTNS-3.

For purification of proteins < 70 kDa and ≥ 70 kDa, a Superdex 75 10/300 GL column or a Superdex 200 10/300 GL were used, respectively, connected to an Äkta Purifier system (GE Healthcare). After equilibration of the column with at least three column volumes (CV) PBS, the samples were loaded with a syringe in a volume of 0.5-1 ml and injected with a suitable sample loop connected to the Äkta system. Proteins larger than the protein of interest passed

earlier through the column and were detected by absorption at 280 nm wavelength. Fractions containing the peak of the target protein were collected in 0.25-0.5 ml fraction size and checked for the absence of contaminating higher or lower molecular weight proteins by SDS-PAGE and either Coomassie staining or Western blotting. For some experiments, the PBS-eluted proteins were concentrated with Vivaspin 6 centrifugal concentrators (Sartorius Stedim Biotech) to a working concentration of 0.5-1 mg/ml.

11.8. Affinity chromatography

Reversible interactions of proteins with each other are the basis of affinity chromatography for purification of proteins. A ligand is covalently bound to a gel matrix (solid phase) in a column and the soluble protein of interest (liquid phase) is passed over the matrix. Unbound proteins flow through and the target protein binds and can be eluted by lowering the pH.
Here, it was intended to purify rabbit-anti-hTNS-3 IgG antibodies from serum. Coupling of the immunogen to HiTrap NHS-activated HP 1 ml columns (GE Healthcare) through formation of an amide linkage between primary amino groups of the protein and the ester linkage of the N-hydroxysuccinimide-activated spacer arm of the sepharose was performed according to the manufacturer's recommendations. A buffer exchange of rabbit serum to binding buffer (20 mM Na_2HPO_4, 0.5 M NaCl, pH 7.4) was performed and the serum proteins then passed over the column using the Äkta Purifier. After washing with binding buffer, unbound proteins were detected by absorption at 280 nm wavelength and discarded. Bound antibodies were eluted in elution buffer (0.1 M glycine, 0.5 M NaCl, pH 3.0) and fractions containing the detected peak were saved and tested for specific recognition of Tensin-3 using Western blotting and indirect immunofluorescence.

12. Cell Culture and Cell Biological Methods

12.1. Cell lines

Cell line	Description	Reference
FN -/-	Fn-deficient mouse fibroblasts	(Nyberg et al. 2004; T. Sakai et al. 2001)
FN fl/fl	Wild-type Fn (including two *loxP* sites) expressing mouse fibroblasts	(Nyberg et al. 2004; T. Sakai et al. 2001)
FN RGE/RGE	RGD>RGE-mutated Fn-expressing mouse fibroblasts	(Takahashi et al. 2007)
GD25	β1 integrin-deficient mouse cells	(Wennerberg et al. 1996)
GD25-β1A	β1A-complemented GD25 mouse cells	(Wennerberg et al. 1996)
beta1-YY MEF	Wild-type β1 integrin-expressing mouse embryonic fibroblasts	(Czuchra et al. 2006)
beta1-FF MEF	Membrane proximal and distal NPXY>NPXF-mutated β1 integrin-expressing mouse embryonic fibroblasts	(Czuchra et al. 2006)
HUVEC	Primary human umbilical cord vein endothelial cells	

All cells were cultured in incubators at 37 °C, supplied with 5 % CO_2 and 90 % humidity. Except for HUVEC, all cell lines were kindly provided by Reinhard Fässler (MPI of Biochemistry, Martinsried [D]).

FN -/-

Fn-deficient fibroblast-like cell line that was derived from FN fl/fl fibroblast-like mouse cells after Cre recombination. Cells were cultured in serum-free AIM-V medium (Invitrogen), containing streptomycin sulfate (50 µg/ml) and gentamicin sulfate (10 µg/ml).

FN fl/fl

Fibroblast-like cells derived from FN fl/fl mice expressing wild-type Fn that includes two *loxP* sequences in the Fn gene. Cells were cultured in serum-free AIM-V medium (Invitrogen), containing streptomycin sulfate (50 µg/ml) and gentamicin sulfate (10 µg/ml).

FN RGE/RGE

Fibroblast-like cells derived from FN RGE/RGE mice expressing Fn that contains a RGD>RGE mutation in the Fn III(10) domain. Cells were cultured in serum-free AIM-V medium (Invitrogen), containing streptomycin sulfate (50 µg/ml) and gentamicin sulfate (10 µg/ml).

GD25

Differentiated and immortalized cell line derived from mouse embryonic stem cell clone G201, which is deficient in integrin subunit β1. Cells were cultivated in DMEM supplemented with 10 % fetal calf serum (FCS) and 100 µg/ml penicillin/streptomycin.

GD25-β1A

Cell line that derived from GD25 cells after stably introducing integrin β1A cDNA. Cells were cultivated in DMEM supplemented with 10 % FCS and 100 µg/ml penicillin/streptomycin.

Beta1-YY MEF

Mouse embryonic fibroblasts expressing wild-type integrin β1 subunit. Cells were cultivated in DMEM supplemented with 10 % FCS and 100 µg/ml penicillin/streptomycin.

Beta1-FF MEF

Mouse embryonic fibroblasts derived from β1A-YY783/795FF mice, where the two NPXY motifs were mutated to NPXF. Cells were cultivated in DMEM supplemented with 10 % FCS and 100 µg/ml penicillin/streptomycin.

HUVEC

Human umbilical cord vein endothelial cells were isolated from human umbilical cord veins and cultured in Endothelial Cell Growth Medium (ECGM, PromoCell) supplemented with 2 % FCS, 50 µg/ml gentamicin sulfate and 0.05 µg/ml Amphotericin B. Cells were used from passage 2-4.

12.2. Isolation of HUVEC

Human umbilical vein endothelial cells (HUVEC) were obtained by trypsin treatment of human umbilical cord veins by a method adapted from Jaffe (Jaffe et al. 1973). The cord was inspected and all areas with clamp marks were cut off. The umbilical vein was cannulized at one end with a blunt 2 cm long needle and the needle was secured by clamping the cord over the needle with two compressors. After perfusing the umbilical vein with sterile PBS to wash out the blood, the other end of the vein was clamped shut and 0.1 % α-chymotrypsin in PBS was infused into the umbilical vein. The umbilical cord was incubated at 37 °C for 20 min. After incubation, the chymotrypsin solution was flushed from the cord by perfusion with sterile PBS. The effluent was collected in a sterile 50 ml conical centrifuge tube (BD Biosciences) containing 2 ml of FCS to stop the trypsinization reaction. The cells were sedimented at 200 g for 8 min at 25 °C, resuspended in endothelial cell growth medium, transferred to 0.2 % gelatin-coated culture flasks (Nunc) and incubated at 37 °C, 5 % CO_2 and 90 % humidity. After 3 h, non-adherent cells and debris were removed by replacement of culture medium. Cell culture medium was replaced every 2-3 days.

12.3. Passaging of cells

Cell culture medium was removed. HUVEC, FN -/-, FN fl/fl and FN RGE/RGE cells were treated with TrypLE Express (Invitrogen), GD25, GD25-β1A, beta1-YY and beta1-FF cells were treated with Trypsin-EDTA (0.05 % Trypsin, 0.53 mM EDTA x 4 Na; Invitrogen) until they rounded up under microscopic observation. Trypsinization was stopped by adding culture medium and the cell suspension was transferred to a 15ml conical centrifugation tube (BD Biosciences). The cells were sedimented at 200 g for 5 min at 25 °C, resuspended in culture medium and split at a ratio of 1:5-1:10 into gelatin-coated (except for GD25, GD25-β1A, beta1-YY and beta1-FF cells) culture flasks (Greiner or Sarstedt) or dishes (Sarstedt). The medium was changed every 2-3 days and cells were not used at passages greater than 20.

12.4. Freezing and thawing of cells

Freezing of cells

Cells were trypsinized from cell culture flasks, centrifuged for 5 min at 1,000 rpm and the cell pellet was resuspended in 1ml sterile-filtered pre-cooled freezing medium (FCS + 10 % dimethylsulfoxide [Sigma-Aldrich]; or CryoSFM [PromoCell] for FN -/-, FN fl/fl and FN RGE/RGE cell). Cells were transferred to 1.5 ml Cryo-vials, incubated for 10 min on ice and subsequently transferred to -80 °C in a Cryo-box filled with isopropanol allowing a temperature decrease of approx. 1 °C/min.

Thawing of cells

Cryo-vials were removed from -80 °C and quickly thawed in a 37 °C water bath. Thawed cells were transferred into 10 ml of 37 °C warm growth medium provided in a (coated) culture flask. After 2-3 h, cell culture medium was changed to remove substances from the freezing medium.

12.5. Coating of coverslips, culture flasks and dishes

Most cells attached and proliferated only poorly on uncoated substrates. Accordingly, culture flasks and dishes and glass coverlips were coated, if necessary, with 0.2 % gelatin in PBS (gelatin solution from bovine skin, 2 %, Sigma-Aldrich). Coating solution was spread over the surface and immediately removed, and coverslips were shortly dipped into it.

For FN -/-, FN fl/fl and FN RGE/RGE cells, glass coverslips were coated with 62.5 µg/ml collagenIV-PBS (collagen type IV from human placenta, Sigma-Aldrich) for 3 h at 37 °C or 4 °C overnight to avoid any possible contaminations with Fn in gelatin that would interfere with downstream assays.

12.6. Transfection with Nucleofector

In HUVEC, transfection of siRNA was performed with the Amaxa Nucleofector system, which is a combination of electroporation and lipofection, and resulted in rapid and high cellular expression. Transfection was performed according to the protocol of the manufacturer. In brief, cells were trypsinized, pelleted and 1 million cells were then transfected with 1 µg of siRNA. Transfected cells were transferred to glass coverslips or cell culture flasks and incubated at 37 °C until experiments were performed.

12.7. Transfection with Neon Transfection System

FN -/- cells were transfected with the Neon Transfection System (Invitrogen), which is an electroporation method. According to the manufacturer, cells were trypsinized, washed with warm PBS and resuspended in transfection buffer R at 10^7 cells per ml. 100 µl tips were used to transfect a maximum number of 10^6 cells at once. A self-determined protocol was applied to transfect large Fn-expression plasmids. The settings were voltage 1400 V, duration 20 ms, and 2 pulses. Cells were immediately seeded in 2 ml pre-warmed medium in a single well of a 6-well plate (Nunc / Thermo Scientific). Each tip was used for a maximum of 6 pulses and changed between the different constructs. The cuvettes were changed after 20 pulses.

12.8. Coating of latex beads

Fluorescent polystyrene microspheres (latex-beads, diameter 1 µm, blue, Ex./Em.=350 / 440 nm) with sulfate groups on the surface for passive adsorption of proteins were purchased from Molecular Probes (Invitrogen). Non-fluorescent sulfate-modified latex-beads were purchased from Polysciences Inc. In Protein LoBind reaction tubes (Eppendorf), 50 µl bead slurry were washed with 500 µl PBS and purified GST-FnBPA(DuD4) was added at a concentration of 630 µg/ml. To generate BSA-coated beads as a negative control, beads were resuspended in 1 % BSA in PBS. Protein was allowed to adsorb to the beads for 3 h at room temperature or overnight at 4 °C. Beads were pelleted, resuspended in 500 µl 1 % BSA in PBS to block unspecific binding and incubated for another 1 h at room temperature. Beads were washed in 1 % BSA-PBS and stored in 0.02 % BSA in PBS at 4 °C. Coupling efficiency was determined by measuring protein concentration before and after coating of beads.

12.9. Immunofluorescence methods

For immunofluorescence staining of cells, three different fixation/permeabilization methods were performed, depending on the antibody and the assay that was used.

Formaldehyde/Triton fixation – permeabilization

Cells seeded on coverslips were fixed in 3.7 % formaldehyde in PBS for 10 min and permeabilized with 0.05 % Triton X-100 in PBS for 20-30 min at room temperature.

Methanol/acetone fixation – permeabilization

Cells seeded on coverslips were fixed and permeabilized by incubating in ice-cold methanol for 10 min and subsequently in ice-cold acetone for 10 min, both at -20 °C.

Paraformaldehyde fixation

Paraformaldehyde fixation was used for bacterial internalization assays to distinguish between intra- and extracellular bacteria. For minimal disruption of cell membranes, cells were fixed with freshly made 4 % paraformaldehyde in PBS by dissolving 2 g of paraformaldehyde in 50 ml of PBS (addition of NaOH and heating to 60 °C were required for dissolving). Cells were fixed in paraformaldehyde for 10 min at room temperature.

Indirect immunofluorescence staining

Indirect immunofluorescence staining of cells seeded on glass coverslips was performed in a wet chamber on a layer of parafilm (American National Can, Menasha, USA). For antibody incubations, 25 µl of the solution was placed on the parafilm and glass coverslips were applied with the cellular side oriented downwards. After fixation and permeabilization, cells were blocked with 2 % BSA in PBS-Triton (0.05 % Triton X-100) for 30-60 min and then incubated with primary antibody for 1 h. Cells were washed three times with PBS and incubated with secondary antibody for 1 h. For specific staining of F-actin or DNA, AlexaFluor488 or -568 labeled phalloidin and DAPI, respectively, was added instead of, or additionally to a secondary antibody. After three washing steps with PBS, coverslips were air dried, mounted on a drop of Mowiol (including DABCO as an anti-fading reagent; Calbiochem) and sealed with nail polish.

Quantification of particle-coating with Fn by indirect immunofluorescence

Fn-coated particles were immobilized on immunofluorescence slides by drying and stained for Fn as described above. Five random positions were imaged with the same settings for each position and specimen. In ImageJ software (National Institutes of Health), phase contrast pictures were used to create selections of particles and this mask was applied to determine the mean fluorescence in the corresponding fluorescence channel.

Inside/Outside staining (double-fluorescence staining)

To distinguish between extracellular (adherent) and intracellular (ingested) bacteria or beads, a double-fluorescence staining method was used that is based upon the fact that cell

membranes are impermeable to antibodies after fixation with paraformaldehyde but permeable after treatment with Triton X-100. Thus, extracellular bacteria/beads were stained before permeabilization with primary and secondary antibody and intracellular bacteria/beads (together with extracellular bacteria/beads) after permeabilization for 20 min with 0.05 % Triton X-100. When fluorescent beads were used, the second labelling was dispensable. This resulted in internalized bacteria/beads stained in one color and extracellular bacteria stained with two colors. By comparison of fluorescence channels, numbers of intracellular and cell-associated extracellular bacteria/beads were determined microscopically. In total, 5 positions with each 2 fluorescence channels and 1 phase contrast channel were imaged at a total magnification of 400x with a Zeiss Axioplan epifluorescence microscope. The overlay-image of the fluorescence-channels was shift-corrected and the phase contrast channel allowed for distinguishing of cell-associated and non-cell adherent bacteria/beads. Only cell-associated beads/bacteria were analyzed and counted.

In the case of Fn-plasmid transfected FN -/- cells, a fourth channel with immunostained Fn was acquired to solely count bacteria that were associated with Fn-expressing cells. For this, images were captured at a total magnification of 400x with a Zeiss Axiovert 200M epifluorescence microscope.

12.10. Infection of cells

Preparation of conditioned medium

Fn expressing cells secrete soluble Fn in the culture medium, which can be used for coating beads or bacteria (see chapter 5 for an overview of the Fns). To obtain conditioned medium from Fn expressing cells (FN fl/fl or FN RGE/RGE) and FN -/- cells as a negative control, 2 million cells were seeded per 5 ml AIM-V medium in a gelatin-coated T-25 cell culture flask (Nunc) for 2 days. Conditioned media from Fn RGD, Fn Syn^- or empty vector control-transfected FN -/- cells were collected from 1 million cells per 2 ml AIM-V medium in a gelatin-coated 6-well after 3 days. These media had to be concentrated 10-fold using Vivaspin 2 centrifugal concentrators (Sartorius Stedim Biotech), because of the low amount of secreted Fn. All supernatants were collected using a syringe, sterile-filtered through a 0.2 µm SFCA-filter (Nalgene) and used immediately or kept at 4 °C for 1-24 h.

Seeding of cells on glass coverslips

The day before infection, 4 x 10^5 FN -/- cells (slower growing) or 2 x 10^4 of the other cells were seeded in 80 µl medium on a 12 mm collagenIV- or gelatin-coated coverslip in a single well of a 12-well plate (Nunc). After cells were allowed to adher for at least 2 h in the cell culture incubator, 1 ml medium was added to each well. For infection via cellularly organized Fn, 10 µg human plasma Fn or the 30 kDa and 70 kDa proteolytic fragments were added for 24 h.

Transfected FN -/- cells were seeded directly after transfection on 5 collagenIV-coated coverlsips that were placed in a single well of a 6-well plate (Nunc) and incubated for 2 days to produce sufficient amounts of Fn on the cell-surface.

Infection via soluble Fn bound to the surface of particles

For the infection of cells with *FnBPA-S. carnosus*, overnight cultures grown at 37 °C in LB-medium containing chloamphenicol were diluted to an OD_{600} of 0.15-0.2 in fresh LB-medium with antibiotics. When an OD_{600} of 0.72 was reached, 1 ml aliquots of bacteria were pelleted in Protein LoBind reaction tubes (Eppendorf) for 1 min at 13,000 g and resuspended in 1 ml of either conditioned medium from cells (FN fl/fl, FN RGE/RGE or FN -/-) or 10 µg/ml proteolytic Fn fragments in PBS. For concentrated Fn RGD, Fn Syn^- and vector control-conditioned media, only 200 µl could be used for coating 1 ml of pelleted bacteria. If FnBPA-beads were used instead of bacteria, 21 µl beads (GST-FnBPA[DuD4] or GST-control) were utilized per coating. After coating for 30 min at 4 °C on a rotating mixer, bacteria/beads were pelleted, washed once in PBS and resuspended in 1 ml of ice-cold PBS. To ensure reproducible infection numbers and facilitate counting, particles were singularized with 2 successive ultrasonic pulses at 30 %, followed each time by 10 s on ice in order to avoid high temperatures that could harm the bacteria. This procedure did not disrupt the Fn-coat as checked by western-blot. After adding 63 µl of bacteria or 200 µl of beads to each well of a 12-well plate, infection was synchronized by centrifugation of the plates for 1 min at 200 g, resulting in a MOI of ~50. At designated time-points, cells were fixed and processed for immunofluorescence assays.

To verify that the presence of antibiotics in the cell culture medium did not interfere the infection assay, the same assay was performed without antibiotics. The results showed no major influence on the adhesiveness or invasiveness of the bacteria.

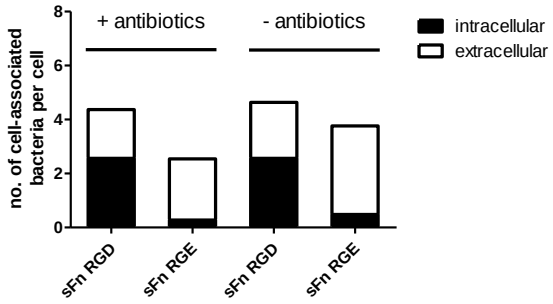

Figure 25: Influence of antibiotics on the infection assay.
FnBPA-S. carnosus coated with Fn-containing conditioned medium from FN fl/fl (sFn RGD) and FN RGE/RGE cells (sFn RGE) were used to infect FN -/- cells. The conditioned medium contained gentamicin and streptomycin (+ antibiotics) or no antibiotics (- antibiotics). The number and localization of cell-associated bacteria was determined microscopically by inside/outside staining of the bacteria. Values represent mean ± s.d. from a single experiment with at least 150 cells counted per experimental condition at a MOI of 50.

Infection via cellularly organized Fn

Bacteria and beads were prepared the same as for infecting via soluble Fn, but without incubating with conditioned media or Fn fragments. Instead, singularized PBS-resuspended bacteria/beads were used directly for infecting the cells. Before adding the particles, medium was removed from the cells, which were washed once with medium before fresh culture medium was added to remove soluble Fn that could coat the bacteria. In some cases, cells were treated for 1 h with 10 µg/ml cyclic peptides (cycRGD or cycRAD) prior to infection in order to inhibit the αVβ3 receptor.

Live cell imaging of bacterial motility

In order to quantify the dynamic behavior of bacterial motility on the surface of cells during infection, time-lapse imaging was performed using a Spinning Disk microscope equipped with an EM-CCD camera (Improvision).

The day before infection, cells were seeded at 1 x 10^5 per 35 mm dish (ibi treat, ibidi), infected with 50 µl *FnBPA-S. carnosus* (OD_{600} of 0.72), which, if desired, were spun onto the cells for 1 min at 200 g. The treatment of bacteria depended on the purpose of investigation (infection through soluble or cellularly organized Fn, see paragraph before). Cells were imaged every 30 s for 1-2 h and the tracks of bacteria analyzed with Volocity software (PerkinElmer). Manual object tracking was applied to determine the position of a bacterium in every single frame from attachment in the cell periphery until movement to the perinuclear region. If bacteria did not remain near or move towards the perinuclear region, they were tracked throughout the infection period. Three parameters were utilized for characterizing bacterial motility:

- Displacement [µm], which is the straight line distance from the first position in the track to the last.
- Directionality, which is displacement / total track length and provides a measure of a track's deviation from a straight line. The value is always ≤ 1, meaning 1 would be a perfectly straight line, and the smaller the value the more random is the movement.
- Track velocity [µm/min], which is the calibrated average speed over the track. Volocity provides this parameter in µm/s, so that it was multiplied by 60.

12.11. Immunization of rabbits

Rabbits were immunized with recombinant hTNS-3, a fragment spanning aa 399-597 in the isoform-specific and non-homologous sequence of human Tensin-3 (reference sequence NP_073585.8). The fragment was expressed as a GST fusion-protein in *E. coli* and verified by tandem mass-spectrometry. The GST-tag was cleaved off and the protein used to immunize two New Zealand rabbits in the animal facility "Versuchstierhaltung Universitätsklinikum Hamburg-Eppendorf". Immunization was applied by authority of "Behörde für Soziales, Familie, Gesundheit und Verbraucherschutz, Fachabteilung Lebensmittelsicherheit und Veterinärwesen, Freie und Hansestadt Hamburg", grant number A 10a/354, according to "§ 10a Tierschutzgesetz".

Pre-immune serum was obtained before immunization. 100 µg of protein in 250 µl PBS was mixed with 250 µl complete Freund's adjuvant until a homogenous suspension was achieved. Rabbits were immunized subcutaneously by technicians at the animal facility. After 4 and 8 weeks, animals received a boost-immunization with the same amount of antigen mixed with incomplete Freund's adjuvant. Rabbits were bled under anesthesia and the blood clot removed from serum via centrifugation after overnight incubation. The serum was tested for the presence of Tensin-3-specific antibodies using the immunogen as antigen for Western blot analysis. The pre-immune serum was not able to detect the hTNS fragment above a serum-dilution of 1:100, compared to 1:50,000 with the post-immune serum. Fibrillar adhesions in HUVECs and mouse fibroblasts, specific adhesion structures rich in tensin (see B.2.2, *introduction*), could also be stained by indirect immuofluorescence, confirming the presence of tensin antibodies and also showing an interspecies reactivity of the antibody.

F. Abbreviations

°C	degree celsius
µg	microgram
µl	microliter
µm	micrometer
µM	micromolar
A	A domain
A	adenosine
A	absorption
A	alanine
aa	amino acid
ADMIDAS	adjacent to MIDAS
AFM	atomic force microscopy
AH2	actin-homology 2 region
Ala	alanine
ALU	arbitrary light units
Arg	arginine
Arp2/3	actin-related protein 2/3
ASAP1	ADP ribosylation factor-GAP containing SH3, ANK repeats, and PH domain
Asp	aspartate
ATP	adenosine triphosphate
beta1-FF	MEF with two tyr>phe mutations in the β1A MD/MP NPXY motifs
beta1-YY	MEF with wild-type β1A integrin tails
BSA	bovine serum albumin
C	cytosine
c	concentration
CDC42	cell division cycle 42 GTP binding protein
CDN	Canada
cDNA	complementary DNA
cFn	cellularly organized Fn
CH	Switzerland
CHO	Chinese hamster ovarian
CLIC	clathrin-independent carriers
cm	centimeter
cm²	square centimeter
CME	clathrin-mediated endocytosis
ColIV	collagen type IV
cycRAD	cyclic peptide cyclo-(Arg-Ala-Asp-D-Phe-Val)
cycRGD	cyclic peptide cyclo-(Arg-Gly-Asp-D-Phe-Val)
Csk	c-src tyrosine kinase
CV	column volume
Cys	cysteine
D	Germany
DAPI	4',6-diamidino-2-phenylindole
DABCO	1,4-diazabicyclo[2.2.2]octane
dd	double –distilled
DLC1/3	deleted in liver cancer 1/3
DMEM	Dulbecco's Modified Eagle's Medium
DNA	deoxyribonucleic acid
dNTP	deoxynucleoside triphosphate (dATP, dCTP, dGTP, dTTP)
Dok1	docking protein 1
DTT	dithiothreitol
Eap	extracellular adherence protein
ECGM	Endothelial Cell Growth Medium
ECM	extracellular matrix
EDTA	ethylenediamine-N,N,N',N'-tetra acetic acid
EGF	epidermal growth factor
EIIIA	extra domain A of Fn type III module
EIIIB	extra domain B of Fn type III module
EM-CCD	electron multiplier charge coupled device
Emp	ECM protein binding protein
FAK	focal adhesion kinase
Fc	fragment crystallizable
FCS	fetal calf serum
FD	fast digest
FERM	protein 4.1, ezrin, radixin, moesin

Fn	fibronectin
Fn hpl	human plasma Fn
FnBP	Fn binding protein
FnBR	Fn binding repeats
Fn III7-10	type III repeats 7-10 of Fn
g	gram
g	relative centrifugal force
G	guanine
G	glycine
GAP	GTPase activating protein
GEEC	GPI-enriched endocytic compartments
GEF	GTP exchange factor
GFP	green fluorescent protein
Glu	glutamate
Gly	glycine
GPI	glycophosphatidylinositol
GST	Glutathion-S-transferase
h	hour
H	histidine
Hg	mercury
His	histidine
HUVEC	human umbilical cord vein endothelial cells
Ig	Immunoglobulin
IIICS	type III connecting segment of Fn
ILK	integrin-linked kinase
iPALM	photo-activated localization microscopy
IPTG	isopropyl β-D-1-thiogalactopyranoside
J	Japan
kbp	kilo base pairs
kDa	kilodalton
l	liter
L	leucine
LB	Luria-Bertani
LPXTG	membrane anchoring motif in staphylococcal surface adhesins
LTA	lipoteichoic acids
M	membrane-spanning domain
M	molar
m²	square meter
mA	milliampere
MAPK	mitogen-activated protein kinase
Mbp	mega basepairs
MD	membrane distal
MEF	mouse embryonic fibroblasts
MEK	MAPK/extracellular signal related kinase kinase
mg	milligram
MGE	mobile genetic elements
MIDAS	metal ion dependent adhesion sites
min	minute
ml	milliliter
mm	millimeter
mM	millimolar
MOI	multiplicity of infection
MOPS	3-(N-morpholino)propanesulfonic acid
MP	membrane proximal
Mr	relative molecular mass
MRSA	meticillin resistant *Staphylococcus aureus*
ms	millisecond
MSCRAMM	microbial surface components recognizing adhesive matrix molecules
N	asparagine
ng	nanogram
NHS	N-hydroxysuccinimide
NL	Netherlands
NPXY	binding motif in cytosolic β-integrin tails
nt	non-targeting
OD	optical density
Opa	opacity protein
p	plasmid
P	proline
PAGE	polyacrylamide gel electrophoresis

PBP	penicillin-binding proteins
PBS	phosphate buffered saline
PBST	PBS with Tween-20
PCR	polymerase chain reaction
PDGF	platelet-derived growth factor
Ph	phase contrast
Phe	phenylalanine
PHSRN/PPSRN	recognition motif in the synergy site of Fn
PI3 kinase	phosphoinositide-3 kinase
PINCH	particularly interesting Cys-His-rich protein
PKC	protein kinase C
PMSF	phenylmethanosulfonylfluoride
PRR	proline-rich region
PTB	phosphotyrosine binding domain
PtdIns(3,4,5)P3	phosphatidylinositol-(3,4,5)-triphosphate
PtdIns(4,5)P2	phosphatidylinositol-(4,5)-bisphosphate
PTK	protein tyrosine kinases
PVDF	polyvinylidene fluoride
pY	phosphotyrosine
R	arginine
RefSeq	reference sequence
RGD	integrin recognition motif in Fn
RGE	Asp>Glu mutated RGD motif
RNA	ribonucleic acid
rpm	revolutions per min
RPTPα	receptor protein-tyrosine phosphatase α
RT	reverse transcription
rxn	reaction
S	Sweden
s	second
S	serine
s.d.	standard deviation
SCV	small colony variant
SDS	sodium dodecyl sulfate
SERAM	secretable expanded repertoire adhesive molecules
SFK	src-family kinases
sFn	soluble Fn
SH2	src homology domain 2
SH3	src-homology domain 3
SHP-2	SH2 domain containing tyrosine phosphatase
siRNA	small interfering RNA
SV40	simian virus 40
Syn	synergy site
Syn^-	RR1495/1500AA mutated Syn
T	thymine
TAE	Tris-acetate-EDTA
TEMED	N,N,N',N'-tetramethylethylenediamine
Tns3	Tensin-3
Tris	Tris(hydroxymethyl)-aminomethane
Tyr	tyrosine
UK	United Kingdom
USA	United States of America
UV	ultraviolet
V	volt
Val	valine
W	cell wall anchoring domain
W	watt
WTA	wall teichoic acids
X-gal	bromo-chloro-indolyl-galactopyranoside
YadA	Yersinia adhesin A

G. References

Abercrombie, M., and Dunn, G. A. (1975). Adhesions of fibroblasts to substratum during contact inhibition observed by interference reflection microscopy. Experimental Cell Research 92, 57-62.

Aderem, A., and Underhill, D. M. (1999). Mechanisms of phagocytosis in macrophages. Annual Review of Immunology 17, 593-623.

Agerer, F., Lux, S., Michel, A., Rohde, Manfred, Ohlsen, K., and Hauck, C. R. (2005). Cellular invasion by Staphylococcus aureus reveals a functional link between focal adhesion kinase and cortactin in integrin-mediated internalisation. Journal of cell science 118, 2189-200.

Agerer, F., Michel, A., Ohlsen, K., and Hauck, C. R. (2003). Integrin-mediated invasion of Staphylococcus aureus into human cells requires Src family protein-tyrosine kinases. The Journal of biological chemistry 278, 42524-31.

Alexandrova, A. Y., Arnold, K., Schaub, S., Vasiliev, J. M., Meister, J.-J., Bershadsky, A. D., and Verkhovsky, A. B. (2008). Comparative dynamics of retrograde actin flow and focal adhesions: formation of nascent adhesions triggers transition from fast to slow flow. PloS one 3, e3234.

Allen, L.-A., and Aderem, A. (1996). Molecular definition of distinct cytoskeletal structures involved in complement- and Fc receptor-mediated phagocytosis in macrophages. The Journal of Experimental Medicine 184, 627-637.

Anderson, R. G. (1998). The caveolae membrane system. Annual Review of Biochemistry 67, 199-225.

Aota, S.-ichi, Nomizu, M., and Yamada, K. M. (1994). The short amino acid sequence Pro-His-Ser-Arg-Asn in human fibronectin enhances cell-adhesive function. The Journal of Biological Chemistry 269, 24756-24761.

Askari, J. A., Buckley, P. A., Mould, A. P., and Humphries, M. J. (2009). Linking integrin conformation to function. Journal of cell science 122, 165-70.

Atkin, K. E. et al. (2010). The Streptococcal Binding Site in the Gelatin-binding Domain of Fibronectin Is Consistent with a Non-linear Arrangement of Modules. Journal of Biological Chemistry 285, 36977-36983.

Bae, E., Sakai, T., and Mosher, D. F. (2004). Assembly of exogenous fibronectin by fibronectin-null cells is dependent on the adhesive substrate. The Journal of biological chemistry 279, 35749-59.

Bearman, G. M. L., and Wenzel, R. P. (2005). Bacteremias: a leading cause of death. Archives of medical research 36, 646-59.

Berrier, A. L., and Yamada, K. M. (2007). Cell – Matrix Adhesion. Journal of Cellular Physiology, 565-573.

Bingham, R. J., Rudiño-Piñera, E., Meenan, N. A. G., Schwarz-Linek, U., Turkenburg, J. P., Höök, M., Garman, E. F., and Potts, Jennifer R (2008). Crystal structures of fibronectin-binding sites from Staphylococcus aureus FnBPA in complex with fibronectin domains. Proceedings of the National Academy of Sciences of the United States of America 105, 12254-8.

Bledzka, K., Bialkowska, K., Nie, H., Qin, J., Byzova, T., Wu, C., Plow, E. F., and Ma, Y.-Q. (2010). Tyrosine phosphorylation of integrin beta3 regulates kindlin-2 binding and integrin activation. The Journal of biological chemistry 285, 30370-4.

Brakebusch, C., and Fässler, R. (2005). Beta 1 Integrin Function in Vivo: Adhesion, Migration and More. Cancer metastasis reviews 24, 403-11.

Bronze, M. S., and Dale, J. B. (2010). Progress in the development of effective vaccines to prevent selected gram-positive bacterial infections. The American journal of the medical sciences 340, 218-25.

Cai, Y. et al. (2006). Nonmuscle myosin IIA-dependent force inhibits cell spreading and drives F-actin flow. Biophysical journal 91, 3907-20.

Caron, E., and Hall, A. (1998). Identification of two distinct mechanisms of phagocytosis controlled by different Rho GTPases. Science 282, 1717-1721.

Chabria, M., Hertig, S., Smith, M. L., and Vogel, V. (2010). Stretching fibronectin fibres disrupts binding of bacterial adhesins by physically destroying an epitope. Nature communications 1, 135.

Chen, H., Zou, Z., Sarratt, K. L., Zhou, D., Zhang, M., Sebzda, E., Hammer, D. A., and Kahn, M. L. (2006). In vivo beta1 integrin function requires phosphorylation-independent regulation by cytoplasmic tyrosines. Genes & development 20, 927-32.

Chen, L. B., Murray, A., Segal, R. A., Bushnell, A., and Walsh, M. L. (1978). Studies on intercellular LETS glycoprotein matrices. Cell 14, 377-391.

Choquet, D., Felsenfeld, D. P., and Sheetz, M. P. (1997). Extracellular matrix rigidity causes strengthening of integrin-cytoskeleton linkages. Cell 88, 39-48.

Clark, K., Pankov, R., Travis, M. A., Askari, J. A., Mould, A. P., Craig, S. E., Newham, P., Yamada, K. M., and Humphries, M. J. (2005). A specific alpha5beta1-integrin conformation promotes directional integrin translocation and fibronectin matrix formation. Journal of cell science 118, 291-300.

Conner, S. D., and Schmid, S. L. (2003). Regulated portals of entry into the cell. Nature 422, 37-44.

Coombes, J. L., and Robey, E. A. (2010). Dynamic imaging of host-pathogen interactions in vivo. Nature reviews. Immunology 10, 353-64.

Coussen, F., Choquet, D., Sheetz, M. P., and Erickson, H. P. (2002). Trimers of the fibronectin cell adhesion domain localize to actin filament bundles and undergo rearward translocation. Journal of cell science 115, 2581-90.

Critchley, D. R., and Gingras, A. R. (2008). Talin at a glance. Journal of cell science 121, 1345-7.

Cue, D., Dombek, P. E., Lam, H., and Cleary, P. P. (1998). Streptococcus pyogenes serotype M1 encodes multiple pathways for entry into human epithelial cells. Infection and Immunity 66, 4593-4601.

Cue, D., Southern, S. O., Southern, P. J., Prabhakar, J., Lorelli, W., Smallheer, J. M., Mousa, S. A., and Cleary, P. P. (2000). A nonpeptide integrin antagonist can inhibit epithelial cell ingestion of Streptococcus pyogenes by blocking formation of integrin alpha 5beta 1-fibronectin-M1 protein complexes. Proceedings of the National Academy of Sciences of the United States of America 97, 2858-2863.

Czuchra, A., Meyer, H., Legate, K. R., Brakebusch, C., and Fässler, R. (2006). Genetic analysis of beta1 integrin "activation motifs" in mice. The Journal of cell biology 174, 889-99.

Danen, E. H. J., Aota, S.-ichi, Kraats, A. A. van, Yamada, K. M., Ruiter, D. J., and Muijen, G. N. van (1995). Requirement for the synergy site for cell adhesion to fibronectin depends on the activation state of integrin alpha 5 beta 1. The Journal of biological chemistry 270, 21612-8.

Diao, J., Maniotis, A. J., Folberg, R., and Tajkhorshid, E. (2010). Interplay of mechanical and binding properties of Fibronectin type I. Theoretical chemistry accounts 125, 397-405.

Doherty, G. J., and McMahon, H. T. (2009). Mechanisms of endocytosis. Annual review of biochemistry 78, 857-902.

Dupuy, A. G., and Caron, E. (2008). Integrin-dependent phagocytosis: spreading from microadhesion to new concepts. Journal of cell science 121, 1773-83.

Dziewanowska, K., Carson, A. R., Patti, J. M., Deobald, C. F., Bayles, K. W., and Bohach, G. A. (2000). Staphylococcal fibronectin binding protein interacts with heat shock protein 60 and integrins: role in internalization by epithelial cells. Infection and immunity 68, 6321-8.

Dziewanowska, K., Patti, J. M., Deobald, C. F., Bayles, K. W., Trumble, W. R., and Bohach, G. A. (1999). Fibronectin binding protein and host cell tyrosine kinase are required for internalization of Staphylococcus aureus by epithelial cells. Infection and immunity 67, 4673-8.

Edwards, A. M., Potts, Jennifer R, Josefsson, E., and Massey, R. C. (2010). Staphylococcus aureus Host Cell Invasion and Virulence in Sepsis Is Facilitated by the Multiple Repeats within FnBPA. PLoS pathogens 6, e1000964.

Erickson, H. P. (2002). Stretching fibronectin. Journal of muscle research and cell motility 23, 575-580.

Espersen, F., and Clemmensen, I. (1982). Isolation of a fibronectin-binding protein from Staphylococcus aureus. Infection and immunity 37, 526-31.

Fath, K. R., Edgell, C. J., and Burridge, K. (1989). The distribution of distinct integrins in focal contacts is determined by the substratum composition. Journal of Cell Science 92 (Pt 1), 67-75.

Ffrench-Constant, C. (1995). Alternative splicing of fibronectin--many different proteins but few different functions. Experimental Cell Research 221, 261-271.

Filipenko, N. R., Attwell, S., Roskelley, C., and Dedhar, S. (2005). Integrin-linked kinase activity regulates Rac- and Cdc42-mediated actin cytoskeleton reorganization via alpha-PIX. Oncogene 24, 5837-5849.

Flock, J.-I. et al. (1987). Cloning and expression of the gene for a fibronectin-binding protein from Staphylococcus aureus. The EMBO 6, 2351-2357.

Foster, T. J. (2009). Colonization and infection of the human host by staphylococci: adhesion, survival and immune evasion. Veterinary dermatology 20, 456-70.

Fowler, T., Johansson, S., Wary, K. K., and Höök, M. (2003). Src kinase has a central role in in vitro cellular internalization of Staphylococcus aureus. Cellular microbiology 5, 417-26.

Fowler, T., Wann, E. R., Joh, D., Johansson, S., Foster, T. J., and Höök, M. (2000). Cellular invasion by Staphylococcus aureus involves a fibronectin bridge between the bacterial fibronectin-binding MSCRAMMs and host cell beta1 integrins. European Journal of Cell Biology 679, 672-679.

Francis, C. L., Ryan, T. A., Jones, B. D., Smith, S. J., and Falkow, S. (1993). Ruffles induced by Salmonella and other stimuli direct macropinocytosis of bacteria. Nature 364, 639-642.

Franco, S. J., Rodgers, M. A., Perrin, B. J., Han, J., Bennin, D. A., Critchley, D. R., and Huttenlocher, A. (2004). Calpain-mediated proteolysis of talin regulates adhesion dynamics. Nature Cell Biology 6, 977-983.

Friedland, J. C., Lee, M. H., and Boettiger, D. (2009). Mechanically Activated Integrin Switch Controls alpha5beta1 Function. Science 323, 642-644.

Fässler, R., and Meyer, M. (1995). Consequences of lack of beta 1 integrin gene expression in mice. Genes Development 9, 1896-1908.

Gardel, M. L., Schneider, I. C., Aratyn-Schaus, Y., and Waterman, C. M. (2010). Mechanical integration of actin and adhesion dynamics in cell migration. Annual review of cell and developmental biology 26, 315-33.

Geiger, Benjamin, Bershadsky, A. D., Pankov, R., Yamada, K. M., and G, C. B. (2001). Transmembrane extracellular matrix– cytoskeleton crosstalk. Nature Reviews Molecular Cell Biology 2.

George, E. L., Georges-Labouesse, E. N., Patel-King, R. S., Rayburn, H, and Hynes, R. O. (1993). Defects in mesoderm, neural tube and vascular development in mouse embryos lacking fibronectin. Development (Cambridge, England) 119, 1079-91.

Giannone, G., Jiang, G., Sutton, D. H., Critchley, D. R., and Sheetz, M. P. (2003). Talin1 is critical for force-dependent reinforcement of initial integrin-cytoskeleton bonds but not tyrosine kinase activation. The Journal of cell biology 163, 409-19.

Giannone, G., Mège, R.-M., and Thoumine, O. (2009). Multi-level molecular clutches in motile cell processes. Trends in cell biology 19, 475-86.

Gottschalk, K.-E. (2005). A coiled-coil structure of the alphaIIbbeta3 integrin transmembrane and cytoplasmic domains in its resting state. Structure London England 1993 13, 703-712.

Grant, S. G. N., Jessee, J., Bloom, F. R., and Hanahan, D. (1990). Differential plasmid rescue from transgenic mouse DNAs into Escherichia coli methylation-restriction mutants. Proceedings of the National Academy of Sciences of the United States of America 87, 4645-4649.

Greene, C., McDevitt, D., François, P. P., Vaudaux, P., Lew, D. P., and Foster, T. J. (1995). Adhesion properties of mutants of Staphylococcus aureus defective in fibronectin-binding proteins and studies on the expression of fnb genes. Molecular microbiology 17, 1143-52.

Heise, T., and Dersch, P. (2006). Identification of a domain in Yersinia virulence factor YadA that is crucial for extracellular matrix-specific cell adhesion and uptake. Proceedings of the National Academy of Sciences of the United States of America 103, 3375-80.

Henderson, B., Nair, S. P., Pallas, J., and Williams, M. A. (2010). Fibronectin: a multidomain host adhesin targeted by bacterial fibronectin-binding proteins. FEMS microbiology reviews, 1-54.

Heying, R., Gevel, J. V. D., and Que, Y.-A. (2009). Contribution of (sub) domains of Staphylococcus aureus fibronectin-binding protein to the proinflammatory and procoagulant response of human vascular endothelial. Thrombosis and Haemostasis, 495-504.

Heying, R., Gevel, J. V. D., Que, Y.-A., Moreillon, P., and Beekhuizen, H. (2007). Fibronectin-binding proteins and clumping factor A in Staphylococcus aureus experimental endocarditis : FnBPA is sufficient to activate human endothelial cells. Society, 617-626.

Hinz, B., Dugina, V., Ballestrem, C., Wehrle-Haller, B., and Chaponnier, C. (2003). Smooth Muscle Actin Is Crucial for Focal Adhesion Maturation in MyofibroblastsV. Molecular Biology of the Cell 14, 2508-2519.

Hoffmann, C., Berking, A., Agerer, F., Buntru, A., Neske, F., Chhatwal, G. S., Ohlsen, K., and Hauck, C. R. (2010). Caveolin limits membrane microdomain mobility and integrin-mediated uptake of fibronectin-binding pathogens. Journal of cell science, 4280-4291.

Honda, S., Shirotani-Ikejima, H., Tadokoro, S., Maeda, Y., Kinoshita, T., Tomiyama, Y., and Miyata, T. (2009). Integrin-linked kinase associated with integrin activation. Blood 113, 5304-5313.

Horton, M. A. (1997). The alphaVbeta3 Integrin " Vitronectin Receptor ." Cell 29.

Hotchin, N. A., Kidd, A. G., Altroff, H., and Mardon, H. J. (1999). Differential activation of focal adhesion kinase, Rho and Rac by the ninth and tenth FIII domains of fibronectin. Journal of cell science 112 (Pt 17, 2937-46.

Hughes, P. E., Diaz-Gonzalez, F., Leong, L., Wu, C., McDonald, J. A., Shattil, S. J., and Ginsberg, M. H. (1996). Breaking the integrin hinge. A defined structural constraint regulates integrin signaling. The Journal of Biological Chemistry 271, 6571-6574.

Humphries, J. D., Wang, P., Streuli, C., Geiger, Benny, Humphries, M. J., and Ballestrem, C. (2007). Vinculin controls focal adhesion formation by direct interactions with talin and actin. The Journal of cell biology 179, 1043-57.

Hynes, R. O. (1990). Fibronectins (Springer-Verlag (New York)).

Hynes, R. O. (2002). Integrins: Bidirectional, Allosteric Signaling Machines. Cell 110, 673-687.

Hynes, R. O. (2009). The extracellular matrix: not just pretty fibrils. Science (New York, N.Y.) 326, 1216-9.

Ingham, K. C., Brew, S. a, Huff, S., and Litvinovich, S. V. (1997). Cryptic self-association sites in type III modules of fibronectin. The Journal of biological chemistry 272, 1718-24.

Ingham, K. C., Brew, S., Vaz, D., Sauder, D. N., and McGavin, Martin J (2004). Interaction of Staphylococcus aureus fibronectin-binding protein with fibronectin: affinity, stoichiometry, and modular requirements. The Journal of biological chemistry 279, 42945-53.

Isberg, R. R., and Barnes, P. (2001). Subversion of integrins by enteropathogenic Yersinia. Journal of cell science 114, 21-28.

Ishibashi, Y., Relman, D. A., and Nishikawa, A. (2001). Invasion of human respiratory epithelial cells by Bordetella pertussis: possible role for a filamentous hemagglutinin Arg-Gly-Asp sequence and alpha5beta1 integrin. Microbial pathogenesis 30, 279-88.

Ithychanda, S. S., Das, M., Ma, Y.-Q., Ding, K., Wang, X., Gupta, S., Wu, C., Plow, E. F., and Qin, J. (2009). Migfilin, a molecular switch in regulation of integrin activation. The Journal of Biological Chemistry 284, 4713-4722.

Jaffe, E. A., Nachman, R. L., Becker, C. G., and Minick, C. R. (1973). Culture of human endothelial cells derived from umbilical veins. Identification by morphologic and immunologic criteria. The Journal of clinical investigation 52, 2745-56. Available at: http://www.pubmedcentral.nih.gov/articlerender.fcgi?artid=302542&tool=pmcentrez&rendertype=abstract.

Johnson, K. J., Sage, H., Briscoe, G, and Erickson, H. P. (1999). The compact conformation of fibronectin is determined by intramolecular ionic interactions. The Journal of biological chemistry 274, 15473-9.

Jönsson, K., Signäs, C., Müller, H.-P., and Lindberg, M. (1991). Two different genes encode fibronectin binding proteins in Staphylococcus aureus. European Journal of Biochemistry 202, 1041–1048.

Kanchanawong, P., Shtengel, G., Pasapera, A. M., Ramko, E. B., Davidson, M. W., Hess, H. F., and Waterman, C. M. (2010). Nanoscale architecture of integrin-based cell adhesions. Nature 468, 580-584.

Kanzaki, H., and Arata, J. (1992). Role of fibronectin in the adherence of Staphylococcus aureus to dermal tissues. Journal of Dermatological Science 4, 87-94.

Katz, B.-Z., Zamir, E., Bershadsky, A., Kam, Z, Yamada, K. M., and Geiger, Benjamin (2000). Physical state of the extracellular matrix regulates the structure and molecular composition of cell-matrix adhesions. Molecular biology of the cell 11, 1047-60.

Kern, W. V. (2010). Management of Staphylococcus aureus bacteremia and endocarditis: progresses and challenges. Current opinion in infectious diseases 23, 346-58.

Klass, C. M., Couchman, J. R., and Woods, A. (2000). Control of extracellular matrix assembly by syndecan-2 proteoglycan. Journal of Cell Science 113 (Pt 3, 493-506.

Kokkoli, E., Ochsenhirt, S. E., and Tirrell, M. (2004). Collective and Single-Molecule Interactions of alpha5beta1 Integrins. Society, 9515-9522.

Kong, F., García, A. J., Mould, A. P., Humphries, M. J., and Zhu, C. (2009). Demonstration of catch bonds between an integrin and its ligand. The Journal of cell biology 185, 1275-84.

Kuusela, P. (1978). Fibronectin binds to Staphylococcus aureus. Nature.

Kuusela, P., Vartio, T., Vuento, M., and Myhre, E. B. (1985). Attachment of staphylococci and streptococci on fibronectin, fibronectin fragments, and fibrinogen bound to a solid phase. Infection and immunity 50, 77-81.

Lan, R., and Reeves, P. R. (2000). Intraspecies variation in bacterial genomes: the need for a species genome concept. Trends in microbiology 8, 396-401.

Le Clainche, C., and Carlier, M.-F. (2008). Regulation of actin assembly associated with protrusion and adhesion in cell migration. Physiological reviews 88, 489-513.

Legate, K. R., and Fässler, R. (2009). Mechanisms that regulate adaptor binding to beta-integrin cytoplasmic tails. Journal of cell science 122, 187-98.

Legate, K. R., Wickström, S. A., and Fässler, R. (2009). Genetic and cell biological analysis of integrin outside-in signaling. Genes & development 23, 397-418.

Leiss, M., Beckmann, K., Girós, A., Costell, M., and Fässler, R. (2008). The role of integrin binding sites in fibronectin matrix assembly in vivo. Current opinion in cell biology 20, 502-7.

Leong, J. M., Morrissey, P. E., Marra, A., and Isberg, R. R. (1995). An aspartate residue of the Yersinia pseudotuberculosis invasin protein that is critical for integrin binding. the The European Molecular Biology Organization Journal 14, 422-431.

Li, F., Redick, S., Erickson, H. P., and Moy, V. (2003). Force Measurements of the α5β1 Integrin–Fibronectin Interaction. Biophysical Journal 84, 1252-1262.

Linder, S. (2003). Podosomes: adhesion hot-spots of invasive cells. Trends in Cell Biology 13, 376-385.

Lindsay, J. A. (2010). Genomic variation and evolution of Staphylococcus aureus. International journal of medical microbiology : IJMM 300, 98-103.

Lindsay, J. A., and Holden, M. T. G. (2004). Staphylococcus aureus: superbug, super genome? Trends in microbiology 12, 378-85.

Loughman, A., Sweeney, T., Keane, F. M., Pietrocola, G., Speziale, P., and Foster, T. J. (2008). Sequence diversity in the A domain of Staphylococcus aureus fibronectin-binding protein A. BMC microbiology 8, 74.

Lowy, F. D. (1998). Staphylococcus aureus infections. The New England Journal of Medicine 339, 520-532.

Luo, B.-H., Carman, C. V., and Springer, T. A. (2007). Structural basis of integrin regulation and signaling. Annual Review of Immunology 25, 619-647.

Ma, Y.-Q., Qin, J., Wu, C., and Plow, E. F. (2008). Kindlin-2 (Mig-2): a co-activator of beta3 integrins. The Journal of cell biology 181, 439-46.

Mack, D., Siemssen, N., and Laufs, R. (1992). Parallel induction by glucose of adherence and a polysaccharide antigen specific for plastic-adherent Staphylococcus epidermidis: evidence for functional relation to intercellular adhesion. Infection and Immunity 60, 2048-2057.

Malachowa, N., and DeLeo, F. R. (2010). Mobile genetic elements of Staphylococcus aureus. Cellular and molecular life sciences : CMLS 67, 3057-71.

Mao, Y., and Schwarzbauer, J. E. (2006). Accessibility to the fibronectin synergy site in a 3D matrix regulates engagement of alpha5beta1 versus alphavbeta3 integrin receptors. Cell communication & adhesion 13, 267-77.

Mao, Y., and Schwarzbauer, J. E. (2005). Fibronectin fibrillogenesis, a cell-mediated matrix assembly process. Matrix biology : journal of the International Society for Matrix Biology 24, 389-99.

Maurer, L. M., Tomasini-Johansson, B. R., Ma, W., Annis, D. S., Eickstaedt, N. L., Ensenberger, Martin G, Satyshur, K. A., and Mosher, D. F. (2010). Extended binding

site on fibronectin for the functional upstream domain of protein F1 of Streptococcus pyogenes. The Journal of biological chemistry 285, 41087-99.

McCarthy, A. J., and Lindsay, J. A. (2010). Genetic variation in Staphylococcus aureus surface and immune evasion genes is lineage associated: implications for vaccine design and host-pathogen interactions. BMC microbiology 10, 173.

McCleverty, C. J., Lin, Diane C, and Liddington, R. C. (2007). Structure of the PTB domain of tensin1 and a model for its recruitment to fibrillar adhesions. Protein science : a publication of the Protein Society 16, 1223-9.

McDonald, J. A. (1988). Extracellular matrix assembly. Ann Rev Cell Biol 4, 183-207.

McDonald, J. A., Quade, B. J., Broekelmann, T. J., LaChance, R., Forsman, K., Hasegawa, E., and Akiyama, S. K. (1987). Fibronectin's cell-adhesive domain and an amino-terminal matrix assembly domain participate in its assembly into fibroblast pericellular matrix. The Journal of Biological Chemistry 262, 2957-2967.

McElroy, M. C., Cain, D. J., Tyrrell, C., Foster, T. J., Haslett, C., and Mmun, I. N. I. (2002). Increased Virulence of a Fibronectin-Binding Protein Mutant of Staphylococcus aureus in a Rat Model of Pneumonia. Society 70, 3865-3873.

McKeown-Longo, P. J., and Mosher, D. F. (1983). Binding of plasma fibronectin to cell layers of human skin fibroblasts. The Journal of cell biology 97, 466-72.

Meenan, N. A. G., Visai, L., Valtulina, V., Schwarz-Linek, U., Norris, N. C., Gurusiddappa, S., Höök, M., Speziale, P., and Potts, Jennifer R (2007). The tandem beta-zipper model defines high affinity fibronectin-binding repeats within Staphylococcus aureus FnBPA. The Journal of biological chemistry 282, 25893-902.

Mercer, J., and Helenius, A. (2009). Virus entry by macropinocytosis. Nature Cell Biology 11, 510-520.

Mercer, J., Schelhaas, M., and Helenius, A. (2010). Virus entry by endocytosis. Annual review of biochemistry 79, 803-33.

Michael, K. E., Dumbauld, D. W., Burns, K. L., Hanks, S. K., and García, A. J. (2009). Focal adhesion kinase modulates cell adhesion strengthening via integrin activation. Molecular biology of the cell 20, 2508-19.

Mitchison, T., and Kirschner, M. (1988). Cytoskeletal dynamics and nerve growth. Neuron 1, 761-772.

Moreno-Ruiz, E., Galán-Díez, M., Zhu, W., Fernández-Ruiz, E., D'Enfert, C., Filler, S. G., Cossart, P., and Veiga, E. (2009). Candida albicans internalization by host cells is mediated by a clathrin-dependent mechanism. Cellular Microbiology 11, 1179-1189.

Morens, D. M., Folkers, G. K., and Fauci, A. S. (2008). Emerging infections: a perpetual challenge. The Lancet Infectious Diseases 8, 710-719.

Moser, M., Legate, K. R., Zent, R., and Fässler, R. (2009). The tail of integrins, talin, and kindlins. Science (New York, N.Y.) 324, 895-9.

Moser, M., Nieswandt, B., Ussar, S., Pozgajova, M., and Fässler, R. (2008). Kindlin-3 is essential for integrin activation and platelet aggregation. Nature medicine 14, 325-30.

Mould, A. P., Barton, S. J., Askari, J. A., Craig, S. E., and Humphries, M. J. (2003). Role of ADMIDAS cation-binding site in ligand recognition by integrin alpha 5 beta 1. The Journal of biological chemistry 278, 51622-9.

Navarre, W. W., and Schneewind, O. (1999). Surface proteins of gram-positive bacteria and mechanisms of their targeting to the cell wall envelope. Microbiology and molecular biology reviews : MMBR 63, 174-229.

Nishizaka, T., Shi, Q., and Sheetz, M. P. (2000). Position-dependent linkages of fibronectin-integrin-cytoskeleton. Proceedings of the National Academy of Sciences of the United States of America 97, 692-7.

Nyberg, P., Sakai, T., Cho, K. H., Caparon, M. G., Fässler, R., and Björck, L. (2004). Interactions with fibronectin attenuate the virulence of Streptococcus pyogenes. The EMBO journal 23, 2166-74.

Ohashi, T., Kiehart, D. P., and Erickson, H. P. (2002). Dual labeling of the fibronectin matrix and actin cytoskeleton with green fluorescent protein variants. Journal of cell science 115, 1221-9.

Overholtzer, M., Mailleux, A. A., Mouneimne, G., Normand, G., Schnitt, S. J., King, R. W., Cibas, E. S., and Brugge, J. S. (2007). A nonapoptotic cell death process, entosis, that occurs by cell-in-cell invasion. Cell 131, 966-979.

Oxley, C. L., Anthis, N. J., Lowe, E. D., Vakonakis, I., Campbell, I. D., and Wegener, K. L. (2008). An integrin phosphorylation switch: the effect of beta3 integrin tail phosphorylation on Dok1 and talin binding. The Journal of biological chemistry 283, 5420-6.

Ozeri, V., Rosenshine, I., Mosher, D. F., Fässler, R., and Hanski, E. (1998). Roles of integrins and fibronectin in the entry of Streptococcus pyogenes into cells via protein F1. Molecular microbiology 30, 625-37.

O'Neill, E., Pozzi, C., Houston, P., Humphreys, H., Robinson, D. A., Loughman, A., Foster, T. J., and O'Gara, J. P. (2008). A novel Staphylococcus aureus biofilm phenotype mediated by the fibronectin-binding proteins, FnBPA and FnBPB. Journal of bacteriology 190, 3835-50.

Pankov, R., Cukierman, E., Katz, B.-Z., Matsumoto, K., Lin, D C, Lin, S., Hahn, C., and Yamada, K. M. (2000). Integrin dynamics and matrix assembly: tensin-dependent translocation of alpha5beta1 integrins promotes early fibronectin fibrillogenesis. The Journal of cell biology 148, 1075-90.

Pankov, R., and Yamada, K. M. (2002). Fibronectin at a glance. Journal of Cell Science 115, 3861-3863.

Paradise, R. K., Lauffenburger, D. a, and Van Vliet, K. J. (2011). Acidic Extracellular pH Promotes Activation of Integrin αvβ3. PLoS ONE 6, e15746.

Parsons, J. T., Horwitz, A. R., and Schwartz, M. A. (2010). Cell adhesion : integrating cytoskeletal dynamics and cellular tension. Nature Publishing Group 11, 633-643.

Patel, R. S., Odermatt, E., Schwarzbauer, J. E., and Hynes, R. O. (1987). Organization of the fibronectin gene provides evidence for exon shuffling during evolution. the The European Molecular Biology Organization Journal 6, 2565-2572.

Patti, J. M., Allen, B. L., McGavin, M J, and Höök, M. (1994). MSCRAMM-mediated adherence of microorganisms to host tissues. Annual review of microbiology 48, 585-617.

Peacock, S. J., Foster, T. J., Cameron, B. J., and Berendt, A. R. (1999). Bacterial fibronectin-binding proteins and endothelial cell surface fibronectin mediate adherence of Staphylococcus aureus to resting human endothelial cells. Microbiology (Reading, England) 145 (Pt 1, 3477-86.

Pierschbacher, M. D., and Ruoslahti, E. (1984). Cell attachment activity of fibronectin can be duplicated by small synthetic fragments of the molecule. Nature 309, 30-33.

Piroth, L., Que, Y.-A., Widmer, E., Panchaud, A., Piu, S., Entenza, J.-M., and Moreillon, P. (2008). The fibrinogen- and fibronectin-binding domains of Staphylococcus aureus fibronectin-binding protein A synergistically promote endothelial invasion and experimental endocarditis. Infection and immunity 76, 3824-31.

Plow, E. F., Haas, T., Zhang, L., Loftus, J., and Smith, J. W. (2000). Ligand binding to integrins. The Journal of biological chemistry 275, 21785-8.

Potts, Jennifer R, and Campbell, I. D. (1994). Fibronectin structure and assembly. Current Opinion in Cell Biology 6, 648-655.

Proctor, R. A., Eiff, C. von, Kahl, B. C., Becker, K., McNamara, P., Herrmann, M., and Peters, Georg (2006). Small colony variants: a pathogenic form of bacteria that facilitates persistent and recurrent infections. Nature reviews. Microbiology 4, 295-305.

Que, Y.-A. et al. (2005). Fibrinogen and fibronectin binding cooperate for valve infection and invasion in Staphylococcus aureus experimental endocarditis. The Journal of experimental medicine 201, 1627-35.

Raibaud, S., Schwarz-Linek, U., Kim, J. H., Jenkins, H. T., Baines, E. R., Gurusiddappa, S., Höök, M., and Potts, J R (2005). Borrelia burgdorferi Binds Fibronectin through a Tandem beta-Zipper, a Common Mechanism of Fibronectin Binding in Staphylococci, Streptococci, and Spirochetes. The Journal of Biological Chemistry 280, 18803-18809.

Redick, S. D., Settles, D. L., Briscoe, Gina, and Erickson, H. P. (2000). Defining Fibronectin' s Cell Adhesion Synergy Site by Site-directed Mutagenesis. Cell 149, 521-527.

Retta, S. F., Ferraris, P., and Tarone, G. (1999). Purification of fibronectin from human plasma. Methods in molecular biology (Clifton, N.J.) 96, 119-24.

Roca-Cusachs, P., Gauthier, N. C., and Sheetz, M. P. (2009). Clustering of alpha5beta1 integrins determines adhesion strength whereas alphavbeta3 and talin enable mechanotransduction. PNAS 106.

Roche, F. M., Massey, R. C., Peacock, S. J., Day, N. P., Visai, L., Speziale, P., Lam, A., Pallen, M., and Foster, T. J. (2003). Characterization of novel LPXTG-containing proteins of Staphylococcus aureus identified from genome sequences. Microbiology 149, 643-654.

Romer, L. H., Birukov, K. G., and Garcia, J. G. N. (2006). Focal adhesions: paradigm for a signaling nexus. Circulation Research 98, 606-616.

Sakai, T. et al. (2001). Plasma fibronectin supports neuronal survival and reduces brain injury following transient focal cerebral ischemia but is not essential for skin-wound healing and hemostasis. Nature medicine 7, 324-30.

Sakai, T., Zhang, Q., and Mosher, D. F. (1998). Modulation of beta1A Integrin Functions by Tyrosine Residues in the beta 1 Cytoplasmic Domain. Cell 141, 527-538.

Saoncella, S., Echtermeyer, F., Denhez, F., Nowlen, J. K., Mosher, D. F., Robinson, S. D., Hynes, R. O., and Goetinck, P. F. (2007). Syndecan-4 signals cooperatively with integrins in a Rho- dependent manner in the assembly of focal adhesions and actin stress fibers. Cell.

Sastry, S. K., and Burridge, K. (2000). Focal adhesions: a nexus for intracellular signaling and cytoskeletal dynamics. Experimental cell research 261, 25-36.

Schleifer, K. H., and Fischer, U. (1982). Description of a new species of the genus Staphylococcus: Staphylococcus carnosus. International Journal of, 23-31.

Schröder, A., Schröder, B., Roppenser, B., Linder, S., and Aepfelbacher, M. (2006). Staphylococcus aureus Fibronectin Binding Protein-A Induces Motile Attachment Sites and Complex Actin Remodeling in Living Endothelial Cells. Molecular Biology of the Cell 17, 5198 -5210.

Schubert, W., Frank, P. G., Razani, B., Park, D. S., Chow, C. W., and Lisanti, M. P. (2001). Caveolae-deficient endothelial cells show defects in the uptake and transport of albumin in vivo. The Journal of Biological Chemistry 276, 48619-48622.

Schwarz-Linek, U. et al. (2003). Pathogenic bacteria attach to human fibronectin through a tandem beta-zipper. Nature 423, 177-81.

Schwarzbauer, J. E. (1991). Fibronectin: from gene to protein. Current Opinion in Cell Biology 3, 786-791.

Sechler, J. L., Corbett, S. A., and Schwarzbauer, J. E. (1997). Modulatory roles for integrin activation and the synergy site of fibronectin during matrix assembly. Molecular biology of the cell 8, 2563-73.

Sechler, J. L., Cumiskey, A. M., Gazzola, D. M., and Schwarzbauer, J. E. (2000). A novel RGD-independent fibronectin assembly pathway initiated by α4β1 integrin binding to the alternatively spliced V region. Journal of Cell Science 1498, 1491-1498.

Sechler, J. L., Takada, Y., and Schwarzbauer, J. E. (1996). Altered rate of fibronectin matrix assembly by deletion of the first type III repeats. The Journal of Cell Biology 134, 573-583.

Shi, F., and Sottile, J. (2008). Caveolin-1-dependent beta1 integrin endocytosis is a critical regulator of fibronectin turnover. Journal of cell science 121, 2360-71.

Singh, P., Carraher, C., and Schwarzbauer, J. E. (2010). Assembly of Fibronectin Extracellular Matrix. Annual review of cell and developmental biology, 1-23.

Sinha, B. et al. (1999). Fibronectin-binding protein acts as Staphylococcus aureus invasin via fibronectin bridging to integrin alpha5beta1. Cellular microbiology 1, 101-17.

Sinha, B. et al. (2000). Heterologously expressed Staphylococcus aureus fibronectin-binding proteins are sufficient for invasion of host cells. Infection and immunity 68, 6871-8.

Sobke, A. C. S. et al. (2006). The extracellular adherence protein from Staphylococcus aureus abrogates angiogenic responses of endothelial cells by blocking Ras activation. The FASEB journal official publication of the Federation of American Societies for Experimental Biology 20, 2621-2623.

Sokurenko, E. V., Vogel, V., and Thomas, W. E. (2008). Catch-bond mechanism of force-enhanced adhesion: counterintuitive, elusive, but ... widespread? Cell host & microbe 4, 314-23.

Sottile, J., and Chandler, J. (2005). Fibronectin matrix turnover occurs through a caveolin-1-dependent process. Molecular biology of the cell 16, 757-68.

Sottile, J., Hocking, D. C., and Langenbach, K. J. (2000). Fibronectin polymerization stimulates cell growth by RGD-dependent and -independent mechanisms. Journal of cell science 113 Pt 23, 4287-99.

Stanchi, F., Grashoff, C., Nguemeni Yonga, C. F., Grall, D., Fässler, R., and Van Obberghen-Schilling, E. (2009). Molecular dissection of the ILK-PINCH-parvin triad reveals a fundamental role for the ILK kinase domain in the late stages of focal-adhesion maturation. Journal of cell science 122, 1800-11.

Stepp, M. A., Daley, W. P., Bernstein, A. M., Pal-Ghosh, S., Tadvalkar, G., Shashurin, A., Palsen, S., Jurjus, R. A., and Larsen, M. (2010). Syndecan-1 regulates cell migration and fibronectin fibril assembly. Experimental Cell Research 316, 2322-2339.

Stevens, J. M., Galyov, E. E., and Stevens, M. P. (2006). Actin-dependent movement of bacterial pathogens. Nature reviews. Microbiology 4, 91-101.

Studier, F. W., and Moffatt, B. A. (1986). Use of bacteriophage T7 RNA polymerase to direct selective high-level expression of cloned genes. Journal of Molecular Biology 189, 113-130.

Suree, N., Liew, C. K., Villareal, V. A., Thieu, W., Fadeev, E. A., Clemens, J. J., Jung, M. E., and Clubb, R. T. (2009). The structure of the Staphylococcus aureus sortase-substrate complex reveals how the universally conserved LPXTG sorting signal is recognized. The Journal of biological chemistry 284, 24465-77.

Takagi, J., Erickson, H. P., and Springer, T. A. (2001). C-terminal opening mimics "inside-out" activation of integrin alpha5beta1. Nature Structural Biology 8, 412-416.

Takagi, J., Strokovich, K., Springer, T. A., and Walz, T. (2003). Structure of integrin alpha5beta1 in complex with fibronectin. EMBO Journal 22, 4607-4615.

Takahashi, S. et al. (2007). The RGD motif in fibronectin is essential for development but dispensable for fibril assembly. The Journal of cell biology 178, 167-78.

Talay, S. R., Zock, A., Rohde, M, Molinari, G., Oggioni, M., Pozzi, G., Guzman, C. A., and Chhatwal, G. S. (2000). Co-operative binding of human fibronectin to Sfbl protein triggers streptococcal invasion into respiratory epithelial cells. Cellular microbiology 2, 521-35.

Tomasini-Johansson, B. R., Kaufman, N. R., Ensenberger, M G, Ozeri, V., Hanski, E., and Mosher, D. F. (2001). A 49-residue peptide from adhesin F1 of Streptococcus pyogenes inhibits fibronectin matrix assembly. The Journal of biological chemistry 276, 23430-9.

Toomre, D., and Bewersdorf, J. (2010). A New Wave of Cellular Imaging. Annual Review of Cell and Developmental Biology 26, 285-314.

Tuchscherr, L., Heitmann, V., Hussain, M., Viemann, D., Roth, J., Eiff, C. von, Peters, Georg, Becker, K., and Löffler, B. (2010). Staphylococcus aureus Small-Colony Variants Are Adapted Phenotypes for Intracellular Persistence. The Journal of infectious diseases 202.

Uhlik, M. T., Temple, B., Bencharit, S., Kimple, A. J., Siderovski, D. P., and Johnson, G. L. (2005). Structural and evolutionary division of phosphotyrosine binding (PTB) domains. Journal of molecular biology 345, 1-20.

Underhill, D. M., and Ozinsky, A. (2002). Phagocytosis of microbes: complexity in action. Annual review of immunology 20, 825-52.

Veiga, E., and Cossart, P. (2005). Listeria hijacks the clathrin-dependent endocytic machinery to invade mammalian cells. Nature Cell Biology 7, 894-900.

Veiga, E. et al. (2007). Invasive and adherent bacterial pathogens co-Opt host clathrin for infection. Cell host & microbe 2, 340-51.

Vicente-Manzanares, M., Choi, C. K., and Horwitz, A. R. (2009). Integrins in cell migration--the actin connection. Journal of cell science 122, 199-206.

Vicente-Manzanares, M., Webb, D. J., and Horwitz, A. R. (2005). Cell migration at a glance. Journal of cell science 118, 4917-9.

Vinogradova, O., Velyvis, A., Velyviene, A., Hu, B., Haas, T., Plow, E. F., and Qin, J. (2002). A structural mechanism of integrin alphaIIbbeta3 "inside-out" activation as regulated by its cytoplasmic face. Cell 110, 587-597.

Wang, B., Yurecko, R. S., Dedhar, S., and Cleary, P. P. (2006). Integrin-linked kinase is an essential link between integrins and uptake of bacterial pathogens by epithelial cells. Cellular microbiology 8, 257-66.

Wang, Y.-L. (1985). Exchange of actin subunits at the leading edge of living fibroblasts: possible role of treadmilling. The Journal of Cell Biology 101, 597-602.

Wann, E. R., Gurusiddappa, S., and Höök, M. (2000). The fibronectin-binding MSCRAMM FnbpA of Staphylococcus aureus is a bifunctional protein that also binds to fibrinogen. The Journal of biological chemistry 275, 13863-71.

Watarai, M., Derre, I., Kirby, J., Growney, J. D., Dietrich, W. F., and Isberg, R. R. (2001). Legionella pneumophila is internalized by a macropinocytotic uptake pathway controlled by the Dot/Icm system and the mouse Lgn1 locus. The Journal of Experimental Medicine 194, 1081-1096.

Weaver, A. M., Heuser, J. E., Karginov, A. V., Lee, W. L., Parsons, J. T., and Cooper, J. A. (2002). Interaction of cortactin and N-WASp with Arp2/3 complex. Current Biology 12, 1270-8.

Wegener, K. L., Partridge, A. W., Han, J., Pickford, A. R., Liddington, R. C., Ginsberg, M. H., and Campbell, I. D. (2007). Structural basis of integrin activation by talin. Cell 128, 171-182.

Wennerberg, K., Armulik, A., Sakai, T., Karlsson, M., Fässler, R., Schaefer, E. M., Mosher, D. F., and Johansson, S. (2000). The cytoplasmic tyrosines of integrin subunit beta1 are involved in focal adhesion kinase activation. Molecular and cellular biology 20, 5758-65.

Wennerberg, K., Lohikangas, L., Gullberg, D., Pfaff, M., Johansson, S., and Fässler, R. (1996). beta1 Integrin-dependent and -independent Polymerization of Fibronectin. The Journal of cell biology 132, 227-238.

Wiseman, P. W., Brown, C. M., Webb, D. J., Hebert, B., Johnson, N. L., Squier, J. A., Ellisman, M. H., and Horwitz, A. F. (2004). Spatial mapping of integrin interactions and dynamics during cell migration by image correlation microscopy. Journal of Cell Science 117, 5521-5534.

Xia, G., Kohler, T., and Peschel, A. (2010). The wall teichoic acid and lipoteichoic acid polymers of Staphylococcus aureus. International journal of medical microbiology : IJMM 300, 148-54.

Xiong, J.-P., Stehle, T., Goodman, S. L., and Arnaout, M. A. (2003). New insights into the structural basis of integrin activation. Blood 102, 1155-1159.

Xiong, J.-P., Stehle, T., Zhang, R., Joachimiak, A., Frech, M., Goodman, S. L., and Arnaout, M. A. (2002). Crystal structure of the extracellular segment of integrin alpha Vbeta3 in complex with an Arg-Gly-Asp ligand. Science 296, 151-155.

Yang, J. T., Rayburn, Helen, and Hynes, R. O. (1993). Embryonic mesodermal defects in alpha 5 integrin-deficient mice. Development Cambridge England 119, 1093-1105.

Ythier, M., Entenza, J.-manuel, Bille, J., Vandenesch, F., Bes, M., Moreillon, P., and Sakwinska, O. (2010). Natural variability of in vitro adherence to fibrinogen and fibronectin does not correlate with in vivo infectivity of Staphylococcus aureus. Infection and immunity 78, 1711-6.

Zaidel-Bar, R., and Geiger, Benjamin (2010). The switchable integrin adhesome. Journal of cell science 123, 1385-8.

Zaidel-Bar, R., Itzkovitz, S., Ma'ayan, A., Iyengar, R., and Geiger, Benjamin (2007). Functional atlas of the integrin adhesome. Nature Cell Biology 9, 858-867.

Zaidel-Bar, R., Milo, R., Kam, Zvi, and Geiger, Benjamin (2007). A paxillin tyrosine phosphorylation switch regulates the assembly and form of cell-matrix adhesions. Journal of cell science 120, 137-48.

Zamir, E., and Geiger, Benjamin (2001). Molecular complexity and dynamics of cell-matrix adhesions. Journal of cell science 114, 3583-90.

Zamir, E., Katz, B.-Z., Aota, S.-ichi, Yamada, K. M., Geiger, Benjamin, and Kam, Zvi (1999). Molecular diversity of cell-matrix adhesions. Journal of cell science 112 (Pt 1, 1655-69.

Zhang, X., Jiang, G., Cai, Y., Monkley, S. J., Critchley, D. R., and Sheetz, M. P. (2008). Talin depletion reveals independence of initial cell spreading from integrin activation and traction. Nature cell biology 10.

H. Acknowledgements

This work would have never been possible without the help of many people. I would sincerely like to thank the following people:

My supervisor, Prof. Dr. Martin Aepfelbacher, for giving me the opportunity to work in his research group and supervising the project, for continuous support, help and careful reading of the manuscript. For giving me the chance to establish and promote the microscopic imaging facility at the UKE.

I am grateful to Prof. Dr. Wolfgang Streit for accepting to be my thesis reviewer at the biological department.

All the former and current members of our research group: Anja Röder, Kirsten Egg, Erin Boyle, Kerstin Lardong, Anne Hett, Franziska Albrecht, Claudia Trasak, Andreas Rumm, Manuel Wolters, Gerhard Zenner and Martin Kuhns.
Bernhard Roppenser for a great time in the lab, on various concerts and in Austria.
Holger Rohde for helpful discussions and any support throughout the thesis.
Mirko Himmel and Prof. Dr. Stefan Linder for their confidence in me, great support and enjoying dissussions.
All the members from other groups at the institute for their help and the good atmosphere.
Very special thanks to Rebecca Stanway for proof-reading the manuscript and the great time we spent together imaging parasites using the spinning disk microscope.

My parents, sister, grand-father and friends, who I could not see as much and long as I wanted in the last years, for their comprehension and continous support.

Melanie Michel, who became the most important person in my life, for simply everything.